STUDIES ON THE NUCLEOCAPSID PROTEIN OF

INFECTIOUS BRONCHITIS VIRUS

A Dissertation

by

JYOTHI JAYARAM

Submitted to the Office of Graduate Studies of
Texas A&M University
in partial fulfillment of the requirements for the degree of

DOCTOR OF PHILOSOPHY

May 2004

Major Subject: Microbiology

STUDIES ON THE NUCLEOCAPSID PROTEIN OF

INFECTIOUS BRONCHITIS VIRUS

A Dissertation

by

JYOTHI JAYARAM

Submitted to Texas A&M University
in partial fulfillment of the requirements
for the degree of

DOCTOR OF PHILOSOPHY

Approved as to style and content by:

Ellen W. Collisson (Co-Chair of Committee)	Timothy C. Hall (Co-Chair of Committee)
Paul D. Gershon (Member)	Van G. Wilson (Member)
	Vincent M. Cassone (Head of Department)

May 2004

Major Subject: Microbiology

ABSTRACT

Studies on the Nucleocapsid Protein of Infectious Bronchitis Virus.

(May 2004)

Jyothi Jayaram, B.S., University of Bombay, India;

M.S., Maharaja Sayajirao University of Baroda, India

Co-Chairs of Advisory Committee: Dr. Ellen W. Collisson
Dr. Timothy C. Hall

Because phosphorylation of the infectious bronchitis virus (IBV) nucleocapsid (N) protein may regulate its multiple roles in viral replication, the dynamics of N phosphorylation were examined. In the infected cell, N was the only viral protein that was phosphorylated as shown by ^{32}P-orthophosphate labeling and Western blot analysis and with IBV specific polyclonal chicken antibody. Using pulse-labeling with ^{32}P-orthophosphate, the IBV N protein was found to be phosphorylated in the virion, as well as at all times during infection of Vero cells. One-hour pulse-chase analysis followed by immunoprecipitation of IBV N using rabbit anti-IBV N polyclonal antibody showed that the phosphate on the protein did not fall below 70% of the maximum and remained stable. The small but reproducible drop in phosphorylation could modulate the various functions of the N protein in the infected cell. Simultaneous labeling with ^{32}P-orthophosphate and ^{3}H-leucine of infected CEK cells indicated a 3.5-fold increase in the ratio of the ^{32}P:^{3}H counts per minute (cpm) on the virion N protein as compared to the ^{32}P:^{3}H cpm ratio of the N protein from lysates at 7 h p.i. The ^{32}P:^{3}H cpm ratio of the N

protein from virion from infected-Vero cell lysates was 10.5X more than the ^{32}P:^{3}H cpm ratio of the N protein obtained at 7 h p.i.

It has been shown that the N proteins from the measles and rabies viruses form helical nucleocapsid-like structures when expressed in bacteria (Schoehn *et al.*, 2001; Warnes *et al.*, 1995). The ability of *E. coli* expressed IBV N protein to form helical-nucleocapsid-like structures was investigated using transmission electron microscopy. Full-length, purified histidine-tagged IBV N protein formed nucleocapsid-like structures when expressed in bacteria. Because *E. coli* -expressed histidine-tagged fragments of the IBV N protein did not form helical nucleocapsid-like structures, the full-length protein is probably required for assembly of these structures.

The highly conserved IBV N protein was also used as a diagnostic tool in an ELISA for detecting anti-IBV antibody in chicken serum using a specialized microwave called the BIOWAVE. The BIOWAVE improves the processing time for an ELISA.

DEDICATION

To My Parents

ACKNOWLEDGEMENTS

TABLE OF CONTENTS

Page

TABLE OF CONTENTS (continued)

LIST OF FIGURES

LIST OF FIGURES (continued)

LIST OF FIGURES (continued)

LIST OF TABLES

LIST OF TABLES (continued)

CHAPTER I

INTRODUCTION

INFECTIOUS BRONCHITIS

Coronaviruses are notorious for causing economic losses in agriculture. Since first described in 1931, IBV has remained a primary concern for the poultry industry (Schalk and Hawn, 1931; Cunningham, 1970). Infection caused by IBV is highly contagious and depending on the strain, it causes respiratory, enteric, kidney, and reproductive diseases (Albassam *et al.*, 1986; Avellaneda *et al.*, 1994; Chew *et al.*, 1997; Ziegler *et al.*, 2002). Associated illness is especially severe in young chickens and persisting virus affects the quality of eggs from adult hens. Live, attenuated vaccines have been used to control IBV related losses (Ignjatovic and Sapats, 2000). However because of continuing genetic variations, field outbreaks continue to occur that antigenically differ from the vaccine strains (Collisson *et al.*, 1992; Ignjatovic and Sapats, 2000). It is necessary to develop new methods to control IBV. A thorough understanding of the molecular biology of the virus can lead to the development of more effective control measures.

Classification

Infectious bronchitis virus (IBV) belongs to the *Nidovirales* order and family *Coronaviridae*. The primary features which define membership of the *Nidovirales* are:

The format of this dissertation follows that of the journal Virology.

1) Linear, non-segmented, positive-sense, single stranded RNA genomes. 2) Genome organization: 5'-replicase gene-structural proteins genes-3'. 3) A 3' co-terminal nested set of four or more subgenomic RNAs. 4) The genomic RNA functions as the mRNA for the translation of the replicase polyprotein. 5) The 5' unique regions of the mRNAs, i.e. those absent from the next smaller RNA are translated (Cavanagh, 1997). Comparative sequence analysis of the non-structural and structural proteins of the viruses have led to their classification under the *Arteriviridae*, *Coronaviridae* and *Roniviridae* families (Gonzalez *et al.*, 2003). The classification of the family *Coronaviridae* into the Coronavirus and the Torovirus genera is based on similarities in genome organization and the expression of their genomes and the structures of the viral gene products (Siddell *et al.*, 1995). The genome size ranges from 13 to 15 kilobases for arteriviruses and from 27 to 32 kilobases for coronaviruses. Coronaviruses, like the toroviruses and the arteriviruses, have a unique, discontinuous transcription strategy that produces several subgenomic mRNAs and the genomic RNA. The subgenomic mRNAs form 3' co-terminal nested sets in which each mRNA contains the common 3' untranslated region and 5' leader sequence (Siddell *et al.*, 1995).

Viruses belonging to the genus coronavirus cause respiratory, gastrointestinal, cardiovascular, and neurological disease in domestic animals, including poultry, and in humans (McIntosh et al., 1974). Based on antigenic cross-reactivity and sequence analysis of structural protein genes, coronaviruses are classified into three distinct groups. Group I includes human coronavirus 229E (HCoV-229E), transmissible gastroenteritis virus (TGEV), canine coronavirus (CCV), feline coronavirus (FECV),

and feline infectious peritonitis virus (FIPV). Group II includes human coronavirus OC43 (HCoV-OC43), murine hepatitis virus (MHV), porcine hemagglutinating encephalomyelitis virus (HEV), sialodacryoadenitis virus (SDAV), and bovine coronavirus (BCoV). Group III includes IBV, a type of turkey coronavirus (TCV) and pheasant coronavirus (Siddell *et al.*, 1995). Recently, a new, genetically unique, human coronavirus was isolated as an etiological agent of severe acute respiratory syndrome (SARS). Although coroanviruses are host-specific, the SARS coronavirus (SCoV) was also isolated from a civet and the closely related raccoon dog (Drosten *et al.*, 2003; Ksiazek *et al.*, 2003; Peiris *et al.*, 2003). The genome organization of the SCoV is typical of coronaviruses. Like the group III coronaviruses, the SCoV has several small non-structural open reading frames (ORFs) that are found between the S and E genes and between the M and N genes (Rota *et al.*, 2003). Phylogenetic analysis of different SCoV proteins using unrooted trees showed that SCoV does not segregate into any of the three currently established coronavirus groups (Marra *et al.*, 2003; Rota *et al.*, 2003). However, when ORF1b of the equine torovirus (EToV) was included in the analysis, the SCoV was distantly related to the group II coronaviruses (Snijder *et al.*, 2003).

Morphology

The name coronavirus refers to the corona-like appearance formed by the spike-like projections of the spike (S) glycoprotein on the surface of the virus (Davies and Macnaughton, 1979). These prominent surface projections of up to 20 nm in length cover the entire virion surface. However, TCV, has smaller spikes on the virion surface (Dea and Tijssen, 1988). Coronavirus virions are pleiomorphic, ranging from 80-160 nm

in diameter and are composed of four major structural proteins, the nucleocapsid (N) protein, the matrix (M) protein, the spike (S) protein and small envelope (E) protein. The N protein directly binds viral genomic RNA and forms a helical ribonucleoprotein complex (RNP) with a morphology similar to paramyxovirus (Davies *et al.*, 1981). In the case of TGEV, electron microscopic data suggest a possible icosahedral core shell structure comprising of the N, M and E proteins (Risco *et al.*, 1996). Certain strains of BCoV and MHV also have a hemagglutinin-esterase (HE) protein.

Genome organization

The genomes of the coronaviruses ranging from about 27.6 to 32 kilobases (kb) are the largest genomes of all the known RNA viruses. IBV and other coronaviruses have a positive stranded RNA genome that is transcribed into full-length negative stranded RNA after infection (Lai *et al.*, 1982). The purified genomic RNA is infectious and therefore can also function as an mRNA. The genomic RNA encodes the viral RNA-dependent RNA polymerase (Lomniczi, 1977; Schochetman *et al.*, 1977). In infected cells, depending on the virus, coronaviruses produce from five to seven subgenomic RNAs in addition to the genomic RNA (Lai *et al.*, 1982; Siddell, 1983; Stern and Kennedy, 1980a; Stern and Kennedy, 1980b). All RNAs are 3' polyadenylated and numbered according to their size. IBV has five subgenomic RNAs and the genomic RNA. They are numbered 1 through 6 based on size with the genome as RNA 1 (Fig. 1.1). The polyadenylated mRNAs form a 3' co-terminal nested set that extend for different lengths in the 5' direction (Leibowitz and Weiss, 1981; Stern and Kennedy, 1980a; Stern and Kennedy, 1980b). Genomic and subgenomic RNAs have 3' and 5'
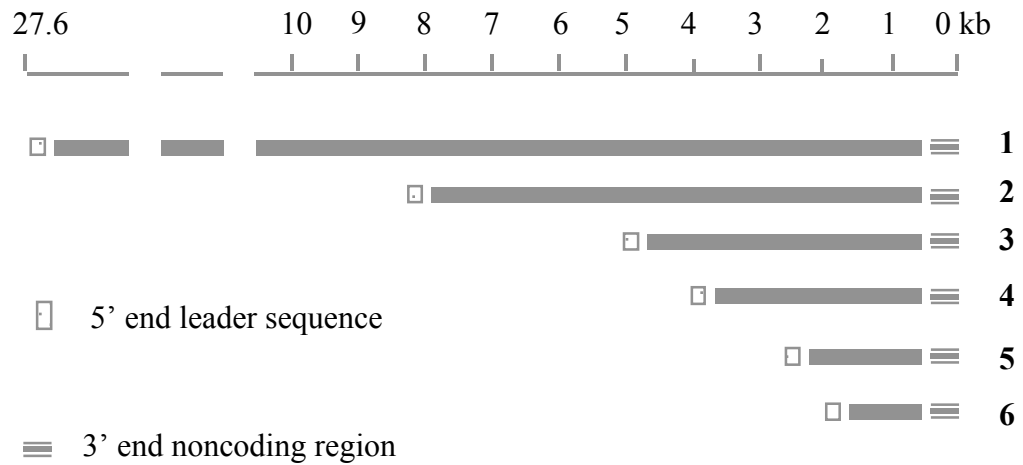
FIG. 1.1. IBV genomic and subgenomic RNA. RNAs 1-6 form a 3'co-terminal nested set. RNA 1 encodes proteins of the replicase complex, 2 encodes the spike protein, 3 encodes the 3a, 3b and E proteins, 4 encodes the M protein, 5 encodes the 5a and 5b proteins and 6 encodes the nucleocapsid protein.

untranslated (UTR) regions. These sequences are believed to function as *cis*-signal sequences for viral replication and transcription. For the various coronaviruses, the 5' end of each mRNA has about 60 to 72 nucleotides common to every RNA called the leader sequence (Lai *et al.*, 1983; Lai *et al.*, 1982; Spaan *et al.*, 1982). In the subgenomic RNA, following the leader sequence, most coronavirus ORFs are preceded by an untranslated region of various lengths that contain a conserved intergenic (IG) or transcription associated sequence (TAS).

The genome organization of IBV is similar to that of other prototype coronaviruses, such as MHV and TGEV, in having the "replicase gene-S-E-M-N" gene order together with small "nonstructural" proteins, such as 3a, b and 5a, b of IBV (thought to be group specific antigens), interspersed between the larger ORFs (Fig. 1.2). Due to its smaller genome size (27 kb) as compared to other coronaviruses (31 kb of MHV), the IBV genome is more efficient and compact. Some of the ORFs overlap with the previous or following ORF, for example, the 3' terminal end of 1b overlaps with the 5' end of the S ORF by about 50 nucleotides (Casais *et al.*, 2003).

IBV proteins

Polymerase: Approximately 70% of the coding potential of the IBV genome encodes the viral polymerase. Nucleotide sequencing has shown that mRNA 1 contains two large overlapping ORFs (1a and 1b), with ORF 1a having the potential to encode a polyprotein of 441 kilodaltons (kDa) (named polyprotein 1a) (Boursnell *et al.*, 1987). Translation of ORF 1b requires a ribosomal frame-shifting event at the 3'-end of ORF 1a, resulting in the synthesis of polyprotein 1ab (741 kDa) (Brierley *et al.*, 1987;
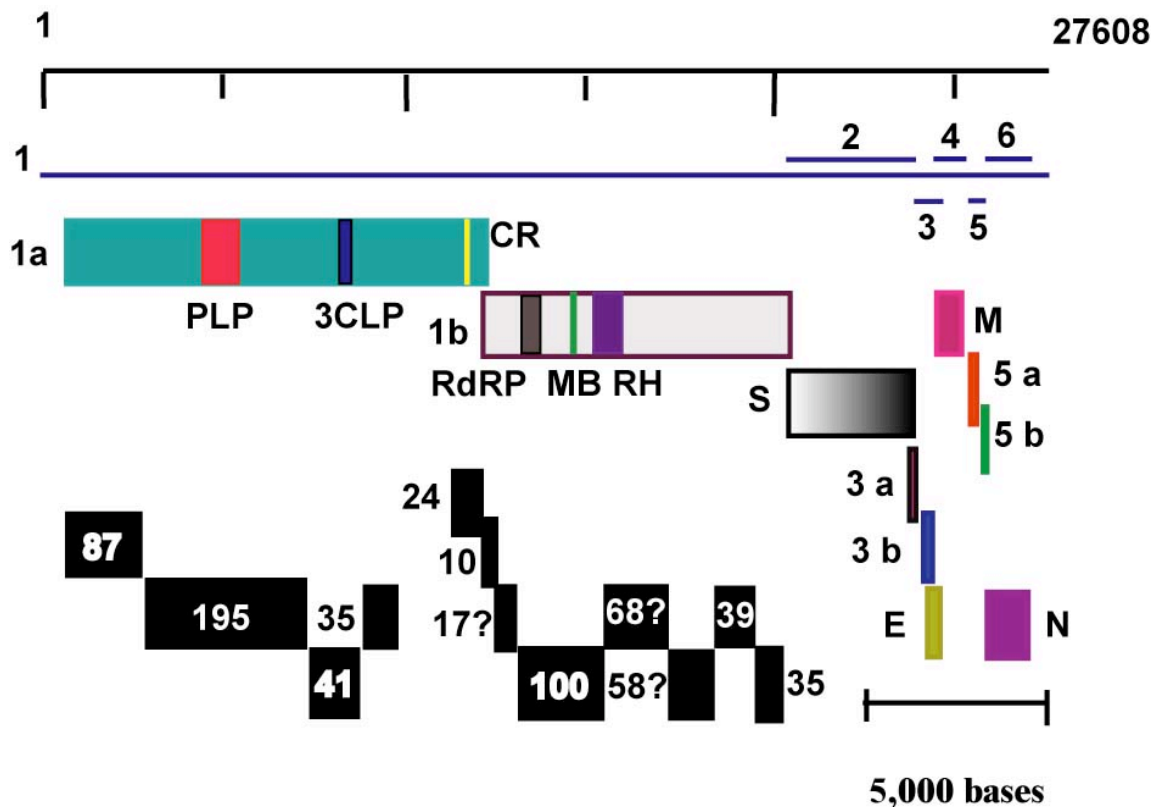
FIG. 1.2. Open reading frames of IBV. Genomic RNA (1) and ORFs (2-6) are represented by *blue* lines. Colored bars denote positions, relative to the RNAs and to each other, for the encoded polypeptides: 1a, 1b (replicase complex); S (spike glycoprotein); 3a, 3b, E (envelope); M (membrane glycoprotein); 5a, 5b and N (nucleocapsid protein). Functional domains indicated within the polypeptides 1a and 1b are: PLP (papain-like protease); 3CLP (3C-like protease); CR (cysteine-rich region); RdRP (RNA-dependent RNA polymerase; MB (metal binding domain) and RH (RNA helicase). Mature and putative (?) products of ORF 1a and ORF 1b are indicated in black with the numbers representing the approximate molecular mass in kilodaltons.

Brierley *et al.*, 1989). This mechanism has proven to be universal in the expression of ORF 1b in all coronaviruses studied so far (Liu *et al.*, 1994). Polyprotein 1ab is post-translationally cleaved by a virus-encoded papain-like proteinase (PLP) and a 3C-like proteinase (3CLP) to form 9 and 15 products in IBV (Fig. 1.2) and MHV respectively (Lim *et al.*, 2000; Liu *et al.*, 1997; Sims *et al.*, 2000). PLP is an accessory proteinase that cleaves polyprotein 1a and 3CLP is the main proteinase that cleaves polyprotein 1ab to give the mature polypeptides (Lim *et al.*, 2000; Liu *et al.*, 1994; Liu *et al.*, 1998; Liu *et al.*, 1997). Both proteinases are encoded by ORF 1a. Sequence analysis has identified four putative functional domains in ORF 1b, namely the RNA-dependent RNA polymerase (RdRP), the metal binding region (MB), the RNA helicase (RH) (Liu *et al.*, 1997) (Fig. 1.2) and a Cap-1 methyltransferase region found in the SCoV (von Grotthuss *et al.*, 2003). With the exception of the experimentally confirmed viral proteinases and the predicted polymerase proteins, the functions of the remaining mature gene 1 proteins have not been determined (Sims *et al.*, 2000). Sequence analysis has shown the presence of two PLP domains in MHV and HCoV, however only one such domain is present in IBV and SCoV (Snijder *et al.*, 2003; Ziebuhr *et al.*, 2000). Two RNA polymerase activities, one early and the other late in infection have been detected in MHV-infected cells. The early polymerase, but not the late polymerase, could be activated by potassium ions in the absence of magnesium ions and it also had a lower optimum pH than the late polymerase (Brayton *et al.*, 1982). Viral RNA in MHV-infected cells was detected in dense membrane fractions containing helicase, p28, and N but not in less dense membrane fractions containing p65 and p1a-22.   p28 and p65 are 28- and 65- kDa

amino-terminal cleavage products of ORF1a respectively, and p1a-22 is a 22-kDa-cleavage product of ORF1a at the C-terminal end. This demonstrates that the multiple gene 1 proteins segregate into two biochemically distinct but tightly associated membrane populations and only one of these sites appears to be the site for viral RNA synthesis (Sims *et al.*, 2000; Xu *et al.*, 2001).

Spike (S) glycoprotein: The spike protein, a type I glycoprotein is a determinant of cell tropism (Casais *et al.*, 2003; Popova and Zhang, 2002). By replacing the ectodomain of the spike gene of FIPV with that of MHV by targeted recombination, the species tropism of FIPV can be altered such that it now infects murine cells instead of feline cells (Haijema *et al.*, 2003). Similar to most coronaviruses, the IBV S glycoprotein (1,162 amino acids) is post-translationally cleaved into two subunits, S1 (535 amino acids; 90 kDa), comprising the N-terminal half of the S protein, and S2 (627 amino acids; 84 kDa), comprising the C-terminal half of the S protein. The S1 subunit contains the receptor-binding activity of the S protein (Casais *et al.*, 2003). The S2 subunit associates noncovalently with the S1 subunit and contains the transmembrane and C-terminal cytoplasmic domains. The ectodomain of the S2 subunit contains a fusion peptide-like region (Luo and Weiss, 1998) and two heptad repeats involved in oligomerization of the S protein (de Groot *et al.*, 1987). Binding of the MHV JHM strain S protein to soluble MHV receptor induces a conformational change in the membrane-anchored fragment of the S protein (Matsuyama and Taguchi, 2002). This activity is probably important in virus entry into the host cell. The S proteins of most coronaviruses are immunogenic and are immune targets for viral inhibition.

Membrane (M) protein: The membrane (M) protein, a type III integral membrane protein, is the most abundant glycoprotein in the viral envelope. It consists of a short amino-terminal ectodomain, three successive transmembrane domains, and a long carboxy-terminal domain on the inside of the virion (Fig. 1.3) (Siddell *et al*.; 1995). The 225-amino acid IBV M protein has a predicted molecular weight of approximately 25 kDa. However, the molecular weight in infected cells is approximately 30 kDa (Siddell *et al*.; 1995). Depending on the coronavirus, the M protein may have O or N linked glycosylation. MHV M protein has O-linked glycosylation and targets to the *trans*-Golgi apparatus (Locker *et al.*, 1995; Niemann and Klenk, 1981; Sturman and Holmes, 1977). However, IBV M has N-linked glycosylation (Cavanagh, 1983; Locker *et al.*, 1992) and targets to the *cis*-Golgi (Machamer *et al.*, 1990).

Small envelope (E) protein: The E protein is a minor but essential component of the virion. It was only recently recognized as a structural protein. The IBV E protein is composed of 108 amino acids with a predicted molecular mass of approximately 10 kDa. In contrast to other viral structural proteins, the coronavirus E protein is expressed by a cap-independent translation mechanism that uses the internal ribosome entry site (IRES) located between ORFs 3a and 3b in the IBV genome and in the 5a region in the MHV genome (Liu and Inglis, 1992; Thiel and Siddell, 1994). The E protein is present in minute amounts in the virus envelope (Liu and Inglis, 1991; Raamsman *et al.*, 2000).

The putative peripheral domain of the E protein interacts with the M protein thereby retaining the M protein in the pre-golgi compartment where the virus buds
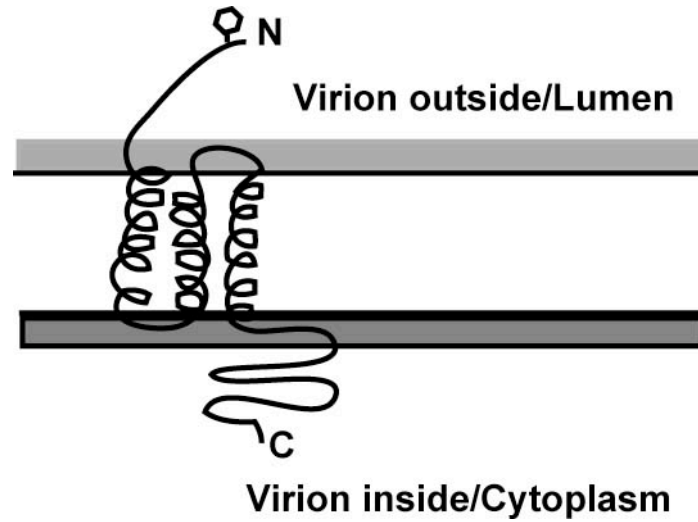
FIG. 1.3. IBV membrane (M) protein. It is a triple membrane spanning protein with the N-terminal end on the outside of the virion and the long C-terminal end in the inside of the virion. The potential N-linked glycosylation site is marked by a hexagon. (Adapted from Siddell *et al*., 1995)

(Lim *et al.*, 2001). Corse and Machamer (2000) have shown that the E protein localizes to the golgi and then interacts with the M protein via the C-terminal tail (Corse and Machamer, 2000; Corse and Machamer, 2002; Corse and Machamer, 2003). The E and M proteins alone can form virus-like particles (i.e. particles that lack any nucleocapsid though resemble the virus in shape and size) when co-expressed in Ver*o* cells (Baudoux *et al.*, 1998; Corse and Machamer, 2000). The E:M stoichiometry in the VLPs have not been determined. Besides the cytoplasmic tail of the E protein, the transmembrane domain may also be important in interacting with the M protein in virus assembly (Corse and Machamer, 2003). The S protein co-localizes with the M protein in the Golgi and is incorporated into virus-like particles when co-expressed with the M and E proteins. S is however dispensable for formation of virus-like particles (Corse and Machamer, 2000; de Haan *et al.*, 1998; Nguyen and Hogue, 1997; Vennema *et al.*, 1996). Since E is present in the particles in very small amounts, interactions between M proteins apparently generate the major driving force for envelope formation. The M protein molecules interact with each other through multiple contact sites, particularly within the lipid envelope (de Haan *et al.*, 2000).

Hemagglutinin esterase (HE) protein: HE, an N-linked glycoprotein is present only in BCoV, TCV, HCoV, and some strains of MHV but is absent in IBV, SCoV and TGEV. This glycoprotein shares some sequence homology with the hemagglutinin protein of influenza C virus and the gene is proposed to be derived from influenza virus by non-homologous recombination. The HE protein of BCoV and some strains of MHV exhibit hemagglutination and esterase activity. Monoclonal antibodies specific for the

HE protein of BCoV can inhibit virus-induced hemagglutination and neutralize viral infectivity implying that at least in BCoV, HE plays a role with S in viral attachment (Snijder *et al.*, 2003).

Nucleocapsid (N) protein: The nucleocapsid (N) protein is the only protein known to be phosphorylated in MHV, TGEV, IBV and HCoV (Siddell, 1995). IBV N protein is 409 amino acids long (approximately 48 kDa). It is a basic protein rich in lysine (39 residues) and arginine (34 residues) amino acids, with a predicted isoelectric point of 9.69. The IBV N protein has thirty-three serine, eighteen threonine, and eight tyrosine residues, any of which could be potential sites for phosphorylation (Table 1.1). MHV N is found in the cytosol of infected cells as well as being associated with cellular membranes. IBV N protein localizes to the nucleolus in the absence of other viral proteins as well as in the virus-infected cell. TGEV and MHV N also localize to the nucleolus in the absence of other viral proteins, though not in the virus-infected cell as 90 % of the infected cells do not have detectable N in the nucleolus (Hiscox *et al.*, 2001; Wurm *et al.*, 2001). IBV N protein has many arginine and lysine residues but lacks any domain characteristic of known RNA binding proteins (Williams, 1993). The N protein is multifunctional. It has been implicated in playing a role in genome replication, transcription of subgenomic RNA, translation and in formation of the nucleocapsid (Masters *et al.*, 1990; Masters and Sturman, 1990; Tahara *et al.*, 1998). It interacts with the cellular heterogenous ribonuclear protein A1 *in vivo* and *in vitro* (Wang and Zhang, 1999). It has been proposed that phosphorylation might regulate the multifunctionality of

Table 1.1.

Physicochemical properties of the IBV N protein

Characterisitc	
Molecular weight	~ 48 kDa
Predicted isoelectric point	9.69
Actual isoelectric point	unknown
Number of serine residues	33
Number of threonine residues	18
Number of tyrosine residues	8
Number of lysine residues	39
Number of arginine residues	34

the protein (Masters and Sturman, 1990). In MHV, a protein kinase activity was found associated with purified virus preparations of MHV indicating the presence of a kinase in the virion (Siddell *et al.*, 1981).

IBV life cycle

Coronaviruses are host-specific. The virion binds to the cell membrane receptors by either the S glycoprotein, or by sequential binding of HE followed by binding of S. Conformational changes either in the S protein or the receptor or both, may be induced by virus binding and lead to fusion of the viral envelope with host cell membranes. MHV-A59-induced fusion is optimal at neutral or mildly alkaline pH. For HCoV-229E, IBV and some MHV variants, fusion does not occur at neutral pH and the virus envelope may fuse with the endosomal membrane rather than the plasma membrane (Gallagher, 1997; Sturman *et al.*, 1990). In some of the coronaviruses, binding of the spike protein to the receptor causes the cleavage or maturation of the spike protein (Siddell, 1995). The receptor for some of the coronaviruses has been identified. The MHV receptor (MHVR) belongs to the carcinoembryonic antigen (CEA) related glycoprotein in the biliary glycoprotein subgroup (Dveksler *et al.*, 1993; Dveksler *et al.*, 1991). Both TGEV and HCV-229E utilize amino peptidase (APN) glycoproteins as receptors (Siddell, 1995). SCoV uses angiotensin-converting enzyme 2, a metallopeptidase, as the receptor (Li *et al.*, 2003).

Coronaviruses replicate in the cytoplasm. Following uncoating to release the nucleocapsid, coronaviruses express the largest known replicase polyproteins (741 kDa), which in turn are proteolytically processed to yield a large number of mature proteins,

including the RNA-dependent RNA polymerase (Fig. 1.2). During infection, virion RNA is initially copied by an early (detected 1 hour post-infection) polymerase activity into a genome-sized negative stranded RNA (Brayton *et al.*, 1982). The negative stranded RNA is transcribed by a late (detected 6 hours post-infection) polymerase activity into a full-length genomic RNA that is bound to polysomes and detected in EDTA resistant forms. Maximum virus production occurs at approximately 13 hours post-infection (Brayton *et al.*, 1982). Fractionation of the membranes by sucrose gradient sedimentation showed that the early polymerase activity was homogeneous, while the late polymerase was associated with two distinct membrane fractions. The light peak of the late polymerase synthesized genomic-sized RNA of positive sense, while the heavy peak of the activity synthesized positive-sensed genomic and subgenomic mRNAs. These findings suggest that the light peak of the late polymerase represents a replication complex while the heavy peak represents a transcription complex (Brayton *et al.*, 1984).

Processes that lead to the formation of the mature virus are membrane associated. Besides the polymerase, other viral proteins are synthesized from the subgenomic RNA. The subgenomic RNAs are created by some type of discontinuous synthesis, rather than by splicing of a genomic precursor (Siddell, 1995). At least one stage of their synthesis requires base-pairing interactions between the positive strand of the leader and the negative strand of the intergenic sequence (IGS) or transcription associated sequence (TAS). The exact nature of the discontinuous leader-body fusion step, whether it occurs during positive strand or negative strand synthesis, and the significance of the negative-

strand counterparts of the subgenomic RNAs are all matters of controversy (Jeong and Makino, 1992; Sawicki and Sawicki, 1990; Sethna *et al.*, 1989).

The discovery of subgenomic negative strands has led to two different models for coronavirus transcription based on the nature of the template(s) for mRNA synthesis. The first model is a leader-primed transcription model (Fig. 1.4A). According to this model, discontinuous transcription occurs during positive stranded RNA synthesis. Leader RNAs are transcribed from one end of the negative stranded RNA template. The leader RNA then dissociates from the template, and subsequently binds to any IGS or TAS on the negative stranded template. This serves as the primer for subgenomic RNA transcription, resulting in subgenomic positive strand RNA synthesis that contains a leader RNA fused to the body RNA. This model is based on the presence of genome-length replicative intermediates (RIs) (the double-stranded structure that "produces" RNA is designated the RI) in MHV-infected cells and of free leader RNAs in infected cells (Baric *et al.*, 1983; Baric *et al.*, 1985). Visualization of double-stranded RNAs by gel electrophoresis and fluorography usually involves digestion of the excess single-stranded RNA by RNase A. The remaining double-stranded RNase-resistant molecules are referred to as the replicative forms (RFs). The RFs do not always correspond to the RIs because the RIs could have been digested at certain RNase-sensitive sites to yield smaller RFs. Several small leader sequence-related RNA species have been detected in the cytoplasm of MHV-infected cells (Baric *et al.*, 1985) These leader RNAs are distinct in size and reproducible in different cell types. However, most of these leader RNAs are either larger or smaller than the leader sequence present at the 5' end of the mRNAs
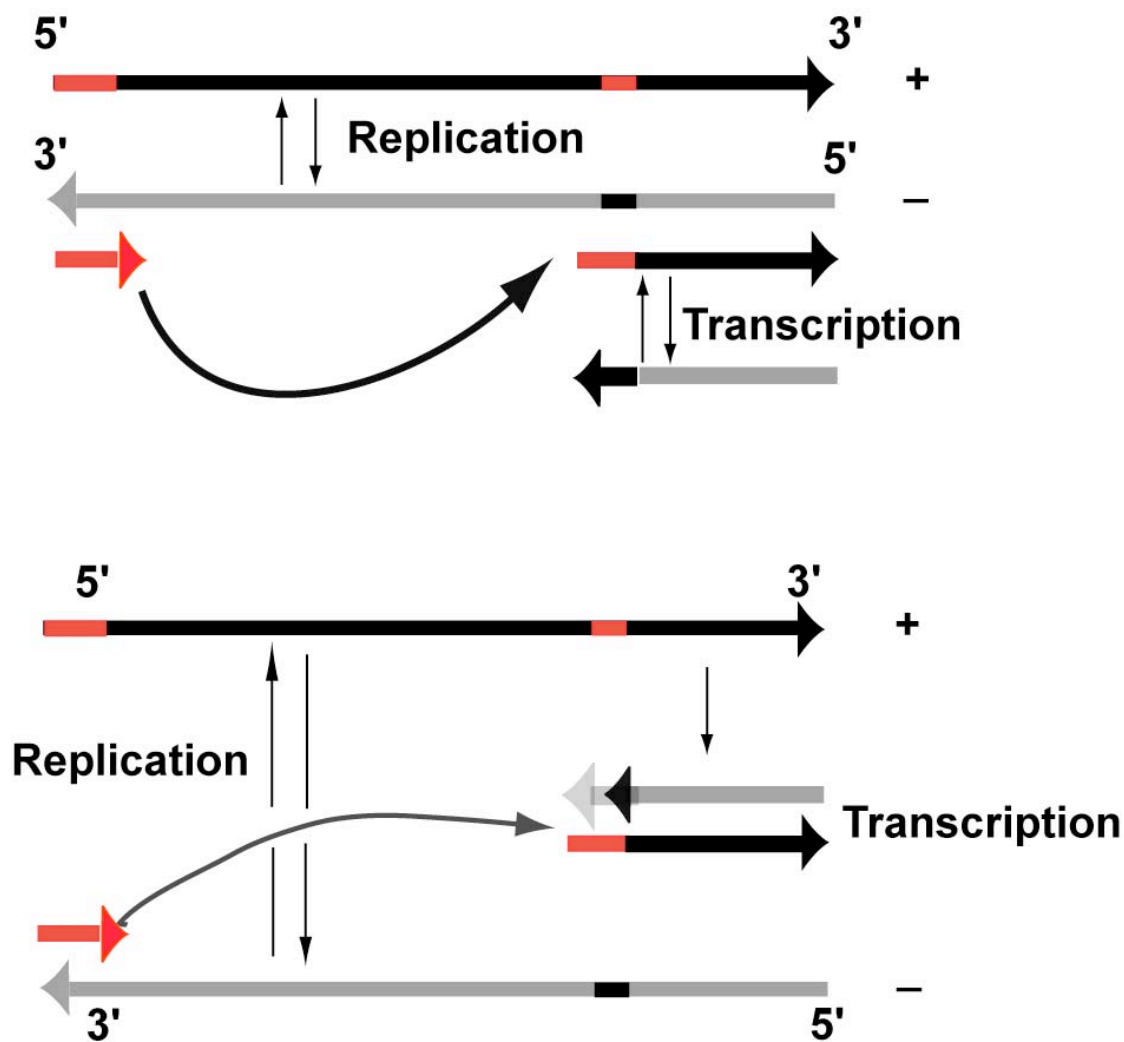
FIG. 1.4. Schematic representation of two transcription models. Plus- and minus-strands are represented by black and gray arrows respectively. On the plus-strand, the leader sequence and intergenic region are indicated in red; on the minus-strand, the intergenic sequence is shown in black. The two models differ in that the template for the subgenomic mRNAs is different. (A) A genomic minus-strand is the template for subgenomic mRNA synthesis. The subgenomic mRNAs are first synthesized by leader-primed transcription and are then amplified. (B) Subgenomic minus-strands are synthesized by premature termination of transcription and serve as templates for leader-primed transcription.

implying that additional processing of these leader RNAs may occur during mRNA transcription. Temperature-sensitive (ts) mutants have been isolated that synthesize only the small leader-related RNAs but not mRNAs at the non-permissive temperature (Baric *et al.*, 1985). Thus it is possible that the synthesis of the leader RNA and mRNAs are two separate and discontinuous events. *In vivo* and *in vitro* studies support this model. When cells with different strains of MHV were co-infected or exogenous leader RNA was introduced into virus infected cells, leader sequence from different strains of MHV or the exogenous leader RNA was incorporated *in trans* into subgenomic mRNAs at precisely the leader-mRNA junction sites (Baker and Lai, 1990). This process is called leader switching and is also observed in IBV (Stirrups *et al.*, 2000).

The second model is a discontinuous transcription model. A discontinuous transcription step potentially occurs during negative strand RNA synthesis (Fig. 1.4B). During negative strand RNA synthesis from the full-length genomic RNA template, the RNA dependent RNA polymerase (RdRp) pauses at one of the IG or TAS sequences and then jumps to the 3' end of the leader sequence at the 5' end of the genomic RNA template, generating a subgenomic negative stranded RNA with an antisense leader sequence at its' 3' end. This subgenomic negative stranded RNA then serves as a template for synthesis of mRNAs. Several studies have shown that both genomic and subgenomic sized negative stranded RNAs are present even though positive stranded RNA are present at higher levels (Baric and Yount, 2000; Sawicki and Sawicki, 1990; Schaad and Baric, 1994; Sethna *et al.*, 1991). Schaad and Baric (1994) have shown that, at least late in infection, the subgenomic negative-strand RNAs were the functional

templates for subgenomic mRNA synthesis. All the negative stranded RNAs were in double-stranded form and no free negative stranded RNA was detected.

Defective interfering (DI) particles of viruses typically accumulate in stocks of virus that are passaged serially at high multiplicity or they can be assembled by genetic manipulation of the parent virus. The following are the defects of DI particles: (a) they have defects (either point mutations or deletions) in essential genes, (b) they interfere with the growth of the parent or helper virus and (c) they enrich themselves at the expense of the parents or helper virus (Lai and Holmes, 2001). Since infectious cDNA clones of coronaviruses have only recently become available, either naturally occurring or artificially constructed DI RNA of bovine coronavirus and mouse hepatitis virus have been used to identify five putative UTR-localized, *cis*-acting replication elements. Four of these elements within the 3'-UTR are phylogenetically conserved in various coronaviruses. They include the 3'-terminal poly (A) tail (Spagnolo and Hogue, 2000), a long range stem interaction between nt 65 to 71 and 124 to 130 from the base of the poly (A) tail in BCoV (nt 68 through 74 and 136 through 142 in MHV-JHM) (Liu *et al.*, 2001), a hairpin-type pseudoknot consisting of nt 173 through 226 in BCoV (nt 185 through 238 in MHV A59) (Williams *et al.*, 1999), and a 5'- proximal extended bulged stem-loop consisting of nt 222 through 289 in BCoV (nt 234 through 301 in MHV-A59) mapping immediately downstream of the N gene stop codon and overlapping the pseudoknot by 5 nt (Hsue *et al.*, 2000; Hsue and Masters, 1997). A 65 nt leader, comprising an identified stem-loop I and part of an identified stem-loop II has been shown to function in BCoV DI replication (Chang *et al.*, 1994). Stem loop III in the 5'

UTR of BCoV has been shown to function as a *cis*-acting element for DI RNA replication. An ORF associated with this stem-loop region may function to enhance replication. It is postulated that these two elements function similarly in the virus genome (Raman *et al.*, 2003). There is evidence to suggest that coronavirus transcription involves interaction between leader mRNA and the intergenic (IG) sequences, probably via RNA-protein interactions (Zhang and Lai, 1994). The 5'-terminal 544 nucleotides (nt) and 3'-terminal 338 nt contain the necessary signals for IBV DI RNA replication. Phylogenetic analysis of 19 strains of IBV and 3 strains of turkey coronavirus predicted a conserved stem-loop structure at the 5' end of region II of the 3' UTR. Removal of the predicted stem-loop structure abolished replication of the DI-RNAs (Dalton *et al.*, 2001).

Various cellular proteins are known to bind to the coronavirus *cis*-acting RNA regulatory elements (Furuya and Lai, 1993). These include polypyrimidine-tract-binding protein (PTB) (Li *et al.*, 1999), heterogenous ribonucleoprotein (hnRNP) A1 (Li *et al.*, 1997), mitochondrial aconitase (Nanda and Leibowitz, 2001), poly (A)-binding protein (PABP) (Spagnolo and Hogue, 2000), and several other unidentified proteins. HnRNP-A1 binds *in vitro* to probe RNAs containing negative-sense strand of MHV IGS (Li *et al.*, 1997; Zhang and Lai, 1995). Although coronavirus RNA has not been shown to enter the nucleolus, the N-protein of MHV has been shown to interact with cellular hnRNP A1, a protein that has been shown to participate in alternative splicing in the nucleus, mRNA export from the nucleus to the cytoplasm, and telomere biogenesis and maintenance. hnRNP A1-N protein interaction has been shown *in vitro* and *in vivo* using the yeast two-hybrid system and by immunoprecipitation from MHV-infected cells. The

interaction between these proteins may be important in regulating RNA transcription (Wang and Zhang, 1999). hnRNP A1 and PTB bind to complementary sequences at the 5' end of MHV RNA and together mediate the formation of an RNP complex involving the 5'- and 3'-end fragments of MHV RNA *in vitro*. DI RNAs containing a mutated hnRNAP A1-binding site have lower RNA transcription and replication activities. These results and the finding that hnRNP A1 binds to the 3'-UTR is compatible with the interpretation of the authors that hnRNP A1 mediates potential 5'-3'-end cross talk of MHV RNA (Huang and Lai, 2001). Contradictory evidence exists to show that this protein regulates MHV RNA synthesis (Shi *et al.*, 2000), and also that it is not necessary for MHV replication. The absence of hnRNP-A1 has no detectable quantitative or qualitative effect on MHV RNA synthesis (Shen and Masters, 2001). Work done by Nanda *et al.* (2001) suggests that binding of mitochondrial aconitase to the MHV 3'-UTR substantially increases the production of infectious virus and the expression of MHV proteins during the early stages of infection (Nanda and Leibowitz, 2001).

A packaging signal sequence within ORF 1b for MHV and BCoV and within the 5' 649 nucleotides of the genome for TGEV confers packaging ability to non-viral RNA (Cologna and Hogue, 2000; Escors *et al.*, 2003; Fosmire *et al.*, 1992). The IBV packaging signal sequence has not yet been identified although a similar sequence can be found in its 1b ORF as in MHV and BCoV. RNA-independent interaction between MHV M and N proteins occurs in MHV infected cells (Narayanan *et al.*, 2000). Co-expression of MHV M and E proteins and RNA containing the MHV packaging signal sequence results in the production of VLPs containing the RNA transcripts; the N and S

proteins are indispensable for this process (Narayanan *et al.*, 2003a; Narayanan and Makino, 2001). Nucleocapsid independent-assembly of VLPs is possible by co-expressing the M and E proteins from transfected plasmids. A combination of M-M, M-N, M-RNA, N-RNA interactions are all likely to be important in specifically packaging the viral genome (Vennema *et al.*, 1996).

A critical part of viral morphogenesis is the assembly of the helical nucleocapsid, made up of the viral RNA and the N protein (Spaan *et al.*, 1981; Stohlman *et al.*, 1983). The order of events leading to virion formation is not known. It is not known if the nucleocapsid is preformed in the cytoplasm and rapidly transported to the membranes where assembly occurs or whether it is assembled in association with cellular membranes. The nucleocapsid associates with smooth membranes belonging to the endoplasmic reticulum-Golgi intermediate compartment (ERGIC) that constitutes the "budding compartment" for coronaviruses (Krijnse-Locker *et al.*, 1994). Two types of virus-related particles are found during coronavirus morphogenesis. The virus that is assembled and found near the perinuclear region is larger than the virus that is finally released from the cell. The virus that is released from the cell is formed as a result of maturation by passing through the Golgi and emerging from the *trans*-Golgi network (Risco *et al.*, 1998; Salanueva *et al.*, 1999).

RNA-PROTEIN INTERACTIONS

Introduction

Specific interactions between RNA and proteins are fundamental to many

cellular processes including the assembly and function of ribonucleoprotein particles (RNPs), such as ribosomes and spliceosomes and the post-transcriptional regulation of gene expression (Draper, 1995). These interactions are also important in DNA and RNA viruses. Motifs characteristic of RNA and DNA binding proteins have been identified in several proteins. Multiple copies of ribonucleoprotein (RNP) motifs have been identified in heterogenous nuclear RNP (hnRNP) and in yeast poly (A) binding protein (Sachs *et al.*, 1986; Adams *et al.*, 1996). Although these domains may bind RNA/DNA non-specifically, they typically bind their natural sequences with greater affinity. An arginine-rich motif present in the carboxyl terminus of the HIV tat protein binds to a small hairpin of the HIV TAR RNA (Calnan *et al.*, 1991). Closely spaced Arg-Gly-Gly (RGG) box and KH motifs have been found to interact with RNA sequences (Burd and Dreyfuss, 1994). Zinc-finger motifs have been identified in a number of proteins as associated with nucleic acid interactions (Draper, 1995). Zinc-fingers of TFIIA, which are repeats of $CX_4CX_{12}HX_3$-4H, interact with 5S RNA and the same sequences in duplex DNA (McCall *et al.*, 1986). The RNA recognition motif 2 (RRM 2) of guanine-rich sequence factor-1 (GRSF-1) is required for regulating translation of viral RNA. Cellular and viral mRNAs containing 5' UTR GRSF-1 binding sites are recruited by GRSF-1 to polyribosomes. This recruitment is mediated through interactions with cellular proteins (Kash *et al.*, 2002). The KH domains of *Xenopus* Vg1 RNA binding protein (Vg1RBP) mediate RNA binding and self-association (Git and Standart, 2002).

RNA motifs

Several RNA motifs, important in RNA folding, in RNA-RNA interactions and in RNA-protein interactions have been identified: terminal loop motifs, internal loop motifs, and tertiary motifs. U-turns and tetraloops are terminal loop motifs of stem loops; Internal loops may be classified as cross-strand purine stacks, bulged-G motifs, A-platforms, bulge-helix-bulge motif and/or metal binding motifs; RNA tertiary structural motifs include the ribose zipper and the tetraloop-helix interactions. The coaxial stack and the pseudoknot also contribute to RNA tertiary structure (Moore, 1999). The most frequently occurring and better-studied tetraloop sequences are the cUNCGg, the cGNRAg, and the gCUUGc sequences. The uCACGg tetraloop occurs naturally within the cloverleaf RNA structure of the 5'-UTR of coxsackievirus B3. The cloverleaf structure is the main determinant for interaction with the viral 3C protease, which is a component of the RNP complex that is involved in regulating viral RNA replication and translation (Du *et al.*, 2003). The central domain of the foot-and-mouth disease (FMDV) IRES contains a conserved GNRA motif, essential for IRES activity. Mutants bearing the UNCG or GUAG tetraloops instead of the GNRA tetraloop revealed lack of protection to chemical attack in native RNA at specific nucleotides relative to the parental GUAA, suggesting that the GNRA motif dictates the organization and stability of the central domain of the IRES. This suggests that the GNRA motif plays a crucial role in the organization of IRES structure with important consequences on activity (Fernandez-Miragall and Martinez-Salas, 2003). The CUUG tetraloop is commonly found in bacterial 16S rRNA (Baumruk *et al.*, 2001). Bacterial ribosomal protein L5

specifically interacts with the bulged nucleotides at the top of loop C of 5S rRNA. The rRNA and protein contact surfaces are strongly stabilized by intramolecular interactions. Charged and polar atoms forming the network of conserved intermolecular hydrogen bonds are located in two narrow planar parallel layers belonging to the protein and rRNA, respectively. The regions, including these atoms in the RNA and the protein, conserved in bacteria and archaea, can be considered an RNA-protein recognition module (Perederina *et al.*, 2002). The internal loop/bulge and hairpin loop of the iron-responsive element of ferritin mRNA, contribute to maximal iron regulatory protein 2 binding and translational regulation in the iso-iron-responsive element/iso-iron regulatory protein family (Ke *et al.*, 2000). RNA elements that bind cellular proteins have been used as a decoy to regulate mRNA transcription and translation (Coulis *et al.*, 2000; Garcia-Gras *et al.*, 2000). The 5' UTR of turnip yellow mosaic virus (TYMV) contains two conserved hairpins with internal loops consisting of C-C and C-A mismatches. Packaging occurs at a pH below N1 pKa of cytosine, and the hydrogen bond arising there from permits a C-C or C-A mismatch, the presence of the latter being proven by mutagenesis. It has been suggested that this RNA-protein interaction is a new type of interaction that is accompanied by base pairing of protonatable bases under acidic conditions (Bink *et al.*, 2002). Both sequence specific and nonspecific interactions between the *Escherichia coli* DEAD protein DbpA and the small RNA hairpin in 23S rRNA are required for activation of the ATPase activity of the DEAD protein (Tsu *et al.*, 2001). Translation initiation factors such as eIF3, eIF4B, and eIF4G bind to the internal

ribosome entry site (IRES) of certain viruses and some of these interactions affect translation efficiencies (Lopez de Quinto *et al.*, 2001).

Purine-rich sequences

Certain purine-rich regions are important in RNA-protein interactions. Replication of human immunodeficiency virus requires Tat protein which activates elongation of RNA polymerase II transcription at the HIV-1 promoter through interaction with the cyclin T1 (CycT1) subunit of the positive transcription elongation factor complex (P-TEF) and the TAR RNA element. CycT1 does not bind TAR RNA in the absence of Tat, and Tat binding to TAR, while detectable, is very inefficient in the absence of CycT1. It is conceivable that the CycT1-Tat heterodimer directly binds to TAR RNA in the U-rich RNA bulge region and this binding facilitates the interactions of the CycT1-Tat heterodimer to the O6 and N7 functional groups at nucleotide positions 32 and 34 in the RNA loop region (Richter *et al.*, 2002). Heterogeneous ribonucleoprotein C1 and C2 (hnRNP-C1/C2) bind U tracts. Using the yeast-three hybrid system, Koloteva-Levine *et al.* have shown that hnRNP-C1 and -C2 binding to U tracts is sequence dependent (Koloteva-Levine *et al.*, 2002). The 3' UTR of the mouse Cas-1 mRNA, encoding the antioxidant enzyme catalase, has a U-rich motif that is conserved across species. This motif is an active site for complex and dynamic interactions involving RNA-binding proteins. Proteins that bind to this motif have been identified. One protein had a motif similar to the RNA recognition motif (RRM) protein superfamily, implicated in splicing, stability, localization, and translation of RNAs (Song and Singh, 2001). A cellular protein p36, identified as glyceraldehyde 3-

phosphate dehydrogenase binds hepatitis delta virus (HDV) anti-genomic RNA. RNase footprinting indicated that the UC-rich domain between nucleotides 379 and 414 of the HDV antigenomic RNA was involved in the GAPDH binding (Lin *et al.*, 2000). Insulin like growth factor-1 (IGF-1) mRNA stability may be mediated by binding of certain cytoplasmic proteins to the adenosine-uridine rich elements (AURE's) present in the 3' untranslated region (Hou *et al.*, 2000). Uridine-rich sequences have also been identified as protein binding sites for poly (A) polymerase from vaccinia virus (Deng and Gershon, 1997; Johnson and Gershon, 1999). AU-Rich elements in the 3' untranslated region of epidermal growth factor receptor mRNA confer stability to the RNA, probably by binding to proteins that stabilize the mRNA. These proteins are cellular proteins identified by gel shift assays. The proteins bound only one of the AU-rich elements present in the 3-cis acting element (Balmer *et al.*, 2001). RNA-protein interactions are also important in regulating the turnover rate of mRNA (Alterio *et al.*, 2001). Bamboo mosaic potexvirus satellite RNA (satBaMV RNA)-encoded P20 protein preferentially binds to satBaMV RNA, primarily to the 5' and 3' –UTR's. Binding is competed out by poly (U) and poly (G) sequences (Tsai *et al.*, 1999).

Specificity of RNA binding

RNA sequence specificity for RNA binding proteins is critical for splice site selection in RNA processing (Singh, 2002). Sequence specificity is exhibited in nucleocapsid protein binding to viral RNA elements for packaging the viral genome (Paoletti *et al.*, 2002). Binding of *E. coli* glutaminyl-tRNA synthetase to its cognate tRNA is a very specific interaction. In general, binding of the tRNA synthetase to the

3'end, requires certain identity determinants, such as base pairs in the acceptor stem and the bases in the anti-codon loop, that contribute to specific interaction between the synthetase and the tRNA leading to correct charging of the tRNA (Steitz *et al.*, 1990).

Tertiary structure of RNA

Besides sequence specificity and secondary structure of the RNA, the steric organization of bases is also important in RNA-protein interactions. The U73 binding site for cysteine-tRNA synthetase is sterically optimized to accommodate a 2'-OH group in the backbone, but the hydroxyl group itself is not involved in specific hydrogen bonding interactions (Hou *et al.*, 2001). An aptamer based on glutamine tRNA in which the five-nucleotide variable loop sequence 5'-44CAUUC48-3' is replaced by 5'-44AGGU48-3' bound glutaminyl-tRNA synthetase with a 30-fold improved affinity as compared to the wild type tRNA. This suggests that enhanced protein binding to a mutant globular RNA can arise from stabilization of RNA tertiary interactions rather than optimization of RNA-protein contacts (Bullock *et al.*, 2000).

OBJECTIVES

As a highly conserved protein, the N protein has been associated with multiple functions in the viral replication cycle and is also a convenient diagnostic tool. It is not known if phosphorylation can regulate the multiple functions of the N protein. Hence the objectives of this study are:

A) To determine the phosphorylation status of the IBV N protein in infected cell lysates and virion particles.

B) To determine the ability of IBV N protein to form nucleocapsid-like structures in the absence of other viral proteins.

C) To determine the significance of uridylates in N binding to viral RNA.

D) To develop a rapid ELISA technique using IBV recombinant N protein for detecting IBV antibody in chickens.

CHAPTER II

PHOSPHORYLATION OF THE IBV N PROTEIN

INTRODUCTION

Infectious bronchitis virus (IBV) is a prototype of the *Coronaviridae* family (Collisson *et al*., 1992; Siddell *et al*., 1983). Coronaviruses are positive stranded RNA viruses that primarily cause respiratory and enteric infections in a broad range of species. Infection with IBV causes a highly contagious, respiratory disease in chickens with a high mortality in young chicks. It also affects the genital and urinary systems (Alexander *et al*., 1978; Crinion and Hofstad, 1972).

IBV has four structural proteins: membrane (M), spike (S), nucleocapsid (N) and the small membrane (E) proteins. IBV N protein, 409 amino acids long, as that of other coronaviruses is a basic, phosphorylated structural protein, that is highly conserved from amino acid residues 238 to 293 (Hogue, 1995; Hogue and Brian, 1986; Wilbur *et al*., 1986; Williams *et al*., 1992). The N protein directly binds viral genomic RNA and forms a helical ribonucleoprotein complex (RNP) (Davies *et al.*, 1981). It has been implicated in playing a role in genome replication, transcription of subgenomic RNA, translation and in formation of the nucleocapsid (Masters *et al.*, 1990; Masters and Sturman, 1990; Tahara *et al.*, 1998).

MHV N protein is the major protein synthesized almost four to five hours post-infection in Sac (-) cells infected at a high multiplicity of infection (M.O.I.) (Siddell *et*

al., 1980). In MHV, a 57 kilodaton (kDa) (p57) non-phosphorylated form is the precursor to the 60 kDa (p60) phosphorylated form of the protein. p57 is present only in the cytosol whereas, p60 is found associated with membranes as well (Anderson and Wong, 1993). Anderson and Wong (1993) showed that single-stranded RNA and DNA inhibit membrane binding of the N protein (Anderson and Wong, 1993).

Phosphorylation of coronavirus N protein

Two plaque morphology variants of JHM (strain of MHV), named DL and DS, with minor differences in their RNA nucleotide fingerprints but with distinct neurovirulence for mice, have been identified. Only two of the twenty-two serine-containing tryptic peptides were found to be phosphorylated (Wilbur *et al.*, 1986). In the case of MHV, no differences in the tryptic peptide maps of the N-protein purified from the virion, the infected cytosol and the infected cellular membranes were detected (Wilbur *et al.*, 1986). While two phosphorylated forms of the N-protein, 50 kDa and 55 kDa, were detected in BCoV infected cells, only the 50 kDa form was detected in the virion. Although the 55 kDa form was susceptible to calf intestinal alkaline phosphatase (CIAP) treatment, the 50 kDa form was not susceptible to CIAP treatment (Hogue, 1995; King and Brian, 1982).

The IBV N protein has been shown to be phosphorylated in infected cells (Lomniczi and Morser, 1981). We show here that both the cellular and virion N proteins are phosphorylated. It has been proposed that phosphorylation might regulate the multifunctionality of the N protein (Masters and Sturman, 1990). We performed some studies to determine the kinetics of phosphorylation and the variation in phosphorylation

between the cellular and virion N proteins. Our work shows that IBV N is phosphorylated at all times during infection. Our results suggest hat the IBV virion N protein is more phosphorylated than the N protein present in infected cells.

MATERIALS AND METHODS

Virus and cells

The infectious bronchitis virus Beaudette strain, used for all experiments in this study was propagated on Vero and chicken embryo kidney (CEK) cells in Dulbecco's modified Eagle's medium (DMEM) containing 10% fetal bovine serum (FBS) or 10% chicken serum respectively. Virus infections were carried out with DMEM containing 2% serum.

Phosphate labeling of *E.coli* during expression of recombinant IBV N protein

An overnight culture of *E.coli* containing the recombinant IBV N gene expression construct was grown at 37°C in Tris-glucose medium (120 mM Tris-Cl, 80 mM NaCl, 20 mM KCl, 20 mM NH_4Cl, 3 mM Na_2SO_4, 0.2 mM $CaCl_2$, 2 nM $FeCl_3$ and 20% glucose) containing 100 mM phosphate and 25 µg/ml kanamycin and 50 µg/ml ampicillin. This culture was added to fresh Tris-glucose medium (without phosphate and with the above mentioned antibiotics) to bring it to an optical density of 0.5. The bacteria were cultured at 37°C on a shaker at 200 rpm for three hours. Protein expression was induced with isopropyl-β-D-thiogalactopyranoside (IPTG) at a final concentration of 2 mM. The bacteria were cultured for another five hours at 37°C on a shaker at 200 rpm in the presence of 100 µCi/ml ^{32}P-orthophosphate and the bacteria were harvested by

centrifuging at 3000 g. The pellet was processed to purify the histidine-tagged-fusion-proteins under native conditions as described in the Qiagen manual (Qiagen, Chatsworth, CA). The purified protein was resolved by 15% SDS-PAGE analysis under denaturing conditions.

Phosphate labeling during natural virus infection

Vero or CEK cells were infected with IBV Beaudette at a multiplicity of infection (M.O.I.) between 2 and 3 for one hour. Fresh DMEM containing 2% serum was used for virus-infected cells. For one hour prior to labeling with 100 μCi ^{32}P-orthophosphate, cells were starved in phosphate-free DMEM containing 2% phosphate-free serum. The cells were labeled for one hour. The cells were washed with Tris buffered saline (TBS) (Sambrook *et al.*, 1989) and either 0.5 ml of modified lysis buffer [1 mM iodoacetamide, 1 mM phenyl methyl sulfonyl fluoride (PMSF), 100 μM sodium orthovanadate, 4 μg/ml aprotinin, 1 mM EDTA, 1% NP40, 10 mM Tris (pH 8), 0.1% SDS, 150 mM NaCl and 0.025 % sodium azide] was added to the 60 mm dishes or 1 ml lysis buffer was added to the 100 mm dishes (Sefton *et al.*, 1978). Cells were scraped off the dish surface and lysis was carried out at 4°C for 30 minutes. The sample was used for immunoprecipitation of IBV N protein. Protease inhibitors PMSF, EDTA, and aprotinin were added to the lysis buffer to prevent protease digestion of proteins. The serine/threonine phosphatase inhibitor sodium fluoride and tyrosine phosphatase inhibitor sodium orthovanadate were used in the lysis buffer to prevent the loss of labeled phosphate from the N protein in the lysate.

Pulse-chase analysis

Vero cells were infected with IBV Beaudette strain at an M.O.I. between 2 and 3 for one hour after which fresh DMEM containing 2% serum was added. To determine the stability of IBV N protein at 6.5 hours post-infection (h p.i.), 2 ml of hypertonic medium containing 2% serum (DMEM containing 0.335M NaCl) were added to the cells to dissociate the ribosomes and thereby synchronize the cells for protein synthesis. After one hour (7.5 h p.i.), the hypertonic medium was discarded and the cells were washed with phosphate buffered saline (PBS) (Sambrook *et al*; 1989) and 1 ml serum-free, methionine-free DMEM (Gibco, Carlsbad, CA) containing 100 µCi ^{35}S-methionine was added to the virus-infected cells. Labeling was carried out for 30 minutes followed by chase as described below. To determine the phosphate turnover of IBV N protein, one hour prior to labeling the virus-infected cells with 100 µCi ^{32}P-orthophosphate (for a period of one hour), the cells were washed with TBS and starved in phosphate free DMEM containing 2% serum (phosphate free).

^{35}S and ^{32}P pulsed cells (above) were chased by removing the labeling medium, washing the cells with PBS, and adding 3 ml of chase medium, either DMEM containing 2% serum and 1 mM L-methionine or DMEM containing 2% serum and 10 mM phosphate buffer for ^{35}S and ^{32}P pulses, respectively. The cells were chased for 2.5 or 3 hours depending on the experiment. At the end of the chase period, the cells were washed with PBS and 0.5 ml of lysis buffer was added to the plate after scraping the cells with a rubber policeman. The cells were lysed for 30 minutes at 4°C and processed for immunoprecipitation.

Immunoprecipitation of the IBV N protein

The lysates were centrifuged at 1000 g to pellet the nuclei and cell debris. Rabbit anti-N polyclonal antibody was added to the lysate at saturating concentrations to precipitate all the N protein. The mix was incubated on a shaker at 4°C for one hour. 50 μL of a 50% slurry of protein-A-agarose (Pierce, Rockford, IL) in dilution buffer {10 mM Tris, pH 8; 140 mM NaCl; 0.025% sodium azide (Tris saline azide) and 1% NP40} were added to capture the antigen-antibody complex. This mix was incubated at 4°C for one hour. The protein-A-agarose antigen-antibody complex was washed thrice with TSA and eluted by adding 20 μl of 2X SDS-PAGE loading buffer and heating at 100°C for 10 minutes. The sample was resolved by sodium dodecyl sulfate-polyacrylamide gel electrophoresis (SDS-PAGE) (Sambrook *et al.*, 1989). Following electrophoresis, the gels were dried and exposed to an imaging plate (Fuji Medical Systems, Stamford, CT) or to an X-ray film. Band intensity was quantified using a Fuji2000 phosphorimager (Fuji Medical Systems, Stamford, CT) and represented as photostimulus luminescence (PSL) units. Phosphate and protein stability was represented as percent PSL units measured in comparison to the maximum incorporation of radioisotope in the immunoprecipitated protein.

Western blot analysis

After resolving the proteins by denaturing gel electrophoresis, the proteins were transferred from the gel to a nitrocellulose membrane (Sambrook *et al.*, 1989). The membrane was blocked with blocking solution (5% skim milk 0.02% tween 20 in TBS) for two hours at room temperature (R.T.). Chicken anti-IBV Gray (strain of IBV)

antibody (1:1000 dilution in blocking solution) was added to the blot and allowed to react with the proteins for one hour at R.T. After two washes with washing buffer (TBS-0.02% Tween 20), alkaline phosphatase conjugated goat anti-chicken antibody (KPL) (1:10,000 dilution in blocking solution) was added to the blot and allowed to react for one hour at R.T. After two washes with washing buffer, alkaline phosphatase substrate, 5-bromo-4-choloro-3-indolyl phosphate (BCIP) and nitroblue tetrazolium (NBT), alkaline phosphatase conjugate substrate (Bio-Rad, Richmond, CA) was added to the blot for color development. The substrate was removed and the blot was washed after color development.

Double labeling of IBV N protein

One hour prior to labeling, virus-infected Vero or CEK cells were starved of leucine and phosphate in serum-free, leucine and phosphate-free DMEM (Specialty Media, Phillipsburg, NJ). Cells were labeled with 100 μCi ^{32}P-orthophosphate and 10 μCi ^{3}H-leucine (Perkin Elmer, Wellesley, MA) for one hour. At the end of the labeling period, the cells were harvested as described above and IBV N protein was immunoprecipitated using rabbit anti-N polyclonal antibody. RNA was extracted from the protein using TRIZOL. DNA associated with the protein was removed by precipitating with 0.3 volumes of 100% alcohol per 1 ml of TRIZOL Reagent. IBV N protein was isolated from the organic phase by precipitating with isopropyl alcohol (Invitrogen, Carlsbad, CA). The precipitate was dissolved in 2X SDS-PAGE gel loading buffer and used for TCA precipitation to determine the ^{3}H and ^{32}P counts per minute

(cpm) (Ausubel *et al*., 1987). ^{32}P:^{3}H ratios were calculated. The experiments were done in duplicate.

Purification of IBV virion

Virus from supernatants of five 100 mm tissue culture plates infected at an M.O.I. of 2 to 3, were concentrated on a 20% sucrose cushion, by centrifuging at 35,000 rpm in a SW 55 Ti Beckmann rotor at 4°C for 2.5 hours. The virus pellet was suspended in 100 μl TEN buffer (10 mM Tris pH 7.4, 1 mM EDTA, 150 mM NaCl) and centrifuged through a linear 30%-50% glycerol-tartrate gradient at 35,000 rpm, in a SW 55 Ti Beckmann rotor at 4°C for 18 hours. A distinct band corresponding to the virion was obtained around 1.18 g/ml density. The virus from this band was used for various analyses.

Alkaline phosphatase treatment

IBV N protein isolated from the infected cells or from virions after immunoprecipitation with rabbit anti-N polyclonal antibody was dialyzed against PBS for four hours at 4°C. Equal volumes of this dialyzed protein were used for treatment with calf intestinal alkaline phosphatase (CIAP) (Promega, Madison, WI) and for the controls (untreated IBV N protein and N protein treated with RNase A). The protein was treated with 23 units of CIAP in 20 μl reaction volume. The reaction was incubated at 37°C for 30 minutes and stopped by heating at 70°C for 15 minutes. The protein was resolved by 15% SDS-PAGE followed by a Western blot with chicken anti-IBV Gray antibody (Sambrook *et al*., 1989).

Treatment of virus infected cells with serine-kinase inhibitor U0126

Virus-infected cells were labeled with ^{32}P-orthophosphate and/or ^{3}H-leucine as described previously, for a period of one hour. The serine-kinase inhibitor U0126 (Calbiochem, San Diego, CA) was added to the virus-infected cells at a concentration of 10 μM or 20 μM when the cells were starved of phosphate and/or leucine. The inhibitor was present throughout the labeling period until the cells were harvested for immunoprecipitation of the IBV N protein. After isolating the IBV N protein, it was resolved by electrophoresis in a denaturing 15% polyacrylamide gel (Sambrook *et al*., 1989).

Protein preparation for mass spectrometry analysis

IBV N protein and bacterially expressed IBV recombinant N protein were resolved by denaturing polyacrylamide gel electrophoresis and stained with Coomassie brilliant blue R250 (Sambrook *et al*., 1989). The band corresponding to the N protein was excised and cut into 1 mm-cubes and transferred to a 0.5 ml microfuge tube. The gel pieces were washed with water (two changes) and with 50 mM ammonium bicarbonate (NH_4HCO_3):acetonitrile 1:1 (v/v) for 15 minutes. The liquid was removed and enough fresh acetonitrile to cover the gel particles was added to the tube. The acetonitrile was removed once the gel pieces shrunk and stuck together. The gel pieces were rehydrated in 50 mM NH_4HCO_3. After 5 minutes, an equal volume of acetonitrile was added to the gel mix. All liquid was removed after 15 minutes and fresh acetonitrile was added to cover the gel particles. Once the gel pieces have shrunk, the gel particles were dried in a vacuum centrifuge.

The gel particles were then rehydrated in 10 mM dithiothreitol/25 mM NH$_4$HCO$_3$ before incubating at 56°C for 45 minutes and chilling to room temperature. The excess liquid was removed and replaced with roughly 150 to 200 µl of freshly prepared 55 mM iodoacetamide in 25 mM NH$_4$HCO$_3$. The iodoacetamide solution was removed after incubating the gel mix for 30 minutes at room temperature in the dark. The gel particles were washed twice (15 minute intervals) with 50 mM NH$_4$HCO$_3$ and acetonitrile (1+1, v/v) and after removing the wash fluid the gel pieces were shrunk by adding fresh acetonitrile. The gel pieces were then dried under vacuum (Bruker, Billerica, MA).

For an in-gel digestion, enough sequencing grade trypsin (5 ng/µl) (Promega, Madison, WI) freshly prepared in 25 mM NH$_4$HCO$_3$, was added to cover the gel and digestion was carried out at 37°C for 30 minutes. 25 mM NH$_4$HCO$_3$ was added to cover the gel pieces. After incubating at 37°C, the gel mix was sonicated for 10 minutes and the supernatant recovered for analysis by matrix assisted laser desorption ionization-time of flight spectrometry (MALDI-TOF) (Bruker, Billerica, MA).

The sample was cleaned and concentrated using a C18 Zip-Tip pipette tip (Millipore, Billerica, MA) as per instructions given in the catalog. The matrix for MALDI-TOF α-cyano-4-hydroxycinnamic acid (a-HCAA) was prepared in 33% acetonitrile in 1% trifluroacetic acid (TFA). A 1:1 preparation of the sample or calibration standard (Bruker, Billerica, MA) and matrix was applied to a Scout MTP^{TM}-384 ground steel target (Bruker, Billerica, MA) for MALDI-TOF analysis.

MALDI-TOF analysis

The MALDI-TOF autoflex instrument (Bruker, Billerica, MA) was calibrated using the ~ 1000 to ~ 4000 Da calibration standards in the linear mode. The monoisotopic mass of the standards and the standards are as follows: Angiotensin II (1046.54 Da), angiotensin I (1296.69 Da), substance P (1347.74 Da), bombesin (1620.81 Da), adenocorticotropic hormone (ACTH) (1-17) (2093.09 Da), ACTH (18-39) (2465.20 Da), somatostatin 28 (3147.47 Da). The "FLEXcontrol" software was used for controlling the autoflex instrument. The tryptic peptide digest of IBV N protein was analyzed using the autoflex MALDI-TOF instrument. The sample was ionized at ~ 60% LASER. Analysis was in a linear acquisition mode. The spectrum was annotated and monoisotopic peaks identified, providing lists of monoisotopic peak m/z values using the "Xmass" software. The resulting peak lists were used for MASCOT database searching using the "BIOTOOLS" software package (Bruker, Billerica, MA).

RESULTS

Phosphate labeling of the bacterially expressed recombinant IBV N protein

N protein expression was detected in *E. coli* when induced in Tris-glucose medium. The protein, corresponding to an approximate molecular mass of 48 kDa reacted with chicken anti-IBV Gray antibody in a Western blot assay (Fig. 2.1). A band higher in electrophoretic mobility than the N protein also reacted with the antibody. This is likely a breakdown product of the recombinant N protein (Fig. 2.1). ^{32}P-orthophosphate labeling in Tris-glucose medium of the *E.coli* expressed recombinant
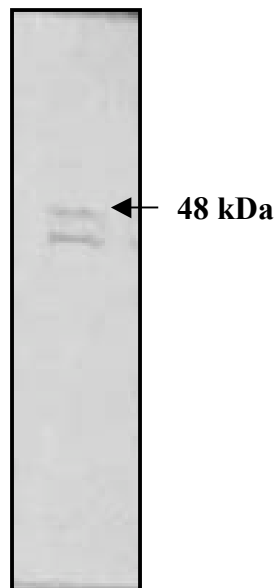
FIG. 2.1. Western blot analysis of recombinant IBV N protein from *E. coli* expressed in Tris-glucose medium. Recombinant IBV N protein expression was induced in *E. coli* in Tris-glucose medium and purified by Ni^{+2}-NTA chromatography (Qiagen). The protein was resolved by 15% denaturing SDS-PAGE analysis and reacted with chicken anti-IBV Gray antibody. The N protein is marked by an arrow. The lower band is likely a degradation product of the N protein.
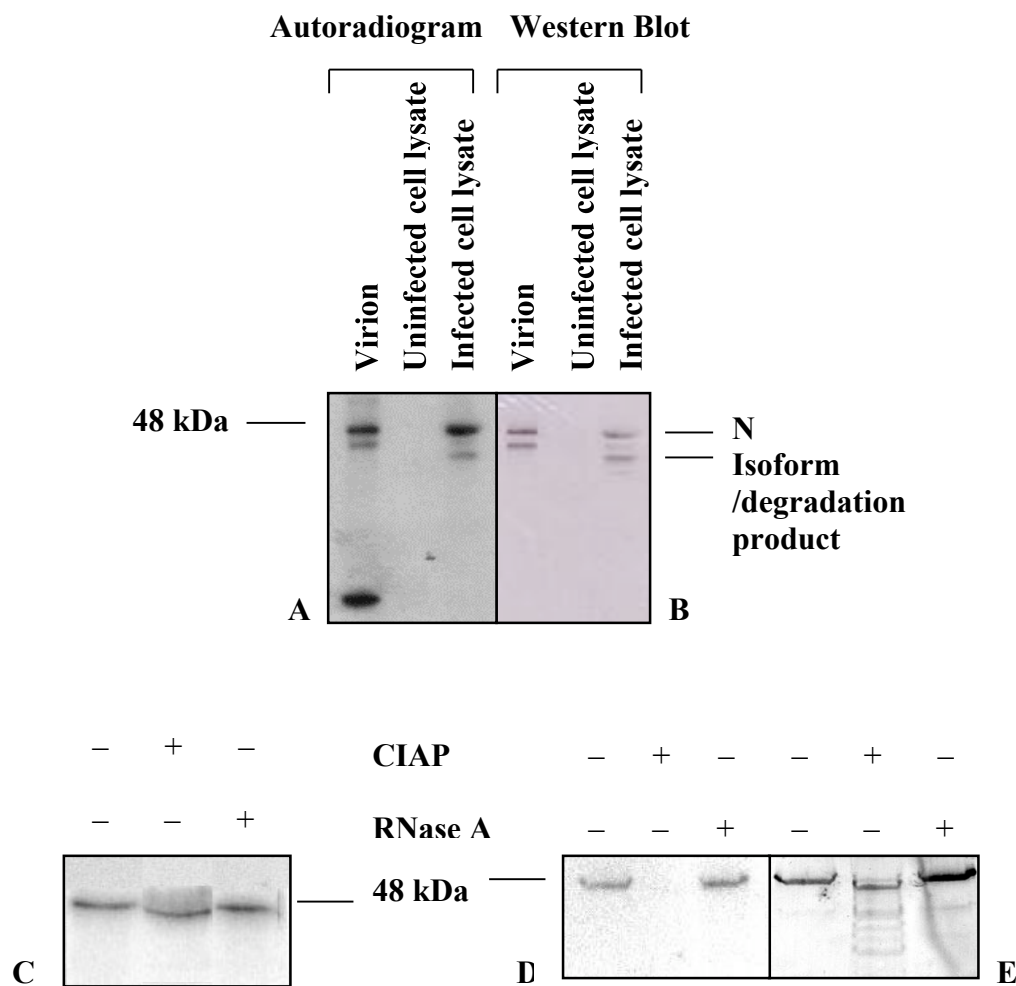
FIG 2.2. Calf intestinal alkaline phosphatase treatment (CIAP) of IBV N protein. ^{32}P-orthophosphate labeled IBV N protein from infected Vero cells and from the virion was isolated by immunoprecipitation with chicken polyclonal anti-IBV antibody. Panel A, shows the autoradiogram and panel B shows the Western blot. Virion N protein, immunoprecipitated from lysates of uninfected cells, and cellular N protein were used for the assay. The labeled N protein was treated with 20 units CIAP and resolved by denaturing electrophoresis in a 15% polyacrylamide gel and subject to autoradiography. Panel C, shows an autoradiogram of the virion N protein, panel D, an autoradiogram of cellular N protein and panel E, a Western blot of cellular N protein. Cellular N was obtained 8 h p.i.

IBV N protein showed that the N protein was not phosphorylated in *E. coli* (data not shown).

Alkaline phosphatase treatment of IBV N protein

[32]P-orthophosphate labeled IBV N-protein was isolated by immunoprecipitation from IBV-infected Vero cells 8 hours post-infection (h p.i.) and from virions purified from ^{32}P-treated cells. The virion N protein appeared to be slightly lower in electrophoretic mobility than the cellular N protein as can be seen from the Western blot (Fig. 2.2B). Both the intracellular and virion N proteins were phosphorylated (Fig. 2.2A). Two forms of the N protein are obtained from Vero cells both of which are phosphorylated (Fig. 2.2A) as has been shown with virion N protein from chicken embryo kidney (CEK) cells (Lomniczi and Morser, 1981). Both bands react with chicken anti-IBV polyclonal antibody using Western blot analysis (Fig. 2.2B) suggesting that the protein higher in electrophoretic mobility is either a degradation product or some other isoform of the N protein. ^{32}P-orthophosphate-labeled N proteins from infected cells and virions were treated with calf intestinal alkaline phosphatase (CIAP), an enzyme that removes phosphate from phosphoserine and phosphothreonine residues. The labeled infected-cell N protein was susceptible to CIAP treatment as determined by autoradiography, confirming the presence of phosphate on the N protein from infected-cell lysates. The cellular N protein loses its phosphate completely (Fig. 2.2D). The Western blot confirms that IBV N protein was indeed present in the CIAP treated immunoprecipitate from the cell lysate (Fig. 2.2E). Susceptibility of the virion N protein to CIAP is indicated by a slight increase in mobility of the treated protein (Fig. 2.2C). It

is possible that the alkaline phosphatase to substrate stoichiometry is higher in the virion N protein than the N protein from infected cell lysates. The slight increase in electrophoretic mobility in the case of the CIAP treated sample as compared to the untreated sample might be due to the effect of CIAP or it might be due to the presence of salts in the sample. It is not possible to estimate the amounts of the N protein in a Coomassie stained gel because the heavy chain of the antibody and the N protein co-migrate in a 15% polyacrymaide gel. In the phosphatase assay, the lower bands were not visible even after a twenty-four hour exposure using a phosphorimager. To verify that the band obtained in autoradiography was not due to the presence of labeled RNA bound to the N protein, the N protein from both sources was also treated with 10 μg of RNAse A. There was not a very apparent decrease in the intensity of the RNase A treated samples as compared to the untreated controls (Figures 2.2C and 2.2D). This indicates that either no RNA was associated with the IBV N protein from the cellular and virion N protein or that the RNA was protected.

IBV N protein was phosphorylated at all times during infection

The kinetics of phosphorylation of IBV N protein has not been reported before. It is possible that the N protein might not be phosphorylated at all times during IBV infection. Hence, to determine if IBV N is phosphorylated throughout IBV infection, IBV Beaudette-infected Vero cells were treated before and during labeling with 100 μCi ^{32}P-orthophosphate for one hour with actinomycin-D (5 μg/ml) an inhibitor of RNA synthesis. The IBV cellular lysate was obtained after TRIZOL (Invitrogen, Carlsbad, CA) extraction to remove the labeled RNA bound to the proteins in the lysate. One-

eighth the volume of the cell lysate was used for denaturing gel electrophoresis. As shown by ^{32}P-orthophosphate labeling, IBV N was the only phosphorylated viral protein in infected cell lysates as can be seen by comparison with the uninfected cell lysate control (Fig. 2.3A). IBV N was phosphorylated throughout infection, appearing around 6 hours post-infection until at least 18 hours post-infection, as represented by a phosphorylated band at ca. 48 kilodalton (kDa) molecular mass (Fig. 2.3A). The other phosphorylated band appearing slightly above 36.4 kDa was a cellular protein as it was also present in the uninfected cell lysate control. Western blot analysis of a similar experiment with rabbit anti-N polyclonal antibody was specific for IBV N protein that corresponded to a band around 48 kDa molecular mass (Fig. 2.3B). It was noticed that the mobility of the protein in the various lanes was not very uniform. This is probably a gel artifact, perhaps due to insoluble material in the crude lysates or a stacking effect.

Pulse-chase analysis determined the stability of the IBV N protein

It was important to know the stability of IBV N protein before the stability of phosphate on the N protein could be determined. IBV Beaudette-infected Vero cells were pulse-labeled with ^{35}S-methionine at 7.5 h p.i. before chasing with excess cold methionine between 0.5 (8 h p.i.) and 3.5 hours (11.5 h p.i.) before harvesting the infected cells. The IBV N protein was isolated by immunoprecipitation with rabbit anti-N-polyclonal antibody at saturating concentrations of the antibody such that all N protein in the infected cell lysate was precipitated. Since labeling the cells for 15 minutes was unfruitful, the cells were instead pulsed for 30 minutes followed by the variable chase period. Maximum incorporation of the label was observed after 1.5 hours of chase

Hours post-infection
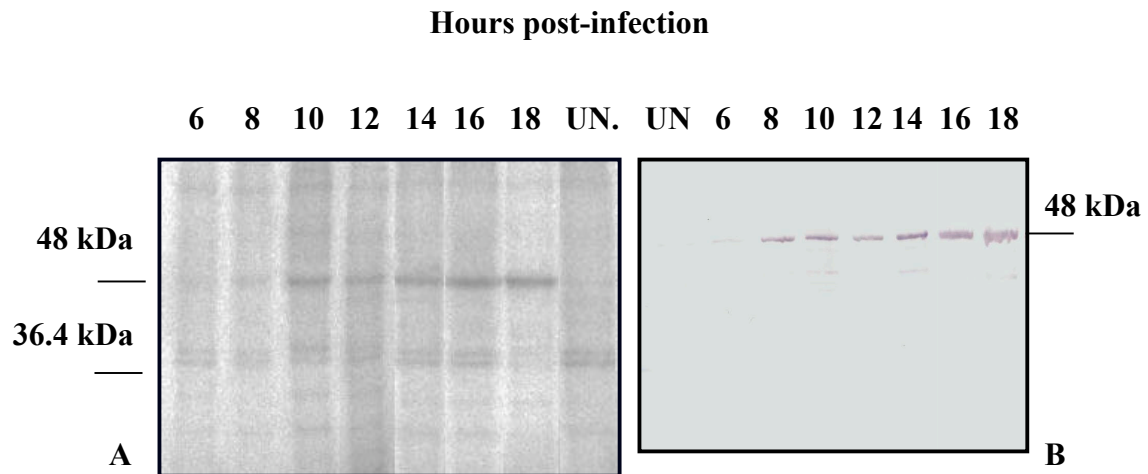
FIG. 2.3. Time-course of phosphorylation of IBV N protein in presence of actinomycin D. Phosphorylation of IBV N protein in IBV-infected Vero cells was studied by labeling with 100 µCi ^{32}P-orthophosphate for one hour in the presence of 5 µg/ml actinomycin-D. At different times post-infection (time is represented above the figure), equal amounts of whole cell lysate from various time points were resolved by gel electrophoresis on a 15 % denaturing polyacrylamide gel followed by autoradiography. Lysate from an uninfected (UN) cell was used as a control. IBV N is ca. 48 kDa in mass. Panel A, represents a phosphorimage and panel B, represents a Western blot.

Chase time in hours

UN PI 0 0.5 1 1.5 2 2.5 3 3.5

——— **48 kDa**

A

B

Chase Time in Hours

PSL units
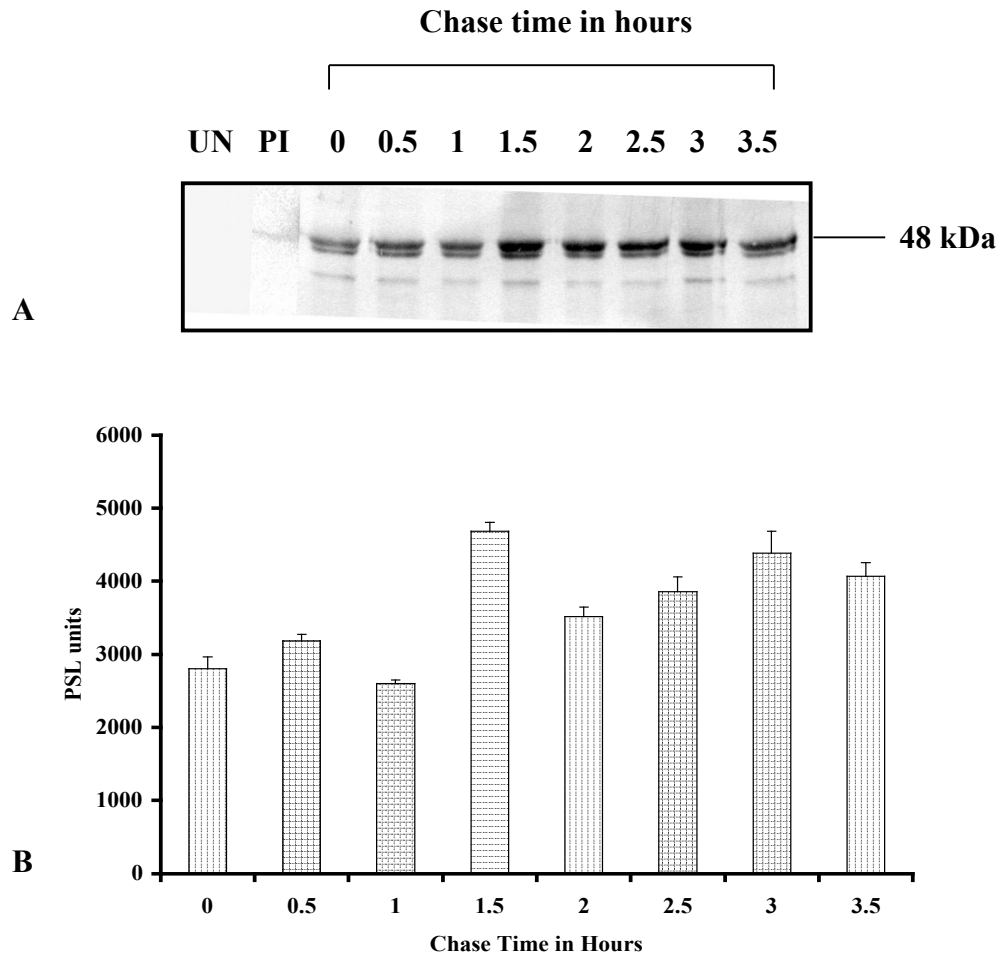
FIG 2.4. Analysis of stability of IBV N protein. Panel A, represents a phosphorimage and panel B, a graphical representation of the densitometric analysis of the bands obtained in the phosphorimage. IBV-infected Vero cells were pulse-labeled with 25 μCi ^{35}S-methionine for 30 minutes and chased with a large excess of cold methionine for 0, 0.5, 1, 1.5, 2, 2.5, 3 and 3.5 hours. The N protein was obtained from IBV-infected cell lysates by immunoprecipitation with rabbit anti-N polyclonal antibody. 0 hour chase time represents 8 hours post-infection. Lysates from uninfected cells precipitated with rabbit anti-N polyclonal antibody (UN) and lysates from infected cell precipitated with preimmune serum (PI) are also shown. Error bars represent standard deviations of two densitometric measurements from one experiment.

period (Figures 2.4A and 2.4B). As can be seen from the graphical representation of the densitometric analysis of the bands using a phosphorimager (Fig. 2.4B), there was a slight decrease in the intensity of the band until the 2.5-hour chase period followed by an increase in the 3- and 3.5-hour chase-periods (Fig. 2.4A). The 2- and 2.5- hour chase period band intensity corresponded respectively to 75% and 82% of the 1.5-hour chase period band intensity. The 3- and 3.5- hour chase period band intensity corresponded respectively to 85% and 92% of the 1.5-hour chase period band intensity. Since the decrease in the band intensity was never greater than 50%, it is likely that the N protein is stable for at least one or maybe two hours. N protein alone was precipitated as shown by Western blot analysis using chicken anti-IBV Gray (strain of IBV) antibody (Figure 2.2B). No bands were obtained when lysates from uninfected cells were used for immunoprecipitation using rabbit-anti-N polyclonal antibody (Figure 2.4A) or when using non-specific antibody such as rabbit-anti-gag antibody to reticuloendotheliosis virus (data not shown) were used as controls. A faint band slightly larger than 48 kDa was obtained on exposure to an imaging plate when rabbit preimmune serum was used for immunoprecipitation of infected cell lysates. This band does not react with anti-IBV-Gray chicken serum as shown by the Western blot analysis (data not shown).

Pulse-chase analysis to determine the stability of phosphate on IBV N protein in Vero cells

^{35}S-methionine pulse-chase analysis indicated that the IBV N protein is stable over at least a two-hour period. Phosphate on a protein can be removed very quickly or slowly thereby regulating the function of the protein. In order to determine the stability
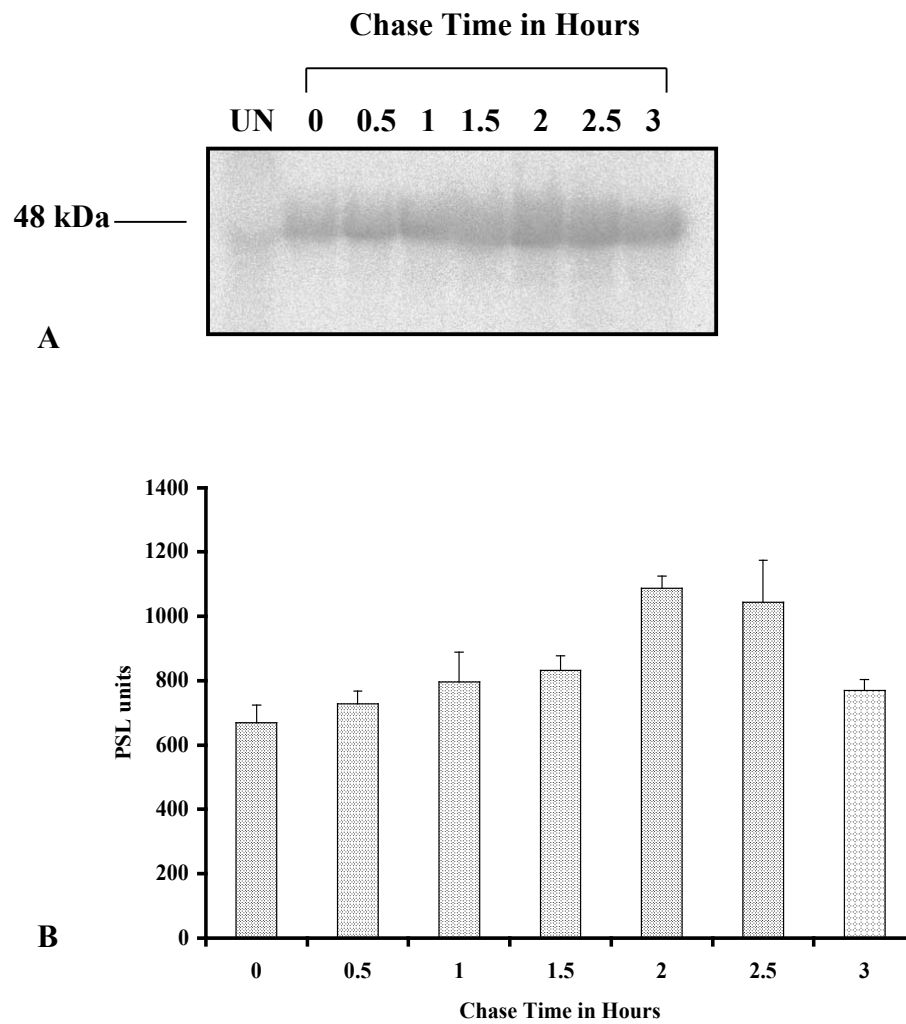
FIG 2.5. Pulse-chase analysis to determine phosphate stability of IBV N protein. IBV infected Vero cells were labeled with ^{32}P-orthophosphate for one-hour and chased with cold phosphate starting at 8 h p.i. until 11 h p.i. Panel A, represents a phosphorimage of labeled N protein resolved by denaturing gel electrophoresis and panel B, represents the densitometric analysis of the bands using a Fuji2000 phosphorimager. Error bars represent standard deviations of two densitometric measurements from one experiment.

of the phosphate on the N protein in terms of half-life, infected cells were labeled with ^{32}P-orthophosphate for one hour and the chase analysis was started at 8 h p.i., and was continued until 11 h p.i. N protein was immunoprecipitated from cell lysates at saturating amounts of the antibody such that all the N protein precipitates out (this has been standardized in the laboratory). From Figures 2.5A and 2.5B we can see that phosphate incorporation continues to occur until the 1.5 h chase period, reaching a maximum at the 2-hour chase period then drops down to 96% and 70% of this value in the 2.5- and 3-hour chase period respectively. Since phosphate is utilized for several processes in the cell, it might be more difficult to replace intracellular phosphate pools. Labeling on the N protein might increase during the chase period due to labeled phosphate from other cellular processes. This experiment has been done twice and similar results were obtained at both times. From these results, the phosphate on the protein does not fall below 70% in a one-hour chase period. This change in phosphate level on the IBV N protein over a one-hour period might have, a positive, negative or no effect on the various functions of the IBV N protein.

Determination of ^{32}P-orthophosphate:^{3}H-leucine ratios of IBV N protein

To determine variations in the amount of phosphate on the N protein during the course of infection in the cell, infected cells were labeled with ^{3}H-leucine and ^{32}P-orthophosphate. The ratio of the counts per minute (cpm) of ^{32}P-orthophosphate:^{3}H-leucine gives an idea of the cpm of phosphate relative to IBV N protein. The ratios of ^{32}P-orthophosphate and ^{3}H-leucine on IBV N-protein were determined in IBV-infected Vero and CEK cells. The ^{32}P:^{3}H cpm ratio for the virion (isolated at 16 hours post-

infection), was almost 3.5 times and 10 times greater than the ratios obtained for the N protein precipitated 7 hours post-infection from CEK cells and Vero cells respectively (Table 2.1).

In order to establish the significance of difference between the ^{32}P:^{3}H ratios of the N protein isolated at different times of virus infection and also establish the significance of increasing trend with time in the proportions, we performed an orthogonal polynomial contrast test across the time points. The various time points were calculated as the treatment variable and the ratio was used as the response. A significant linear trend ($P<0.0001$) in the ratios was obtained (Fig. 2.6). There is a direct correlation in the amount of phosphate on the N protein with time. In order to establish a significant difference in the ^{32}P:^{3}H cpm ratios of the N protein at various time points other multiple comparison procedures were employed to analyze the data. The ratio (0.35 for CEK cells or 0.24 for Vero cells) at time point 1 (7 hours post-infection) was significantly different ($P<0.05$) from the ratio (1.22 for CEK cells or 2.52 for Vero cells) at time point 5 (16 hours post-infection) using Least Significant Difference (LSD) test. These results were also confirmed by other multiple comparison procedures such as Student-Newman Keuls test and Tukey's Studentized Range test (Table 2.1).

Effect of a serine-kinase inhibitor U0126 on phosphorylation of IBV N protein

To determine the role of phosphorylation in the life cycle of the virus, specific inhibitors of phosphorylation could be used. N protein has 33 serine, 18 threonine and 8 tyrosine residues. The sites of phosphorylation on this protein have not been identified and hence site directed mutagenesis might prove a more tedious approach to determine

Table 2.1.

Double labeling of IBV N protein in Vero and CEK cells to determine the ratios of $^{32}P:^{3}H$ on IBV N protein at different times of infection

Time of harvest: hours post-infection (h p.i.)	Chicken Embryo Kidney cells: Ratio of counts per minute (cpm) of $^{32}P:^{3}H$	Vero cells: Ratio of counts per minute (cpm) of $^{32}P:^{3}H$
7	0.35 ± 0.003 *	0.24 ± 0.003 *
9	0.83 ± 0.026 *	0.45 ± 0.002 *
11	0.80 ± 0.052 *	0.84 ± 0.001 *
13	0.73 ± 0.012 *	0.85 ± 0.04 *
16 (Virion N)	1.22 ± 0.003 *	2.52 ± 0.005 *

* Represents standard error values from two identical experiments.

Note. The results are representative of two experiments.
a) A significant linear trend (P<0.0001) in the ratios of $^{32}P:^{3}H$ on IBV N protein is obtained, thus establishing the fact there is an increasing trend in the phosphate on the N-protein with time.

b) The ratio at time point 1 (7 hours post-infection) is significantly different (P<0.05) from the ratio at time point 5 (16 hours post-infection) using Least Significant Difference (LSD) test.

the role of phosphorylation of IBV N in the virus life cycle. Because of the large number of serines, we decided to try specific kinase inhibitors to determine the role of phosphorylation of IBV N protein in the virus life cycle. A preliminary analysis was carried out with U0126, a specific serine-kinase inhibitor that inhibits the MEK 1 kinase pathway. The consensus site of phosphorylation of this kinase was not known. N protein from both the virion and the infected-cell lysates from Vero cells, treated with 10 μM U0126, was decreased in phosphorylation as can been seen with double labeling studies using ^{3}H-leucine and ^{32}P-orthophophate (Table 2.2). However, the difference in ratios between the untreated and treated samples was not significant based on the one-tailed equal variance T-test (P > 0.05). Concentrations higher than 10 μM inhibitor were found to be toxic to the cells. To determine if this marginal effect on N protein phosphorylation affected viral titers, the viral titers from inhibitor-treated and -untreated cells were compared. Slightly higher titers were obtained from inhibitor-treated infected cells. This difference was however not significant based on the T-test (P > 0.05) (Table 2.3). Hence, this specific kinase inhibitor does not affect phosphorylation of IBV N protein nor the virus titer in a significant manner. Other kinases possibly phosphorylate the IBV N protein.

Matrix assisted laser desorption ionization-time of flight (MALDI-TOF) mass spectrometry

The phosphorylation sites on the IBV N protein have not been identified. An attempt was made at identifying phosphorylated peptides using MALDI-TOF mass spectrometry. IBV N from bacteria expressing the recombinant N protein and from t
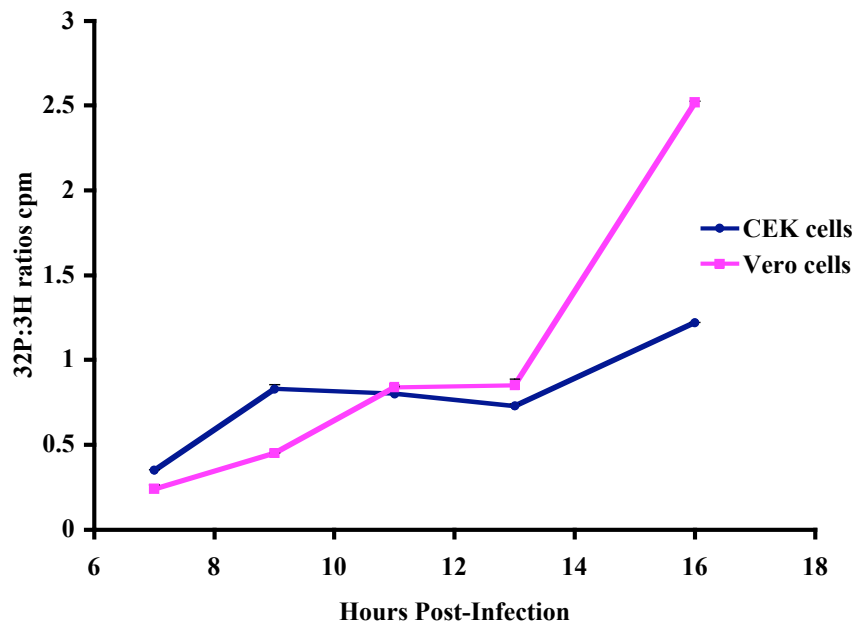
FIG 2.6. Graphical representation of ^{32}P:^{3}H cpm ratios of N protein obtained at different hours post-infection from Vero- and CEK-infected cells. The N protein was obtained by immunoprecipitation with rabbit anti-N polyclonal antibody. It was treated with TRIZOL to remove bound RNA, followed by TCA precipitation to remove unincorporated label and then counted to determine the ^{32}P:^{3}H cpm ratios. Standard error is less than 0.05. A significant linear trend (P<0.0001) in the ratios was obtained.

Table 2.2.

$^{32}P{:}^{3}H$ ratios of IBV N protein in presence and absence of a serine-kinase inhibitor
U0126

Hours post-infection	Untreated samples Ratios of $^{32}P{:}^{3}H$	Samples treated with 10 μM U 0126 serine-kinase inhibitor. Ratios of $^{32}P{:}^{3}H$
5	0.43 ± 0.12 *	0.36 ± 0.14 *
7	0.80 ± 0.14 *	0.68 ± 0.2 *
Virion	1.57 ± 0.2 *	1.45 ± 0.18 *

* Represents standard error values from two identical experiments.

The $^{32}P{:}^{3}H$ ratios of IBV N protein of the untreated and treated samples are not
significantly different as determined by the T-test ($P > 0.05$).

Table 2.3.

Viral titers from IBV-infected Vero cells in the presence and absence of serine-kinase
inhibitor U0126

Inhibitor	Viral titer (pfu/ml)
0 μM	6.3×10^{7}
10 μM	1.97×10^{8}

Viral titers were determined in triplicates and the average values are represented here.
The titers of the untreated and treated samples are not significantly different as
determined by the T-test ($P > 0.05$).

IBV virion was used for the analysis (Figures 2.7A and 2.7C). The band corresponding to ca. 48 kDa for both, virion and bacterially expressed IBV N protein was excised from the gel and used for sample preparation for MALDI-TOF analysis. The bacterially expressed N protein always shows two bands, the lower band is thought to be a degradation product as has been confirmed by Western blot analysis with chicken anti-IBV Gray antibody (Fig. 2.7). Similarly, the N protein from lysates of infected Vero cells has been shown to exist as two bands (Fig. 2.2B).

Predictably, recombinant IBV N protein expressed in bacteria was non-phosphorylated (data not shown). Therefore it was used as a control for MALDI-TOF analysis to compare the phosphorylated peptides obtained from the virion N protein. MALDI-TOF mass spectrometry separates peptides based on the mass:charge ratio (m/z). Trypsin is commonly used to digest the protein for peptide analysis. It digests proteins after lysine or arginine amino acids residues. Using the Sequence Editor software (Bruker, Billerica, MA), 67 tryptics were predicted varying in m/z from 288 to 3857 (Table 2.4). Immediately prior to analysis of the protein, the MALDI-TOF instrument was calibrated using the 1000 to 4000 Da range peptide calibration standards in the linear mode. Either a quadratic (multipoint) or linear (two point) calibration can be performed. A linear calibration employs only two peaks from the calibration standards whereas a quadratic calibration can be configured to take into account multiple peptides. A quadratic calibration is more accurate than a linear calibration because it can interpolate and extrapolate more accurately. Preliminary MALDI-TOF analysis of the virion N protein showed several peaks with a mass:charge (m/z) of less than 200.
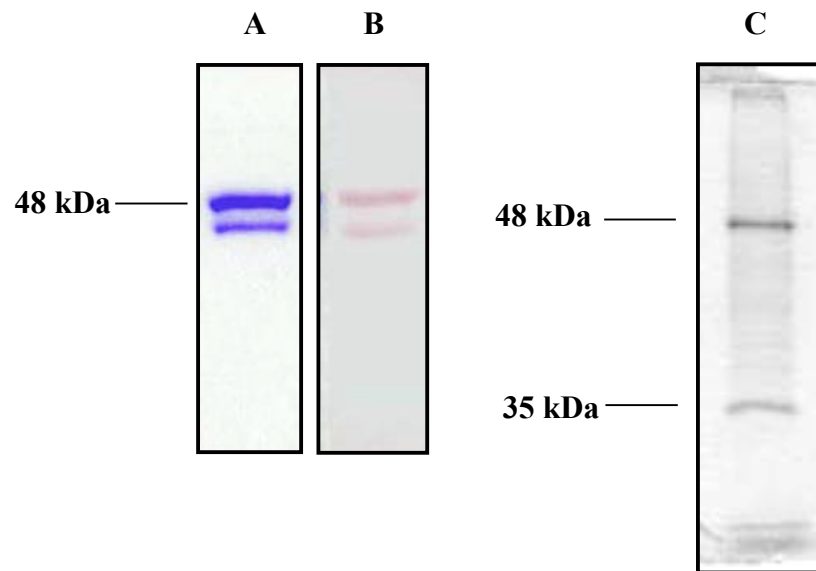
FIG. 2.7. SDS-PAGE and Western blot analysis of IBV N protein. Coomassie Brilliant Blue R250 staining of the bacterially expressed protein is shown in panel A and of the IBV virion is shown in panel C. Panel B, shows the Western blot of the bacterially expressed N protein.

These can be ignored because they corresponded to single amino acid residues obtainethe tryptic digest or ionized products of the matrix. For the virion N protein, very few peaks were observed in the m/z range between 400-900. Ten peaks were obtained in the range 1050-1500 and 9 peaks were obtained in the range 2000 to 2550. Peaks were assigned to specific peptides by comparing predicted with actual m/z ratio. Many peaks could not be assigned to a specific peptide because the m/z ratio did not correspond to any of the predicted peptides that are obtained by trypsin digestion. The peaks obtained here have an m/z ratio greater than that of the predicted peaks, suggesting a partial digestion of the N protein. Only 4 peaks in the range of 400 to 1500 could be assigned with certainty to peptides when compared to the predicted tryptic peptide digest obtained with a zero partial cut (Fig. 2.8 and Table 2.4). GADVK (amino acids 120-124), SGSEDDLIAR (amino acids 190-199), FSDGGPDGNFR (amino acids 144-154) and VGSSGNASWFQAIK (amino acids 27 to 40) are shown in Figure 2.8 and Table 2.4. Four other peptides were identified when a one or more partial cut was used for analysis of predicted tryptic peptides. WDFIPLNR (amino acids 155-162), DPDKFDQYPLR (amino acids 133-143), ALTSDEERNNAQLEFDDEPK (amino acids 376-395) and SNQGTRDPDKFDQYPLR (amino acids 127-143) (Fig. 2.7). In the case of the IBV recombinant N protein used as a control, four peaks in the ratio 399-450, and nine peaks in the 820-1170 range could be assigned to peaks with certainty (Table 2.4.). Besides the 13 peaks that could be assigned to peptides, the other peaks obtained for the recombinant IBV N protein had an m/z ratio greater than that of the predicted peaks, suggesting a partial digestion of the N protein.

Table 2.4.

Comparison of the mass:charge (m/z) ratios of predicted tryptic peptides (using the
Sequence Editor software) with a zero partial cut with that of the peptides identified
positively by MALDI-TOF analysis

	Amino acids	m/z	Sequence	Peak: Recomb -inant N	Peak: Virion N
1	43-43	146.106	K	-	-
2	210-210	146.106	K	-	-
3	362-362	146.106	K	-	-
4	368-368	146.106	K	-	-
5	73-73	174.112	R	-	-
6	84-84	174.112	R	-	-
7	189-189	174.112	R	-	-
8	226-226	174.112	R	-	-
9	230-230	174.112	R	-	-
10	248-249	203.127	GK	-	-
11	41-42	217.143	AK	-	-
12	217-218	217.143	AK	-	-
13	82-83	231.133	GR	-	-
14	163-164	231.133	GR	-	-
15	187-188	231.133	GR	-	-
16	246-247	247.153	TK	-	-
17	360-361	259.190	LK	-	-
18	125-126	261.144	SR	-	-
19	340-341	261.144	SR	-	-
20	363-364	275.148	EK	-	-
21	200-202	288.180	AAK	-	-
22	165-167	318.165	SGR	-	-
23	211-213	318.165	GSR	-	-
24	265-267	346.160	DGR	-	-
25	214-216	360.237	ITK	-	-
26	74-76	373.207	QAR	-	-
27	6-9	375.212	ATGK	-	-
28	365-367	399.259	RPK	+	-
29	227-229	412.178	YCK	-	-
30	357-359	430.229	QQR	+	-
31	287-290	443.274	VTPK	+	-
32	183-186	447.208	EGSR	+	-

Table 2.4. (continued)

	Amino acids	m/z	Sequence	Peak: Recomb-inant N	Peak: Virion N
33	133-136	473.212	DPDK	-	-
34	120-124	488.259	GADVK	-	+
35	1-5	492.237	MASGK	-	-
36	77-81	575.343	FKPGK	-	-
37	127-132	661.314	SNQGTR	-	-
38	350-356	714.366	TSSPAPR	-	-
39	231-237	774.428	TIPPGYK	-	-
40	44-50	782.429	LNSPQPK	-	-
41	258-264	819.380	MNEEGIK	-	-
42	1-6	820.492	LGGPRPPK	+	-
43	333-339	827.402	DDEPKPK	-	-
44	219-225	828.335	ADEMAHR	-	-
45	369-375	847.356	QDDEVDK	-	-
46	342-349	860.446	SSSRPATR	-	-
47	203-209	871.476	IIQDQQK	-	-
48	250-257	880.356	EGNFGDDK	+	-
49	10-18	910.512	TDAPAPVIK	-	-
50	238-245	916.477	VDQVFGPR	+	-
51	376-383	919.425	ALTSDEER	+	-
52	137-143	937.466	FDQYPLR	-	-
53	155-162	1019.576	LQPDGLHLK	-	-
54	155-162	1059.550	WDFIPLNR	+	-
55	190-199	1061.499	SGSEDDLIAR	+	+
56	300-308	1094.576	FEFTTVVPR	+	-
57	64-72	1161.532	TSQQHGYWR	+	-
58	144-154	1167.495	FSDGGPDGNFR	+	+
59	309-318	1239.541	DDPQFDNYVK	-	-
60	384-395	1418.631	NNAQLEFDDEPK	-	-
61	168-182	1431.707	STAASSAASSRPPSR	-	-
62	51-63	1438.636	FEGSGVPDNENFK	-	-
63	27-40	1450.720	VGSSGNASWFQAIK	-	+
64	319-332	1489.702	ICDQCVDGVGTRPK	-	-
65	396-409	1515.721	VINWGDSALGENEL	-	-
66	268-286	2002.013	VTAMLNLVPSSHACLFGSR	-	-
67	85-119	3857.837	KPVPDAWYFYYTGTGPAADLN WGDSQDGIVWVAAK	-	-

(+) indicates peptides that were positively identified using MALDI-TOF

(-) indicates peptides that were not identified using MALDI-TOF
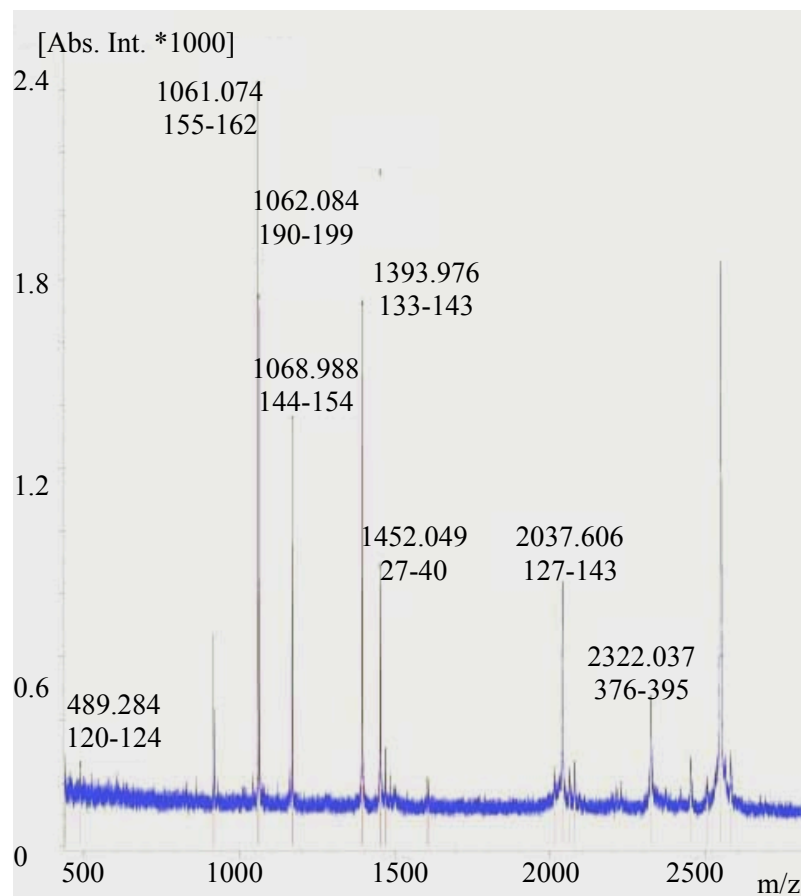
FIG. 2.8. MALDI-TOF analysis of IBV virion N protein. Seven peptides of the virion N protein that correspond to mass/charge (m/z) ratios as indicated in the figure are represented here.

Table 2.5.

Summary of the peaks assigned by MALDI-TOF analysis of the IBV N protein

	Amino Acids	Predicted m/z value	Observed m/z	Δ m/z	Sequence
A	190-199	1061.5	1062.084	0.585	SGSEDDLIAR
B	144-154	1167.5	1168.988	1.493	FSDGGPDGNFR
C	155-162	1059.55	1061.074	1.329	WDFIPLNR
D	133-143	1392.67	1393.976	1.524	DPDKFDQYPLR
E	27-40	1450.67	1452.049	1.309	VGSSGNASWFQAIK
F	376-395	2320.046	2322.037	1.991	ALTSDEERNNAQLEFDDEPK
G	120-124	488.259	489.284	1.025	GADVK
H	127-143	2037.154	2037.606	0.452	SNQGTRDPDKFDQYPLR
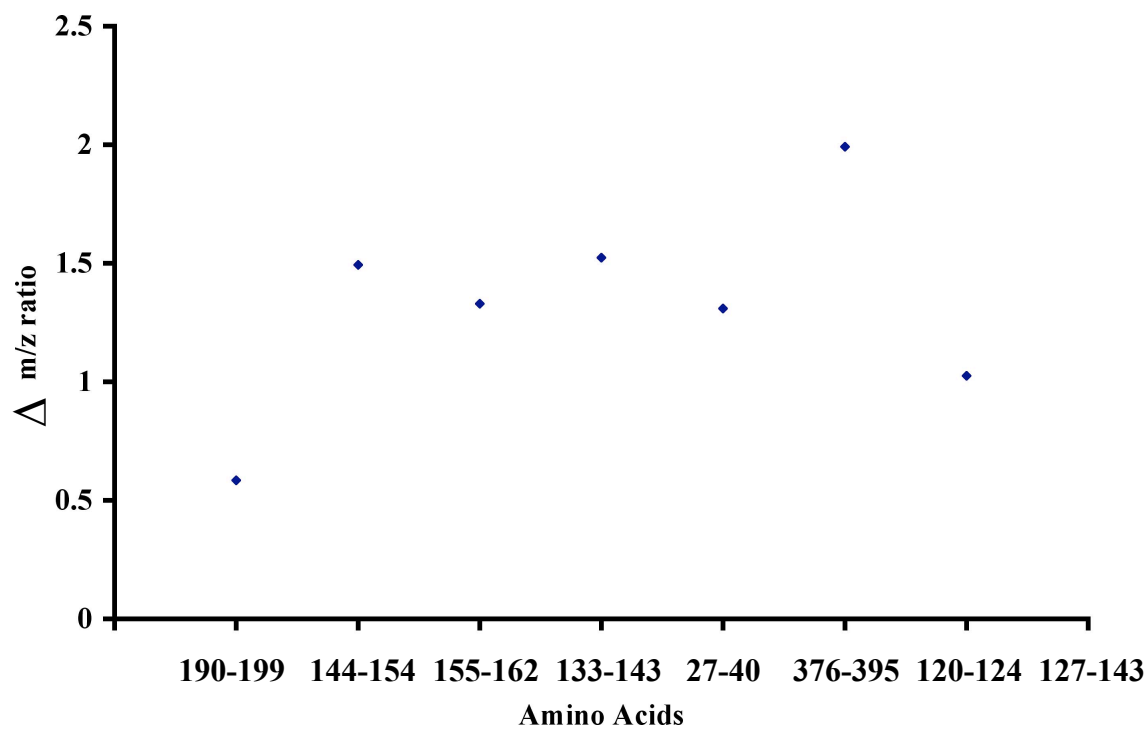
FIG. 2.9. Scatter plot comparing the predicted and obtained values of m/z ratios of some of the assigned peaks in the MALDI-TOF spectrum of the IBV virion N protein.

SGSE is a potential casein kinase II phosphorylation motif. Since the peptide constituting amino acids 190-199 was not phosphorylated, the serine in this motif is not phosphorylated. This motif was absent in the other peptides that were assigned. For the virion N protein, a scatter plot of the Δ m/z values between the predicted and observed m/z of the assigned peaks obtained from the spectrum is presented in figure 2.9. As can be seen the difference between the two values is marginal. The difference between the predicted and obtained values ranges between 0.585-1.99 Da (Table 2.5). Similar differences in m/z ratios were obtained with the recombinant IBV N protein as well (data not shown). Under the conditions tested, phosphorylated peptides of IBV N could not be identified.

DISCUSSION

Coronavirus N proteins are known to be phosphorylated, although the precise sites have not been identified and the mechanism regulating the functions of the N protein are not known. It has been postulated that phosphorylation might control the multiple functions of the N protein (Siddell *et al*., 1995). Coronavirus N has been implicated in transcription, replication, translation and packaging of the viral genome (Siddell *et al*., 1995). With an M.O.I. of 5, synthesis of MHV N protein begins around 4.5 hours post-infection (h p.i.) as determined using ^{35}S-methionine labeling (Cheley and Anderson, 1981). With an M.O.I. between 2 and 3, we find that IBV N protein synthesis can be detected around 6 hours post-infection by Western blot analysis and the N protein was phosphorylated by 6 h until at least 18 h, while cytopathic effect was observed by 14

h p.i. It is possible that differential phosphorylation might regulate the various functions of the N protein. The best way to investigate whether the IBV N is differentially phosphorylated is to isolate the N protein from the infected cell lysates at varying times during infection and identify the sites of phosphorylation by mass spectrometric analysis.

Unlike the MHV N protein, that is stable for one hour, from the results of a ^{35}S-methionine pulse-chase experiment; the IBV N protein was stable for at least a two-hour period (Perlman *et al.,* 1986). The stability of phosphate on the N protein might give an indication of how quickly it is removed from the protein. The phosphate on the protein might be present for very long periods or it might be removed very quickly. Our results show that the labeled phosphate on the protein reached a maximum level of incorporation only when chased for two hours which is probably due to a delay in chasing the intracellular phosphate pool, and then the level dropped down to 70% of this maximum value when chased for another hour. It is possible that even this change in the level of phosphorylation might affect the function of the IBV N protein. It is also likely that differential phosphorylation actually regulates the functions of the IBV N protein.

The IBV N protein for the pulse-chase analysis experiments was isolated by immunoprecipitation using saturating amounts of rabbit polyclonal antibody to the N protein such that it precipitated both labeled and unlabeled N protein from infected cell lysates. All analyses were carried out based on duplicate sets of experiments and gave nearly identical results. MHV M has been shown to co-precipitate with N using anti-MHV N monoclonal antibody (Narayanan *et al.*, 2000). With BCoV, rabbit polyclonal

antibody to N does not co-precipitate M in infected cells (Nguyen and Hogue, 1997). In our experiments, no other proteins co-precipitated with IBV N using the rabbit-anti-N polyclonal antibody. This may be due to differences in the cell type, lysis buffer, as well as antibody used for immunoprecipitation.

Double labeling studies with ^{32}P-orthophosphate and ^{3}H-leucine suggest that the virion N protein is more phosphorylated than the cellular N protein. The ^{32}P:^{3}H cpm ratio of the virion N protein from Vero cells is greater than the ratio from CEK cells. A small difference in electrophoretic mobility between the virion and cellular N protein, with the virion N protein of slightly greater molecular mass, is observed by SDS-PAGE analysis indicative of additional modification of the virion N protein. In the case of measles virus, nucleoprotein phosphorylated on both serine and threonine is preferentially assembled into the nucleocapsids (Gombart et al., 1995). Consistent with our results, greater phosphorylation possibly increases the binding of N protein to viral RNA for packaging or assembly into nucleocapsids. In the case of Chandipura virus, homodimerization of the phosphoprotein (P) protein occurs via the N-terminal 46 amino acids of the protein and occurs only after phosphorylation of this region (Raha et al., 2000). A global conformational change in the N-terminal domain of the P protein is induced by phosphorylation (Raha et al., 1999). It is possible that phosphorylation of the IBV N protein induces some kind of a conformational change thereby promoting N-N interaction. This N-N interaction may be important in RNA binding, in nucleocapsid assembly and in compacting the nucleocapsid. Narayanan et al. (2003) showed that the MHV N protein in the virion nucleocapsid and in the intracellular genome-length RNP

complexes that bound to the viral M protein was tightly self-associated, such that its association was retained even after extensive RNAse A treatment. This was not the case with RNP complexes formed with subgenomic RNA (Narayanan *et al.*, 2003b). It is highly likely that the hyperphosphorylated form of the IBV N protein binds genomic RNA in association with other viral proteins thereby forming tight complexes that are compact and resistant to RNase A treatment. Phosphorylation of the N protein might also affect IBV infectivity. A protein kinase activity was found associated with purified virus preparations of MHV, indicating the presence of a kinase in the virion (Siddell *et al.*, 1981). Studies carried out with JHM strain of MHV (JHMV) showed that dephosphorylation of the nucleocapsid protein of JHMV may be essential for initiating the virus replication cycle (Kalicharran and Dales, 1995). In the case of cauliflower mosaic virus, mutation of the capsid protein phosphorylation sites from serine to alanine abolished infectivity (Chapdelaine *et al.*, 2002). As suggested earlier, the hyperphosphorylated form of the protein might be required for the formation of a compact nucleocapsid. It is possible that dephosphorylation of the N protein might therefore be required to unravel the nucleocapsid making the genome more accessible to RNA dependent RNA polymerase. The ^{32}P:^{3}H cpm ratio of the IBV virion N protein from Vero cells is 7 times more than the ratio of the virion N protein from CEK cells. CEK cells are primary cells whereas Vero cells are a cell line. Also, Vero cells are primate kidney cells and CEK cells are avian kidney cells. There might be a higher level of activity of kinases in the cell line that contribute to these observed differences. CEK

cells produce interferon whereas Vero cells do not produce interferon. Hence, the differences between the cell types might cause this variation.

Viral proteins have been shown to be phosphorylated *in vitro* by casein kinase II (Bontems *et al.*, 2002). Based on sequence gazing, two potential casein kinase II and four potential cAMP and cGMP dependent protein kinase phosphorylation sites were identified on the IBV N protein. In order to determine the sites of phosphorylation, MALDI-TOF mass spectrometry analysis was performed with the IBV virion N protein. With the recombinant IBV N protein expressed in bacteria, 13 tryptic peptides could be assigned to peaks. A partial tryptic digest was obtained with the bacterially expressed protein. In the case of the virion N protein, due to a partial tryptic digest, only eight tryptic peptides could be assigned in the MALDI-TOF spectrum and none of these were phosphorylated. For future analysis the following points need to be considered. Very few peaks of predicted peptides in the m/z range of 400 Da to 900 Da were obtained in the analysis, possibly due to ion suppression which is a phenomenon where the presence of salts, detergents, urea, glycerol or too much of starting sample can interfere in the formation of ions. Even if the protein is digested into peptides, these non-ionized species cannot reach the detector. A partial digest could also result in a situation where predicted tryptic peptides are missing from the MALDI-TOF spectrum. Approximately 200 ng of N protein were used in our analysis. Since the IBV N protein is rich in lysine and arginine residues, a higher trypsin:substrate stoichiometry or a longer digestion time should be employed to ensure a complete digest. In our analysis, several peaks were obtained in the m/z ratio of less than 200 Da. This might have been due to the use of a

high laser output power. However, effective use of laser power is required to achieve ionization of all peptides especially the larger ones. Calibration of the instrument is also critical in the analysis of the results. We used a linear calibration that identified predicted peptides in the MALDI-TOF spectrum that were greater by mass between 0.585-1.99 Da. In the future, the use of a quadratic calibration will give more accurate results of m/z ratios over the range of the standards used. Several modifications of amino acids occur during sample preparation, which change the m/z ratio of the peptide. These mass differences must be taken into account when carrying out the analysis. Commonly occurring modifications are change of N to D, oxidation of methionine and conversion of cysteine to Carbamidomethyl, Carboxymethyl, Propionamide or S-pyridylethyl.

Kinase inhibitors have been used to determine the role of phosphorlyation in the virus life cycle. Kinases affect various cellular functions and hence the use of inhibitors to kinases is likely to have either a direct or indirect or no effect on the virus life cycle. In our studies, U0126, a specific serine-kinase inhibitor did not have any effect on the phosphoryaltion of the IBV N protein.

An infectious cDNA clone has now been constructed (Youn, 2003) and is also readily available. Once the N protein phosphorylation sites have been identified site-specific mutagenesis is a more appropriate approach to determine the role of IBV N protein phosphorylation in the virus life cycle.

CHAPTER III

INFECTIOUS BRONCHITIS VIRUS BACTERIALLY EXPRESSED

RECOMBINANT NUCLEOCAPSID PROTEIN PRODUCES HELICAL

STRUCTURES IN THE ABSENCE OF OTHER VIRAL STRUCTURAL

PROTEINS

IBV has four structural proteins: the spike (S) protein that is important in cell entry, the membrane (M) protein that can interact with the small envelope (E) protein to form virus-like particles and the nucleocapsid (N) protein that binds the viral genome to form a helical nucleocapsid (Davies *et al.*, 1981; Lomniczi and Morser, 1981; Macnaughton and Madge, 1977). The M protein is the most abundant glycoprotein in the virus (Siddell *et al.*, 1995). The E protein is present in very small amounts in the infected cell as well as in the virion. Virus assembly requires the interaction of the helical nucleocapsid with the M, E and S proteins to form the complete virus (Spaan *et al.*, 1981; Stohlman *et al.*, 1983). M and E proteins interact with each other and also with the S protein. M also interacts with the N protein as has been shown by co-immunoprecipitation in MHV and BCV infected cells (Corse and Machamer, 2003; Escors *et al.*, 2001; Kuo and Masters, 2002; Narayanan *et al.*, 2000; Nguyen and Hogue, 1997). The N protein binds genomic as well as subgenomic RNA as shown by immunoprecipitation studies (Stohlman *et al.*, 1988). Although subgenomic RNA is packaged in very small amounts in IBV and TGEV, the genome is the predominant

packaged RNA in coronaviruses. The presence of a packaging signal sequence has been shown to confer packaging of non-viral RNA in TGEV, MHV and BCV. This sequence is present at the 3' end of the pol 1b region in BCV and MHV and in the 5'- untranslated region in TGEV (Cologna and Hogue, 2000; Escors *et al.*, 2003; Woo *et al.*, 1997). The MHV M protein can bind this sequence in the absence of the N protein. It is speculated that the M protein is responsible for the specificity of packaging (Narayanan *et al.*, 2003a; Narayanan *et al.*, 2000; Vennema *et al.*, 1996).

Although it is not known if formation of the helical nucleocapsid requires the presence of other viral structural proteins, nucleocapsid proteins have a tendency to oligomerize, a property that is important for assembly into a nucleocapsid (Alfadhli *et al.*, 2001; Baron and Forsell, 1991; Sandalon and Oppenheim, 1997; Wootton and Yoo, 2003). Nucleocapsid proteins of measles virus, rabies virus, Newcastle disease virus, human immunodeficiency virus (HIV) and respiratory syncytial virus (RSV) form nucleocapsid-like structures when expressed in *E. coli* or Sf9 cells. RNA has been found associated with the nucleocapsid-like structures formed by the heterologous expression of the nucleocapsid proteins of these viruses (Errington and Emmerson, 1997; Fooks *et al.*, 1993; Gross *et al.*, 1997; Iseni *et al.*, 1998; Murphy *et al.*, 2003). Herein, electron microscopy results show that recombinant IBV N protein expressed in *E. coli* also forms nucleocapsid-like structures that resemble extended nucleocapsid structures isolated from the virus.

MATERIALS AND METHODS

Expression and purification of the IBV recombinant nucleocapsid (N) protein and N protein polypeptides

The N gene and several truncations of the N gene were cloned into the pQE8 vector and expressed as a histidine tagged protein in *E. coli* M15 cells (Zhou *et al.*, 1996). Fifty ml of an overnight culture of bacteria grown in SOC medium (Sambrook *et al.*, 1989) containing 50 μg/ml ampicillin and 25 μg/ml kanamycin were inoculated into 450 ml SOC medium containing the same antibiotics. The bacteria were cultured at 37°C on a shaker at 200 rpm for three hours. Protein expression was induced with IPTG at a final concentration of 2 mM. The bacteria were cultured for another five hours at 37°C on a shaker at 200 rpm and harvested by centrifuging at 3000 g. The pellet was suspended in non-denaturing buffer (0.05 M Tris, pH 8, 0.3 M NaCl, 0.01 M imidazole). Lysozyme was added at a final concentration of 0.1 mg/ml and the sample was incubated on ice for 30 minutes. The sample was lysed on ice by sonication at a 100 W power output, 10 s pulses, six times with 10 s intervals. The sample was centrifuged at 5000 rpm at 4°C for 10 minutes, in a JA 21 rotor. The supernatant was collected and 1 ml of a 50% Ni^{+2}-NTA resin (Qiagen, Chatsworth, CA) was added to every 10 ml of cell lysate. The mix was incubated on a shaker at 4°C for one hour. The resin was collected by centrifuging at 1800g, in a Joun CR412 centrifuge at 4°C for 1 minute and washed three times with 10 ml of wash buffer (0.05 M Tris, pH 8, 0.3 M NaCl, 0.02 M imidazole). The protein was eluted from the resin with 1 ml of elution buffer (0.05 M Tris, pH 8, 0.3 M NaCl, 0.25 M imidazole). Approximately 3 mg of N protein were obtained per 500 ml

of bacterial culture. Polypeptides equal to, or greater than, 274 amino acids were further purified by gel permeation chromatography using a Sephadex G200 (16/100 column specifications) (Sigma, St. Louis, MO) or Superdex 200 (16/60 column specifications) (Amersham Biosciences, Piscataway, NJ) column while peptides equal to or smaller than 207 amino acids were purified with Bio-gel P60 (Bio-Rad, Richmond, CA) in a column of 1.6cm inner diameter and 100cm length. Five ml of each sample were loaded onto the column before washing with Tris buffer (Tris 0.05 M pH 8, 0.3 M NaCl). Fractions were monitored with the Bio-Rad protein assay reagent (Bio-Rad, Richmond, CA), and the fractions containing protein, were analyzed by 15% polyacrylamide gel electrophoresis (Sambrook *et al*., 1989). Protein used for electron microscopy was dialyzed in HEPES buffer (25 mM HEPES, 25 mM EDTA, 150 mM NaCl, 5 mM DTT and 5% glycerol).

Western blot assays were used to determine the viral specificity of the recombinant polypeptides (Sambrook *et al*., 1989). Briefly, varying amounts of the proteins were separated by 15% polyacrylamide gel electrophoresis and blotted onto nitrocellulose membranes. After blocking the membranes with 5% skim milk in Tris buffered saline (TBS, pH 7), the membranes were reacted sequentially with chicken anti-IBV Gray serum and alkaline phosphatase conjugated goat anti-chicken IgG (KPL, Gaithersburg, Maryland).

Electron microscopy of IBV N protein and N polypeptides

Specimen preparation was performed according to Valentine (1968) and the droplet on the grid method (Hoppert and Holzenburg, 1998). For the droplet method, 5 µl of various protein preparations in HEPES buffer (25 mM HEPES, 5 mM EDTA, 150

mM NaCl, 5 mM DTT, 5% glycerol) at a concentration of 0.1 mg/ml were placed on glow-discharged carbon-formvar coated copper grids for 30 s. The excess liquid was blotted, and the grids were washed with distilled water. Samples were negatively stained using a 2% (w/v) aqueous solution of uranyl acetate. Specimens were observed using a JEOL 1200 EX transmission electron microscope at an acceleration voltage of 80 kV and micrographs were recorded at a calibrated magnification of 40,000.

An attempt was made at obtaining monodisperse, single particles of the IBV full-length N protein. HEPES buffer (25 mM HEPES, 5 mM EDTA, 150 mM NaCl, 5 mM DTT, 5% glycerol) with various concentrations of magnesium (10 mM, 20 mM, 40 mM, 50 mM, 60 mM, 70 mM, 80 mM, 90 mM and 100 mM) ions were incubated for 20 minutes at room-temperature following which the samples were used for N protein preparation for electron microscopy.

Thin sections of *E.coli* expressing the IBV recombinant N protein

Induced and uninduced bacterial preparations were fixed in 2.5% glutaraldehyde in 0.1 M sodium cacodylate-HCl buffer, pH 7.4 for 1 hour at room temperature (R.T.). The bacterial specimens were then pelleted by centrifugation and washed 3X, 15 min with 0.1 M cacodylate buffer, pH 7.4. Pellets were post fixed overnight at 40°C with 1% osmium tetroxide in 0.1 M cacodylate buffer, pH 7.4. Pellets were washed with 0.1 M cacodylate buffer followed by dehydration in an ethanol series (20, 40, 60, 80, 90, 100% X 2) to propylene oxide. Specimens were then infiltrated and embedded in Araldite-Quetol 651 epoxy resin (Ellis, 2002). Ultra thin sections on 200 mesh copper grids were post stained with 2% aqueous uranyl acetate followed by Reynolds lead citrate

(Reynolds, 1963). Grids were examined and photographed at an accelerating voltage of 80 kV in a JEOL 1200 EX transmission electron microscope (TEM).

Isolation of radiolabeled RNA from IBV recombinant N protein

An overnight culture of *E. coli* containing the N gene expression construct was grown in Tris-glucose medium (Tris 120 mM, NaCl 80 mM, KCl 20 mM, NH_4Cl 20 mM, Na_2SO_4 3 mM, $MgCl_2$ 1 mM, $CaCl_2$ 0.2 mM, $FeCl_3$ 2 mM and Glucose 20%) containing 100 mM phosphate and 25 μg/ml kanamycin and 50 μg/ml ampicillin at 37°C at 200 rpm on a shaker. This culture was added to fresh Tris-glucose medium (without phosphate and with the above mentioned antibiotics) to bring it to an optical density of 0.5. The bacteria were grown at 37°C on a shaker at 200 rpm for three hours following which protein expression was induced with isopropyl-β-D-thiogalactoside (IPTG) at a final concentration of 2 mM. The bacteria were cultured for another five hours at 37°C on a shaker at 200 rpm in the presence of 100 μCi/ml ^{32}P-orthophosphate and the bacteria were harvested by centrifuging at 3000 g. The pellet was processed to purify the histidine-tagged-fusion-proteins under native conditions as described in the Qiagen manual (Qiagen, Chatsworth, CA). RNA was extracted from the N-protein using TRIZOL (Invitrogen, Carlsbad, California) and analyzed by denaturing agaorse gel electrophoresis. Following electrophoresis the gel was dried and exposed to an imaging plate (Fuji Medical Systems, Stamford, CT). RNA from *E.coli* DH5α lacking any vector, induced with IPTG and RNA from uninduced *E.coli* containing the N gene expression construct were used as controls. The procedure for RNA isolation from the controls was identical to that of the test.

RESULTS

Protein preparation

Full length IBV N and its truncation mutants were expressed in *E. coli* (Zhou *et al.*, 1996). N represents whole IBV N protein, N91 represents amino acids 1 to 91, N171 represents amino acids 1 to 171, M173 represents amino acids 101 to 283, C207 represents amino acids 203 to 409 and C140 represents amino acids 268 to 407 of IBV N protein respectively (Fig. 3.1). The polypeptides were used to identify an RNA binding region of the IBV N protein (Zhou *et al.*, 1997). Recombinant polypeptides were first purified by Ni^{2+}-NTA chromatography**.** SDS-PAGE indicated that the samples eluted from the Ni^{2+}-NTA resin were impure (Fig. 3.2). Therefore, N and C207 were further purified with Superdex-200 and Sephadex G-200 respectively, and polypeptides equal to or less than 171 amino acids, C140 and N171 were further purified with a Bio-gel P60 column (Zhou *et al.*, 1996). The column matrices were selected based on the ability to resolve proteins depending on molecular mass.

The further purified proteins were analyzed by SDS-PAGE. Qualitative analysis of each sample showed that the samples contained the polypeptide of expected molecular weight. C207 and full-length N (Fig 3.3) contained additional proteins slightly smaller than the expected molecular weight. The smaller peptides also reacted with the chicken anti-IBV Gray polyclonal antibody in Western blot analyses (data not shown).

Nucleocapsid protein (N)
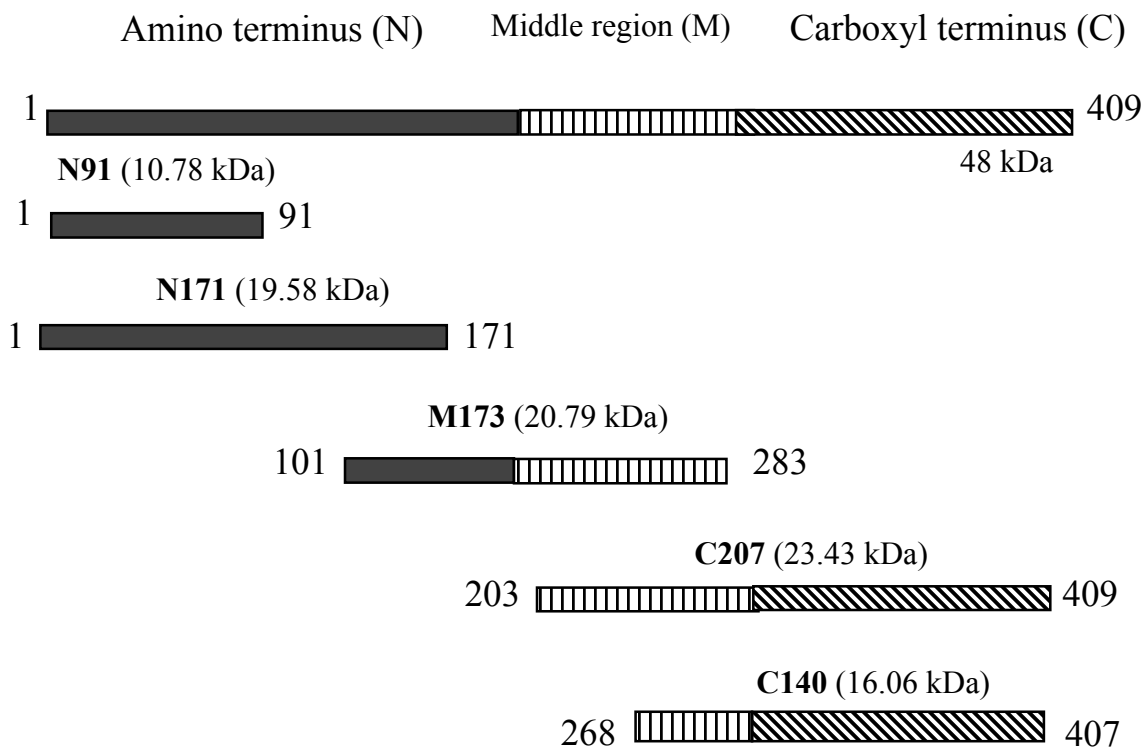
FIG. 3.1. IBV N protein and N-based polypeptides expressed in *E. coli*. Peptides corresponding to the amino terminus and carboxyl terminus are designated . Full-length IBV N is approximately 48 kDa in molecular mass. The predicted molecular mass of N-based polypeptides is given in parenthesis. The number following N, C, and M correspond to the length, in amino acid residues, of the polypeptides. All fragments had an N-terminal polyhistidine tag from the expression plasmid (Qiagen, Chastworth, CA).
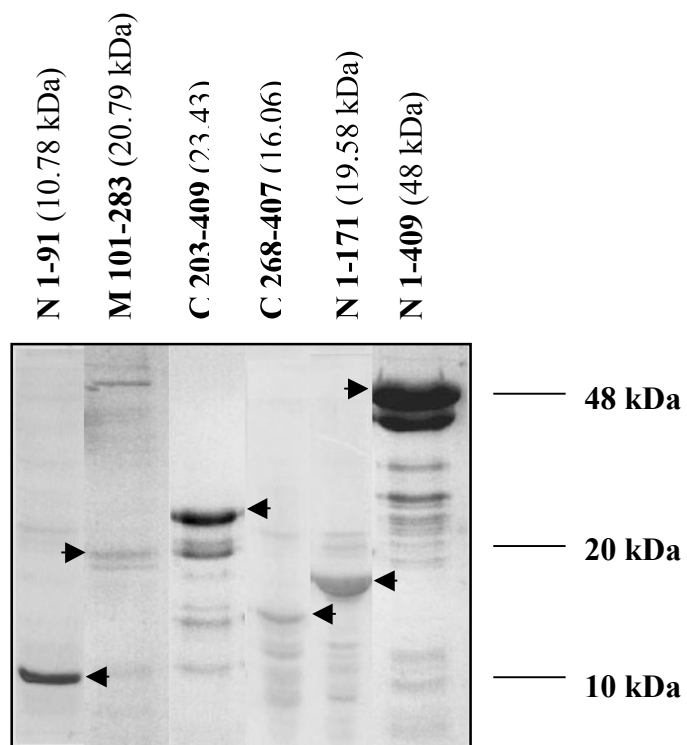
FIG. 3.2. SDS-PAGE analysis of IBV N and polypeptides obtained after Ni^{+2}-NTA chromatography. The gel was stained with Coomassie Brilliant Blue R250. Various amounts of the polypeptides were resolved by 15% SDS-PAGE.
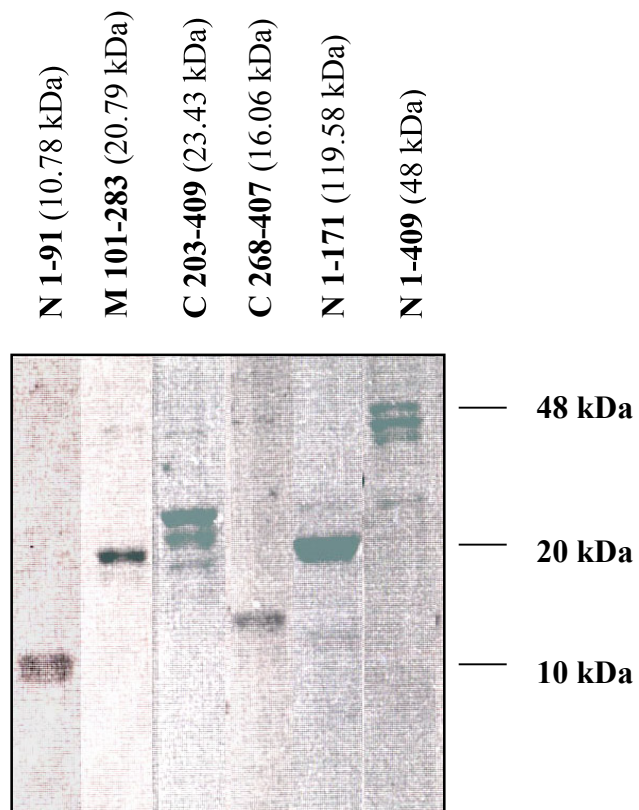
FIG. 3.3. SDS-PAGE analysis of IBV N and truncations thereof after gel-filtration column chromatography. Various amounts of the polypeptides were resolved by 15% SDS-PAGE. The gel was stained with Coomassie Brilliant Blue R250.

The smaller proteins are probable truncations or degradation products. Gel permeation chromatography of IBV N protein through a Superdex 200 matrix resolved four peaks of protein eluting from the column (Table 3.2). Peak 1 corresponded to approximately a 443 kilodalton (kDa) complex eluting from the column at approximately 53.5 minutes as compared to the molecular weight standards also separated by gel permeation chromatography (Tables 3.1 and 3.2 and Fig. 3.4 and Fig. 3.5). Peaks 2, 3 and 4 correspond to proteins much smaller than IBV N (less than 48 kDa) (Fig. 3.4 and Fig. 3.5). No peak corresponding to a 48 kDa molecular mass was obtained. The recombinant N protein degrades over time and hence an abundant peak for the smaller products was obtained (Fig. 3.4).

Electron microscopy (EM)

Since IBV N protein, present in peak 1 corresponded to a very high molecular mass, it was of interest to determine if any structures are formed by IBV N protein. IBV N protein was negatively stained with 2% uranyl acetate and observed by electron microscopy. Aggregates and helical structures of lengths varying from 50 nm to 500 nm and diameters from 6 to 10 nm were found in each of over ten preparations (Fig 3.6). Each grid typically contained 6 to 10 such structures along with N protein aggregates (Fig. 3.6). The size of the IBV virion itself is approximately 100-120 nm in diameter. This suggests that certain other factors are important in compressing the helical nucleocapsid to be encased into the virion or in limiting the growth of the helix.

It was of interest to determine if truncations of IBV N protein are capable of forming these helical structures. Truncations of IBV N that corresponded to the amino

Table 3.1.

Gel permeation chromatography: Elution profile of molecular weight standards (Tris 0.05 M pH7, 0.15 M NaCl) using superdex 200 gel matrix in an HR 16/60 column

Elution time in minutes	Molecular weight (kDa)
48.6	669
53.8	443
60.8	200
66	150
74	66
88.3	29

Table 3.2.

Peaks after gel permeation chromatography of IBV recombinant N protein (Tris 0.05 M pH7, 0.15 M NaCl) using superdex 200 gel matrix in an HR 16/60 column

Elution time in minutes	Peak number
53.5	1
92.5	2
116	3
122.54	4
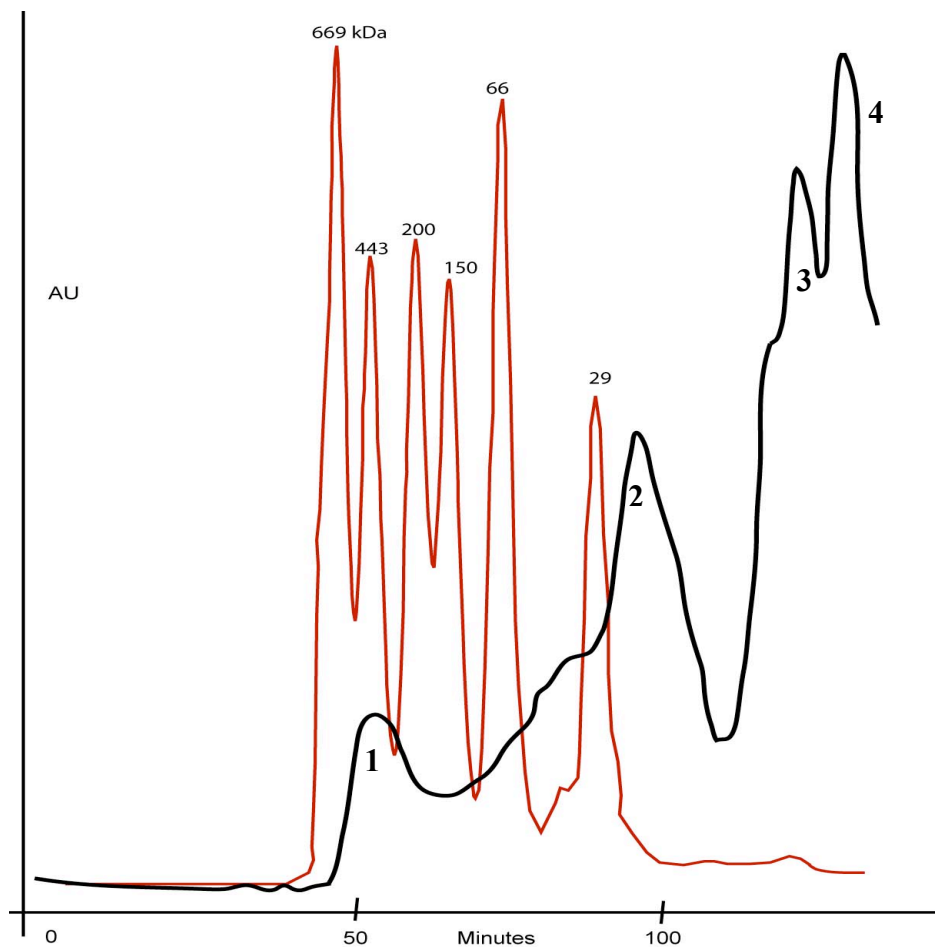
FIG. 3.4. Elution profile of Ni^{+2}-NTA chromatography purified IBV N protein using a Superdex-200 matrix in a 16/60 column. Peak1 corresponds to a molecular mass of approximately 443 kDa as compared to the molecular-weight standards (each standard peak is labeled with the corresponding molecular mass). Peaks 2, 3, and 4 are much smaller than 48kD, the predicted molecular weight of monomeric IBV N protein.
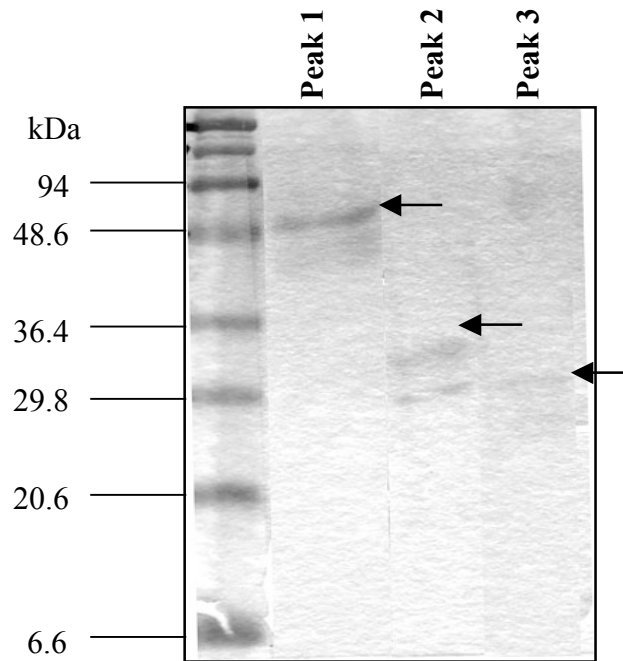
FIG. 3.5. SDS-PAGE analysis of IBV recombinant N protein obtained from fractions eluted from the Superdex-200 (16/60) column. Lane 1, SDS-PAGE molecular weight markers; lane 2, peak 1; lane 3, peak 2 and lane 4, peak 3. Small arrows represent the major protein in the gel lane eluted from the column.

terminal 91 amino acids (N91), amino terminal 171 amino acids (N171), amino acids 101-283 (M173), amino acids 203-409 (C207) and amino acids 268-407 (C140) (Fig 3.1) that had been expressed as histidine tagged fusion proteins (Zhou *et al*., 1996) were negatively stained with 2% uranyl acetate and examined by TEM. These truncations had been used to determine the RNA binding region of the N protein. Except for N91 and M173, all truncations bound the 3'-UTR of IBV as studied using the gel shift assay (Zhou *et al*., 1996). The truncations formed a few protein aggregates similar to that seen in figure 3.6, but no helical structures were observed in the preparations of the truncations (Table 3.3) used for TEM studies.

N protein of several different viruses can form oligomeric structures that are precursors to forming the nucleocapsid. The structures of these oligomers have been determined using single particle image reconstruction of electron microscopic images (Murphy *et al.*, 2003; Schoehn *et al.*, 2001). It was of interest to determine if recombinant IBV N forms such oligomers. Single particle image reconstruction involves constructing a three-dimensional image of a macromolecule typically larger than 500 kDa from electron microscopic images of single particles of the macromolecule. Single particle structure determination typically begins with preparation of a homogenous sample that is placed on an electron microscope grid and prepared for imaging (Thuman-Commike, 2001). TEM studies of the IBV recombinant N protein showed that it consisted of protein aggregates in addition to helical structures, suggesting that it is not a homogenous preparation.

Table 3.3.

RNA binding (as determined using gel-shift assay) (Zhou *et al*., 1996) and ability to form nucleocapsid-like structures by IBV N and its polypeptides

Amino acids	RNA binding to 3'-UTR	Ability to form nucleocapsid-like structures
1-409 (N)	+	+
1-91 (N 91)	-	-
1-171 (N 171)	+	-
101-283 (M 173)	-	Not tested
203-409 (C 207)	+	-
268-407 (C140)	+	-
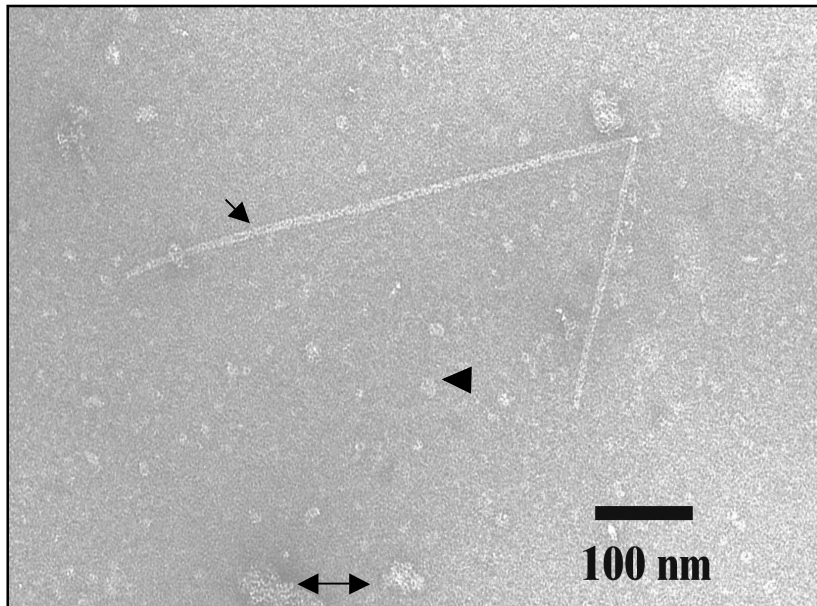
FIG 3.6. Analysis by TEM of affinity-purified IBV recombinant N protein expressed in *E. coli*. The arrow points to the helical nucleocapsid-like structure formed by IBV N protein negatively stained with 2% uranyl acetate. The arrowhead points to small aggregates and the double headed arrow points to large aggregates. The length varies from 50 to 600 nm and the diameter varies from 6 to 10 nm. The bar below represents 100 nm.

A homogenous preparation can be achieved by modifying the type and concentration of ions. As a preliminary analysis, HEPES buffer with varying concentrations of magnesium ions was used to determine the conditions to obtain a homogenous preparation for single particle formation of recombinant IBV N protein. At 10 and 20 mM Mg^{+2} concentrations, large and small aggregates were visible (data not shown). Above 40 mM Mg^{+2} concentrations, and up to 100 mM Mg^{+2} concentrations, a more homogenous preparation without aggregates was obtained. No oligomers were formed under these conditions. High concentrations of magnesium probably destabilize the nucleocapsid-like structures. Other ions should be used to determine the conditions for single particle formation of recombinant IBV N protein.

Thin section preparation of *E.coli* expressing the IBV N protein

Negatively stained thin sections of Sf9 cells expressing the rabies virus nucleocapsid protein showed the presence of helical nucleocapsid-like structures (Pinto *et al.*, 1994). To determine if such structures are visible in *E.coli* preparations expressing the IBV N protein, thin sections of induced and uninduced preparations of bacteria were stained with 2% uranyl acetate and Reynold citrate and observed by TEM. No nucleocapsid-like structures were observed within the thin sections of the induced bacterial preparations (Fig. 3.7B). Fine detail was not clear within both uninduced and induced bacterial preparations (Figures 3.7A and 3.7B) when studied at 40,000X or 80,000X magnification, probably due to dense packing of cell contents. At least five grids of both induced and un-induced preparations of bacteria were studied using TEM. Using bacterial lysates might be a better alternative than whole cells to determine the
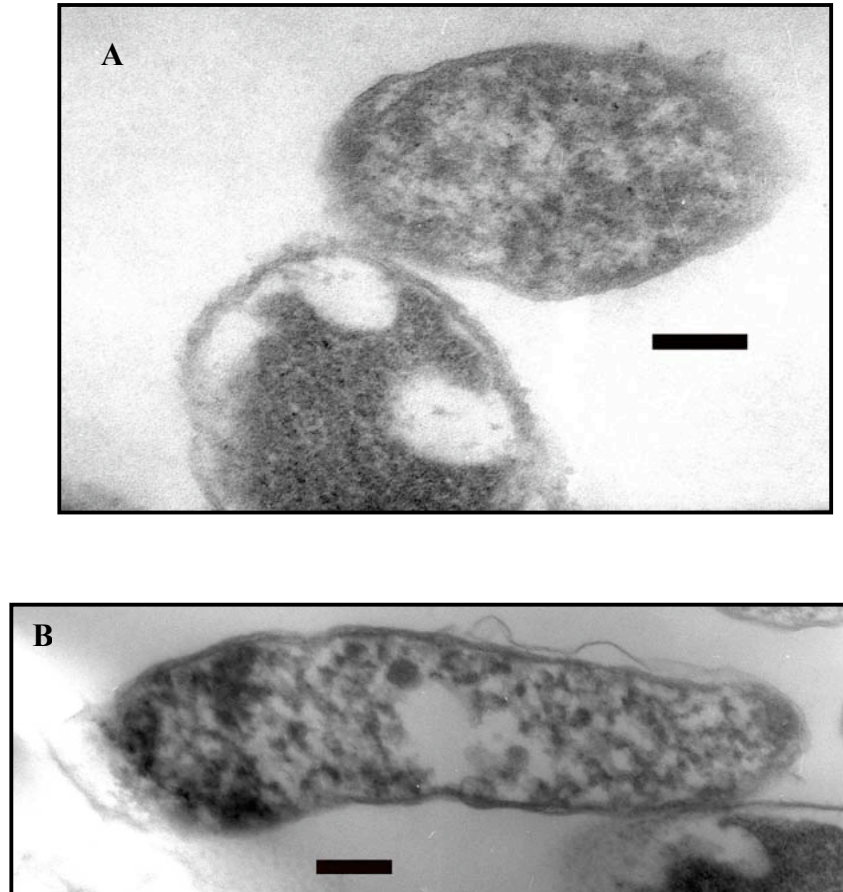
FIG 3.7. TEM images of thin sections of (A) uninduced *E. coli* and (B) induced *E.coli* expressing IBV recombinant N protein using a JEOL 1200 EX transmission electron microscope at an accelerating voltage of 80kV. The bar represents a scale of 100 nm.

presence of these structures in *E. coli*.

Determination of RNA in IBV N protein preparations

Nucleocapsid proteins have a tendency to self assemble and form regular structures in the presence of RNA or DNA (Pinto *et al.*, 1994; Spehner *et al.*, 1991; Warnes *et al.*, 1995). The carboxyl region (C140) of IBV N also forms oligomers as observed by gel permeation chromatography through a BioGel-P60 column. Most of the protein elutes in the void volume of the column indicating the presence of a large complex (data not shown). IBV N is an RNA binding protein (Zhou *et al.*, 1996). To determine if RNA from *E.coli* was associated with the affinity purified N preparations, the nucleic acid was *in vivo* labeled with ^{32}P-orthophosphate during N protein induction. The nucleic acid associated with Ni^{+2}-NTA affinity purified N protein was isolated using TRIZOL reagent. RNA is present in the aqueous phase and the DNA and protein are present in the phenol-chloroform phase. The nucleic acid isolated from the aqueous phase was split in to three parts and two parts were treated with 10 μg RNase A and 2 U DNase I respectively, to determine the nature of the nucleic acid associated with the N protein. Denaturing agarose gel electrophoresis showed the presence of nucleic acid associated with N protein from both uninduced and induced bacteria (Fig. 3.8). Higher amounts of nucleic acids were found associated with samples from induced bacteria as compared to samples from uninduced bacteria. Leaky expression of N protein in the uninduced bacteria can account for the low levels of nucleic acid associated with the preparation. For both uninduced and induced preparations, RNase A treatment degraded the RNA completely, however DNase I treatment (Fig. 3.8) showed a marginal decrease
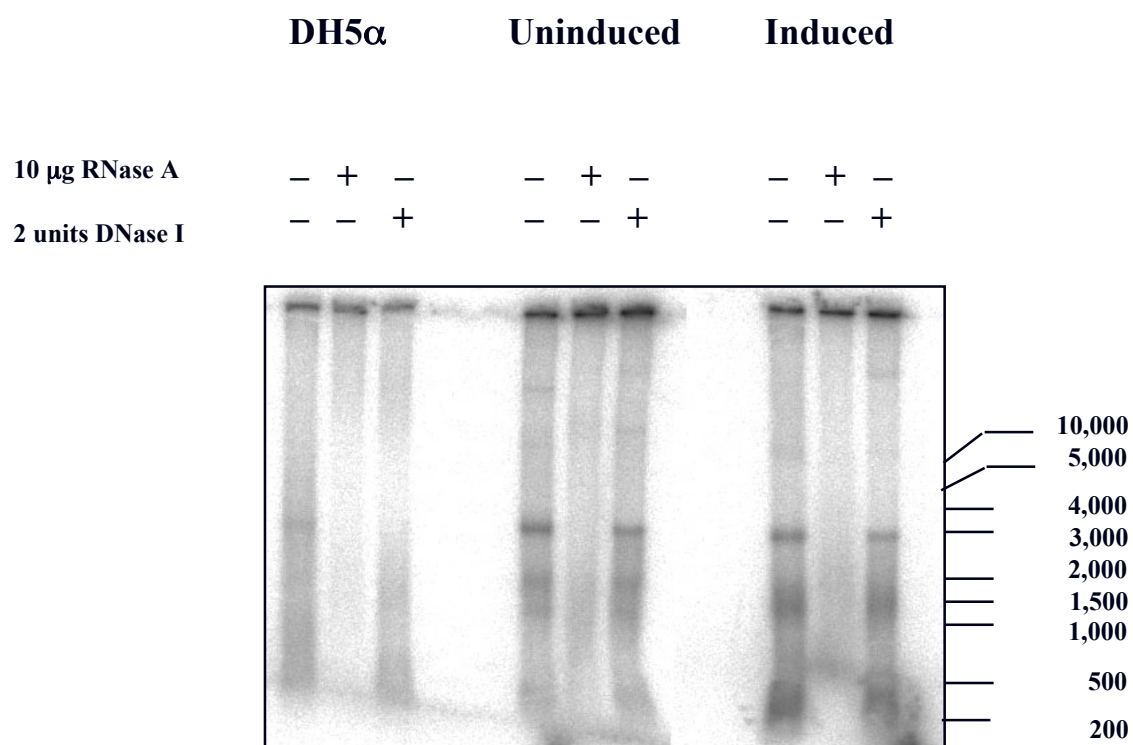
FIG. 3.8. Analysis of presence of RNA in preparations of IBV recombinant N protein purified by affinity chromatography. RNA isolated by Trizol extraction from induced *E. coli* DH5α cells lacking any expression construct, from uninduced bacteria containing the N-gene expression construct, and from bacteria containing the N-gene expression construct induced with 2 mM IPTG.

in the intensity of the bands, which may have been due to a contamination of RNase A or due to the presence of small amounts of DNA associated with the N protein. Small amounts of nucleic acid were isolated from the *E. coli* DH5α cells (Fig. 3.8). The nucleic acid was either RNA or DNA as shown by absence of bands in the samples treated with RNase A or DNase I respectively. The sizes of the RNA obtained from uninduced and induced *E. coli* containing the N gene expression construct were close to 3000, between 1000-1500 and between 200-500 nucleotides (Fig. 3.8). The N gene transcript is 1254 nucleotides in length. The 23S, 16S, and 5S ribosomal RNA (rRNA) from *E. coli* K12 measure 2904, 1543, and 120 nucleotides respectively in length (Blattner *et al*., 1997). The sizes of the RNA associated with the N protein are very close to the sizes of the N gene transcript, 23S and 16S ribosomal RNA. Higher levels of nucleic acid corresponding to 1000-1500 and 200-500 nucleotides (nt) in length were found associated with the induced preparation as compared to the uninduced preparation. IBV N has been shown to bind to its own transcript as well as to non-IBV RNA (Zhou *et al*., 1996). It is possible that the nucleic acid bound to IBV N is the N gene transcript (1254 nt) and/or E. coli 16S rRNA (1543 nt) and other *E. coli* RNA (200-500 nt). Hence, it is possible that RNA is present in the helical-nucleocpasid-like structures observed in the recombinant N protein preparations. RNase A-gold immunolabeling of the structures followed by TEM can conclusively determine the presence of RNA in these structures.

DISCUSSION

The IBV nucleocapsid protein binds viral RNA forming a helical nucleocapsid that interacts with other structural proteins to assemble the complete virion (Davies *et al.*, 1981). Using electron microscopy, we showed that the IBV recombinant nucleocapsid protein expressed in *E.coli* also forms helical nucleocapsid-like structures devoid of other viral structural proteins. When individual, overlapping fragments of the N protein were examined such helical structures were not obtained. This suggests that formation of the helical structures depended on the full length N protein. RNA binding studies have demonstrated that the amino and carboxyl regions of the N protein bind RNA (Zhou *et al.*, 1996). Other experiments with C140 suggest that it aggregates and hence may be important in N interacting with itself. These results once again are consistent with the full length N protein being important in formation of the nucleocapsid-like structure. Nucleocapsid proteins of several viruses are known to self-assemble or in the presence of other viral proteins, to form nucleocapsid-like structures (Errington and Emmerson, 1997; Fooks *et al.*, 1993; Gross *et al.*, 1997; Iseni *et al.*, 1998; Murphy *et al.*, 2003).

Nucleocapsid assembly in measles virus, rabies virus, Newcastle disease virus, human immunodeficiency virus (HIV) and respiratory syncytial virus (RSV) occurs when expressed in Sf9 cells or in *E.coli* in the presence of non-viral RNA (Errington and Emmerson, 1997; Fooks *et al.*, 1993; Gross *et al.*, 1997; Iseni *et al.*, 1998; Murphy *et al.*, 2003). However, it is not known if RNA is present in the nucleocapsid-like structures formed by the IBV N proteins. RNA is associated with the N protein preparation as

confirmed by the sensitivity of the co-purifying radiolabeled nucleic acids isolated from the N protein preparation to RNase A. Small amounts of DNA may also be present in the preparation due to the sensitivity of the oligonucleotide to DNase I. The sizes of the RNA vary from close to 3000, between 1000-1500 and between 200-500 nucleotides. The IBV N protein binds RNA non-specifically as shown by gel shift assays (Zhou *et al.*, 1996). Since varying lengths of nucleocapsid-like structures are formed, it is possible that the N protein binds to either *E. coli* RNA or the N RNA transcript to form these nucleocapsid-like structures. A northern blot assay using a probe to the N gene can help identify if the N gene transcript is present in the recombinant N protein preparation. What is the significance of formation of these structures in *E.coli*? Since the IBV N protein is over expressed, the large amounts of N protein produced in *E. coli* interact with each other, as well as with the RNA, to form these structures. It reflects the self-assembling nature of the IBV N protein. What is the significance in the virus-infected cell? MHV RNP complexes are found in the infected eukaryotic cell wherein the N protein is found associated with genomic and subgenomic RNA (Narayanan *et al.*, 2003b). It is not known if the RNP complexes in the eukaryotic cell have a regular structure. There are several possible explanations of events in the cell associated with the formation of these structures: 1) Other viral or host proteins may prevent formation of these structures so that free RNA is available for transcription and translation and the RNP complexes do not form any regular structures. 2) These nucleocapsid-like structures may be present even in the infected cell. The diameter of these complexes in *E. coli* is varied suggesting that unwinding of the helix was possible, leading to exposure

of the RNA and making it accessible by the transcription and translation machinery. RNP complexes from virions of IBV, MHV3 and HCV 229E have been shown to consist of tightly bound coils of 9 to 13 nm in diameter or of more loosely bound coils of 14 to 16 nm in diameter (Macnaughton *et al.,* 1978; Davies *et al.*, 1981). This suggests that the RNP structure can unwind when released from the virion. 3) The IBV N protein concentrations might reach a certain threshold concentration after which viral assembly is initiated, leading to the formation of helical nucleocapsid-like structures. 4) Other modifications associated with eukaryotic systems might prevent the N protein from forming these nucleocapsid-like structures in the infected cell prior to nucleocapsid assembly.

In respiratory syncytial virus, amino acids 1 to 92 are sufficient for forming the nucleocapsid-like structure (Murphy *et al.*, 2003). N-N interactions are important in the nucleocapsid of bluetongue virus, hantavirus, hepatitis C virus and porcine reproductive and respiratory syndrome virus (Alfadhli *et al.*, 2001; Kunkel *et al.*, 2001; Salanueva *et al.*, 1999; Wootton and Yoo, 2003). N91, N171, C207 and C140, truncations of the IBV N protein (Fig. 3.1) bind an RNA transcript containing the N gene and the 3' untranslated region (UTR) of IBV. M173 does not bind this transcript (Zhou *et al.*, 1996). Binding may be mediated by the 3'-UTR and/or regions of the N gene. The N protein also shows some non-specific binding to RNA (Zhou *et al.*, 1996). It is likely that if RNA is present in the helical structures, although some fragments of N are capable of binding RNA, the protein-protein interaction domain(s) may be lacking, resulting in no formation of helical-nucleocapsid-like structures. Even if formation of

these structures does not require RNA, the protein fragments are probably incapable of forming these structures due to absence of N-N interaction.

Nucleocapsid independent-assembly of virus like particles is possible by co-expressing the membrane and envelope proteins (Vennema *et al.*, 1996). The RNA that is packaged by the VLPs formed as a result of co-expressing the M and E proteins is much smaller than the genome. Extended RNP-like structures from the IBV virion have been shown to be as long as 6.7 μm in length (Davies *et al.*, 1981). Packaging of the 26.7 kb genome (approximately 9μm in length) into the IBV virion requires that the RNA be compacted since the virion itself is 100-120nm in diameter (Davies and Macnaughton, 1979). The volume of the spherical IBV virion 100 nm in diameter is 5.233×10^5 nm^3. The volume of a rod-shaped RNP-like structure from IBV 6.7 μm in length and 10 nm in diameter is 5.259×10^5 nm^3. Although the volume of the spherical virion and the rod-like nucleocapsid-like structure from the virion is fairly close, the radius of the RNP-like structure should be approximately 5 nm so that it can be packaged in to the virion. Hence, other factors that can compress the helical nucleocapsid to accommodate it into a 100-120 nm diameter particle are also important in forming the virion. There are two possibilities: 1) an alternative morphology of N in the presence of other proteins, 2) the helical rod is folded/compacted by other proteins. It is not clear as to what nucleation event leads to the formation of the nucleocapsid and to packaging of the genome. We show here that extended helical-nucleocapsid-like structures are formed when the IBV N protein is expressed in *E. coli* as a recombinant histidine-tagged fusion protein. Therefore, combinations of M-M, M-N, M-RNA, and N-

RNA interactions are all likely to be important in specifically packaging the viral genome. The recombinant N protein used in this study is not phosphorylated. Hence, phosphorylation might not be necessary for the formation of an elongated nucleocapsid-like structure as observed with bacterially expressed recombinant IBV N. Phosphorylation however might be important in specificity of binding viral RNA for nucleocapsid formation or in some other aspect of virus assembly.

CHAPTER IV

INTERACTIONS OF RECOMBINANT IBV NUCLEOCAPSID PROTEIN AND THE 3'-UNTRANSLATED REGION OF THE IBV VIRAL RNA

INTRODUCTION

The IBV nucleocapsid (N) protein is 409 amino acids long (approximately 48 kDa). MHV N is the only phosphorylated protein in the virus. It is present in the cytosol of infected cells, and also binds small leader RNA that are a part of transcription complexes found associated with cellular membranes (Baric *et al.*, 1988). Although the IBV N protein has many arginine and lysine residues, it lacks any domain characteristic of RNA binding proteins (Williams, 1993). This has also been confirmed using the N protein is multifunctional and has been implicated in playing a role in genome replication, transcription of subgenomic RNA, translation and in formation of the nucleocapsid (Masters *et al.*, 1990; Masters and Sturman, 1990; Tahara *et al.*, 1998). Translation of the N protein is required for optimal replication of BCoV DI RNA and in initiating infection with coronavirus molecular clones (Chang and Brian, 1996; Krishnan *et al.*, 1996). Co-transfection of transcripts of the N gene open reading frame and the *in vitro* assembled virus genome sequence is required for the production of coronavirus in cell culture using reverse genetics approaches (Casais *et al.*, 2003; Yount *et al.*, 2000; Yount *et al.*, 2002). The N protein has been shown to bind to the 5'-UTR, 3'-UTR, the leader sequence, and also the intergenic sequence (Nelson *et al.*, 2000; Zhou and

Collisson, 2000; Zhou *et al.*, 1996) of the MHV and IBV viral genomes. Anti-nucleocapsid protein monoclonal antibodies precipitate both full length and subgenomic mRNAs, as well as replicative intermediate RNA (Stohlman *et al.*, 1988). Both MHV and BCV N bind to the 3' end of the N ORF and also to a sequence in the 1b region that encodes the packaging signal sequence. N protein binds viral sequences with a greater affinity than non-viral sequences (Cologna and Hogue, 2000; Zhou *et al.*).

A three-domain structure for the IBV N protein has been suggested based on sequence comparisons of the N protein of the various IBV strains: the amino-terminal region, the middle region and the carboxy-terminal region (Williams *et al.*, 1992). The IBV whole N protein, the amino-terminal and the carboxy-terminal regions of the N protein bind the 3'-UTR of the viral genome (Zhou and Collisson, 2000; Zhou *et al.*, 1996). The middle region does not bind the 3'-UTR but has been shown to bind the 5'-UTR of the viral genome (Zhou, 1997). The N protein binds the different regions of the 3'-UTR with varying affinities. Certain U-rich regions are bound with greater affinity than other regions (Collisson *et al.*, 2001). These interactions are likely to be important in RNA-transcription, replication and translation.

Most techniques examining RNA-protein interactions, such as filter binding assays, electrophoretic mobility shift assays, and structural studies, describe binding under equilibrium conditions. Although these methods provide information about the affinity of the interactions, they provide little or no insight into the kinetic parameters underlying complex formation. RNA-protein interactions are dynamic, and the rates of binding and release can affect many biological processes (Myszka, 2000; Myszka and

Rich, 2000). A more comprehensive approach would be to examine RNA-protein interactions under equilibrium conditions and as a dynamic process. BIAcore, a technology based on   surface plasmon resonance (SPR), provides both equilibrium and kinetic information about intermolecular interactions (Myszka, 1997; Myszka, 2000).

Surface plasmon resonance (SPR)

SPR is an optical phenomenon that arises when incident light is reflected from a thin metal film (gold in BIAcore instruments) between two layers. Light projected through a prism will be reflected from the film at all but one angle, where light is absorbed and converted into an evanescent wave that propagates into the medium on the nonilluminated side of the metal film. Changes in refractive index on the non-illuminated side within 300 nm of the gold surface lead to a change in the identity of the absorbed angle (Fig. 4.1 a). This system allows intermolecular interactions to be visualized in real time: One of the molecules, the ligand, such as biotinylated RNA, is coated onto the surface matrix, and a second molecule, the analyte, IBV N protein, is injected into the flowing buffer. As the N protein reaches the RNA surface, binding occurs, leading to a change in refractive index near the gold surface, which results in a change in the angle at which light is absorbed (Fig. 4.1 a and Fig 4.1 b). This change, closely related to the change in mass near the gold surface due to the protein binding, is recorded by an optical unit and sent to a computer which displays a trace of binding vs. time called a "sensorgram". The rate at which change occurs upon injection of analyte provides readout for the association rate of the molecules (Fig. 4.1 c). After the injected protein has passed over the surface, it is followed by buffer flow and the dissociation can
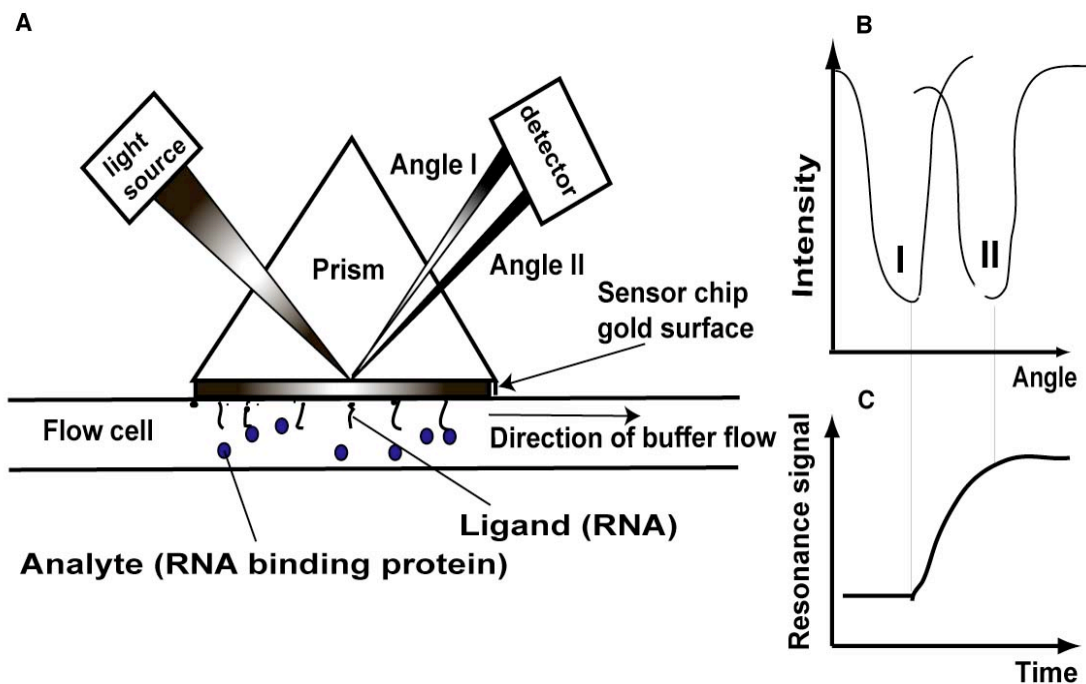
FIG. 4.1. BIAcore system. The BIAcore makes use of the phenomenon of surface plasmon resonance. The instrument has a light source and an optical detection unit that are on one side of the thin gold film (sensor chip). As plane polarized light from the light source shines on the sensor chip, it is reflected at all angles but one, at which it will be absorbed into the gold surface in the form of an evanescent wave (angle I). The identity of the absorbed angle depends on the refractive index of the material close to the nonilluminated side of the gold surface, where the binding reaction takes place. RNA is immobilized on the nonilluminated side of the sensor chip. As a protein sample is injected into the flow cell and binds to the RNA, it causes a change in the refractive index. Such a change will result in a shift in the absorbed angle, to angle II. The change in angle is recorded by the detector and is displayed in the form of a sensorgram. (Adapted from Katsamba *et al.*, 2002).

be observed as the protein gradually dissociates from the RNA, and the absorbed angle returns to the preinjection value. Subsequently, a new injection can be performed. The time it takes for the angle to return to baseline depends on the off-rate of the interaction. Here, SPR is used to study the binding of IBV N protein to the terminal 40 nucleotides of the 3'UTR.

MATERIALS AND METHODS

Expression and purification of the IBV recombinant nucleocapsid protein

The N gene and several truncations of the N gene were cloned into pQE8 vector and expressed as a histidine-tagged protein in *E. coli* M15 cells (Zhou *et al*., 1996). Fifty ml of an overnight culture of bacteria grown in SOC medium containing 50 μg/ml ampicillin and 25 μg/ml kanamycin were inoculated into 450 ml SOC medium containing the same antibiotics. The bacteria were cultured at 37°C on a shaker at 200 rpm for three hours. Protein expression was induced with IPTG at a final concentration of 2 mM. The bacteria were cultured for another five hours at 37°C on a shaker at 200 rpm and harvested by centrifuging at 3000 g. The pellet was suspended in non-denaturing buffer (0.05 M Tris, pH 8, 0.3 M NaCl, 0.01 M imidazole). Lysozyme was added at a final concentration of 0.1 mg/ml and the sample was incubated on ice for 30 minutes. The sample was lysed on ice by sonication at a 100 W power output, 10 s pulses, six times with 10 s intervals. The sample was centrifuged at 5000 rpm at 4°C for 10 minutes, in a JA 21 rotor. The supernatant was collected and 1 ml of a 50% Ni^{+2}-NTA resin (Qiagen, Chatsworth, CA) was added to every 10 ml of cell lysate. The mix

was incubated on a shaker at 4°C for one hour. The resin was collected by centrifuging at 1800g, in a Joun CR412 centrifuge at 4°C for 1 minute and washed three times with 10 ml of wash buffer (0.05 M Tris, pH 8, 0.3 M NaCl, 0.02 M imidazole). The protein was eluted from the resin with 1 ml of elution buffer (0.05 M Tris, pH 8, 0.3 M NaCl, 0.25 M imidazole). Approximately 3 mg of N protein were obtained per 500 ml of bacterial culture. Polypeptides equal to, or greater than, 274 amino acids in length were further purified by gel permeation chromatography using a Sephadex G200 (Sigma, St. Louis, MO) or Superdex 200 (Amersham Biosciences, Piscataway, NJ) while peptides equal to, or smaller than, 207 amino acids were purified with Bio-gel P60 (Bio-Rad, Richmond, CA). Five ml of each sample were loaded onto the column before washing with Tris buffer (Tris 0.05 M pH 8, 0.3 M NaCl). Fractions were monitored with the Bio-Rad protein assay reagent (Bio-Rad, Richmond, CA), and the fractions containing protein, were analyzed by 15% polyacrylamide gel electrophoresis (Sambrook *et al*., 1989). Protein used for electron microscopy was dialyzed in HEPES buffer (25 mM HEPES, 25 mM EDTA, 150 mM NaCl, 5 mM DTT and 5% glycerol).

Western blot assays were used to determine the viral specificity of the recombinant polypeptides (Sambrook *et al*., 1989). Briefly, varying amounts of the various proteins were separated by 15% polyacrylamide gel electrophoresis and blotted onto nitrocellulose membranes. After blocking the membranes with 5% skim milk in Tris buffered saline (TBS, pH 7), the membranes were reacted sequentially with chicken anti-IBV Gray antibody and alkaline phosphatase conjugated goat anti-chicken IgG (KPL, Gaithersburg, Maryland).

Synthesis of RNA

Minus and plus strand DNA oligonucleotides corresponding to the RNA sequences used in this study were synthesized with the T7 promoter at the 5' end of the positive strand. Double strand oligonucleotides were obtained by annealing the genomic sense and anti-genomic sense DNAs. The RNA fragments were transcribed from these synthetic oligonucleotides with 2 μg DNA template, 40 units T7 RNA polymerase, rATP, rCTP and rGTP at a final concentration of 1 mM and 100 μM of rUTP (Invitrogen, Carlsbad, CA), 50 μCi of αP^{32} labeled rUTP (Perkin Elmer, Wellesley, MA), 80 units of RNasin (Promega, Madison, WI), 5X transcription buffer and 1 mM DTT (final concentration). The reaction was incubated at 37°C for 2 hours and terminated with the addition of 1000 units of DNase I (Roche Biochemicals, Indianapolis, Indiana) and incubating at 37°C for 15 minutes. After extracting the RNA probe with phenol chloroform, and cleaning with a spin column (Eppendorf, Boulder, CO) to remove unincorporated nucleotides, the RNA was quantified by gel electrophoresis by comparing with yeast t-RNA. This probe was heated to 70°C for 10 minutes and flash frozen to -20°C to remove any secondary structures. The 40 mer, 15 mer poly U and 40 mer RNA oligonucleotide corresponding to the terminal 40 nucleotides of the 3'-UTR of IBV were synthesized by Dr. Paul Gershon (Institute of Bioscience and Technology, Houston, TX) using phosphoramidite chemistry on a model 392 DNA/RNA synthesizer (Applied Biosystems, Foster City, CA.)

Alkaline phosphatase treatment and end labeling of RNA

10 pmoles of RNA were treated with 0.05 units of calf intestinal alkaline

phosphatase (CIAP) in CIAP buffer in a 50 μl reaction volume at 37°C for 30 minutes. Another 0.05 units of CIAP were added and the reaction was incubated under the same conditions for another 30 minutes. The reaction was terminated with CIAP stop buffer (10 mM Tris-HCl, pH 7.5; 1 mM EDTA, pH 7.5; 200 mM NaCl and 0.5% SDS), followed by phenol chloroform extraction of RNA and precipitation with 0.5 volumes of 7.5 M ammonium acetate and 2 volumes of ethanol at room temperature. At the end of two hours, the RNA precipitate was recovered by centrifugation at 12,000 g, for 20 minutes. This RNA was used for 5' end labeling. End labeling was carried out with 150 μCi of ^{32}P γ-ATP and 20 units of T4 polynucleotide kinase in appropriate buffer in a 30 μl reaction volume. The reaction was incubated at 37°C for one hour and stopped with 1 μl of 0.5 M EDTA. The RNA was extracted by phenol-chloroform and purified by precipitation as mentioned above.

Gel shift assays

Protein-RNA interactions were analyzed by a modified gel-shift assay (Chodosh, 1992). Varying concentrations of RNA and 65.54 picomoles (3 μg) of the nucleocapsid protein were co-incubated for 20 minutes at room temperature (25°C) in 10 μl of gel shift assay buffer {25 mM HEPES, 5 mM EDTA, 150 mM NaCl, 5 mM DTT, 5% glycerol and 20 units rRNAsin (Invitrogen, Carslbad, CA)}. Following the addition of 1 μl 10X RNA loading buffer, the reaction mixtures were loaded onto either 6% polyacrylamide gels or 1% metaphor agarose gels and electrophoresed at 100V in 1X Tris-borate-EDTA (Sambrook *et al*., 1989). Gels were dried and then subject to autoradiography.

Competitive gel shift assays

Competition assays were performed using 65.54 picomoles of nucleocapsid protein and different concentrations of the radiolabeled RNA and unlabeled heterologous competitor RNA in 10 µl reaction volume. Briefly, the probe, protein and cold competitor RNA were mixed together in gel shift assay buffer for 20 minutes at room temperature. After adding gel-loading dye, the complexes, if any, were resolved by agarose gel electrophoresis. The gel was dried and then subject to autoradiography.

Surface plasmon resosnance (SPR)-BIAcore

The CM5 sensor chip was activated using N-hydroxisuccinimide (NHS) and 1-ethyl-3-(3-dimethylaminopropyl) carbodiimide hydrochloride (EDC) (BIAcore) at a flow rate of 5 µl/min. 80 µg/ml of streptavidin in 25 mM sodium acetate pH5 (total volume 100 µl) was injected at a flow rate of 5 µl/min in running buffer (20 mM HEPES, pH 7, 100 mM NaCl, 0.05% Tween 20) until 2800 RU of streptavidin was immobilized on the sensor chip. This was followed by deactivation of unreacted NHS-esters using 35 µl 1 M ethanolamine hydrochloride adjusted to pH 8.5 with NaOH. This was followed by an injection of biotinylated RNA (70 µl) in running buffer till a surface coating of 750 RU was reached. Varying concentrations of protein in different buffers were injected at a flow rate of 5 µl/min to determine the optimum conditions for binding. The bound protein was dissociated by injecting running buffer at a flow rate of 100 µl/min. This was followed by regeneration of the chip by injecting 0.5 M NaCl in running buffer at a flow rate of 40 µl/min. The regenerated CM5 chip could be reused for studying binding for at least ten reactions or till the time the immobilized RNA

remained intact. Buffer A (20 mM HEPES buffer, pH7, 0.05% Tween 20); buffer B (20 mM HEPES, pH 7, 150 mM NaCl, 0.05% Tween 20, 25 mM EDTA, 5 mM DTT).

RESULTS

Purification of IBV recombinant nucleocapsid (N) protein and the amino terminal 171 amino acids of the N protein

Ni^{+2}-NTA affinity purified IBV N and N171 proteins were resolved by denaturing polyacrylamide gel electrophoresis (SDS-PAGE). IBV N protein is approximately 48 kilodalton (kDa) and N171 is approximately 20 kDa in molecular mass. The identity of the proteins was confirmed using chicken anti-IBV Gray antibody using a Western blot assay (Fig.4.2). These purified proteins were used for the gel shift and surface plasmon resonance assays. Recombinant IBV N protein tends to degrade probably due to small amounts of bacterial proteases co-purifying with the protein, in which case additional procedures need to be used to obtain pure protein. However, for this experiment the recombinant proteins appeared pure after a single purification step.

Surface plasmon resonance (SPR)

N171 (the amino 171 amino acid residues of the IBV nucleocapsid protein) was used for the assay, because N171 was of greater purity than IBV N. Binding of N171 to the terminal 155 nucleotides of the 3'-UTR has been demonstrated by Zhou *et al.*
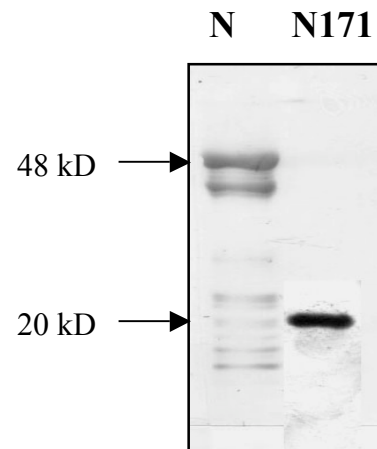
FIG. 4.2. Western blot analysis of the recombinant IBV N protein and the recombinant amino terminal 171 amino acids (N171) of the IBV N protein purified by Ni^{+2}-NTA chromatography.
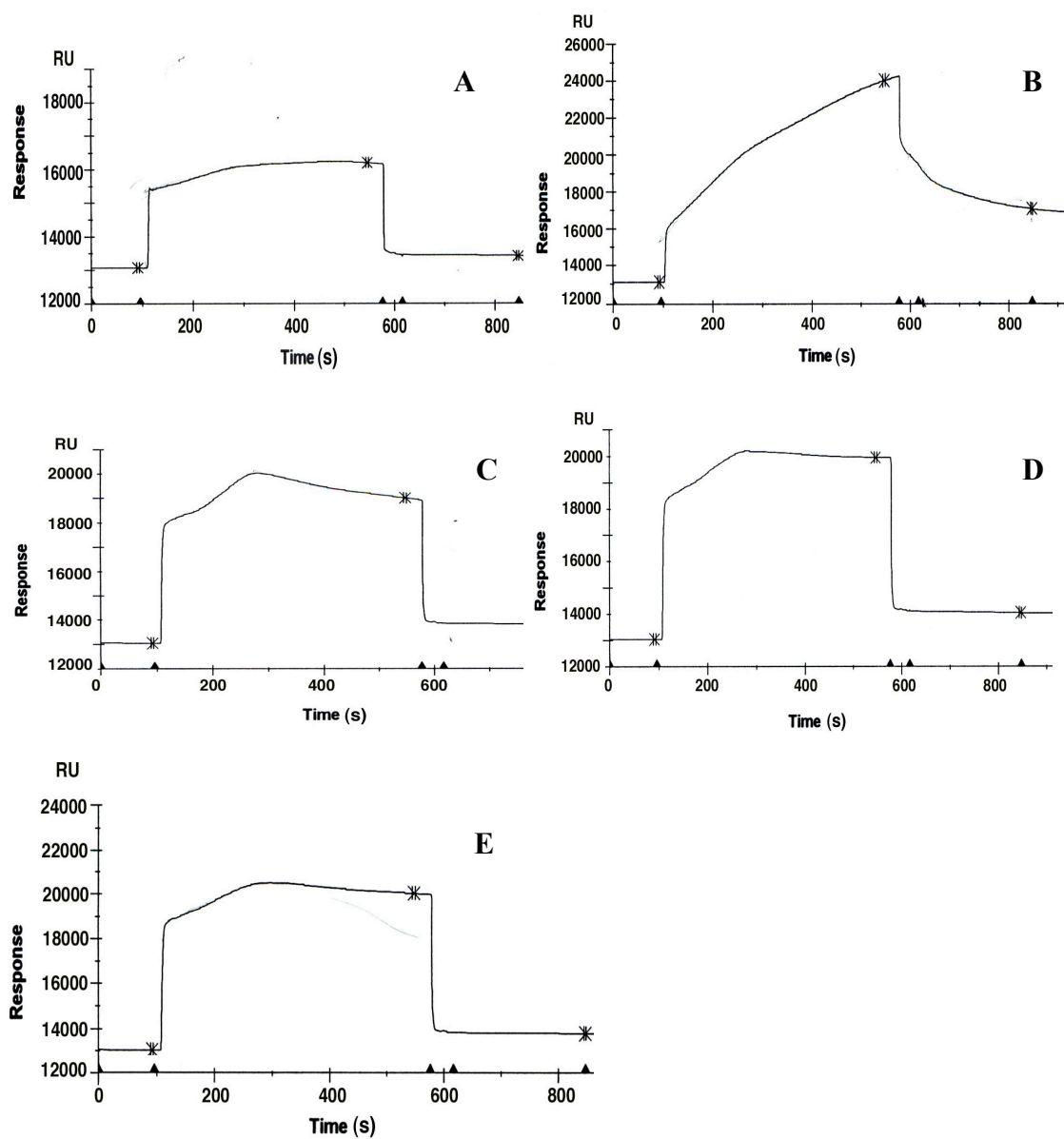
FIG. 4.3. Effect of NaCl concentration on binding of N171 and 3'-UTR 40 mer RNA of IBV using surface plasmon resonance. Binding was carried out with 3.75 μM N171 in running buffer containing (A) 25 mM NaCl, (B) 50 mM NaCl, (C) 100 mM NaCl, (D) 200 mM NaCl and (E) 250 mM NaCl.

(1996). Biotinylated sequences 40 to 50 nucleotides in length were easier to synthesize than the 155 nucleotides of the 3'-UTR used by Zhou *et al*. (1996) for the gel shift assay. Hence, the terminal 40 nucleotides of the 3'-UTR were used to standardize conditions for binding of N171 to viral RNA using SPR. The signal from association of N171 with RNA (in resonance units, RU) was calculated after subtraction from the sensorgram of the baseline due to the immobilization of RNA alone. The maximum level of binding was obtained at 50 mM NaCl concentration with running buffer A and 3.75 µM of the protein (Fig. 4.3, Table 4.1). However, running buffer B has a composition closer to that of the buffer used in our gel shift assays. A higher relative resonance response was obtained using 3.75 µM of N171 and running buffer B (Fig. 4.4, Table 4.2). Binding of 1.875 µM, 3.75 µM, 5.625 µM, 7.5 µM, 9 µM, 11.25 µM and 15 µM of N171 to the 3'-UTR terminal 40 nucleotides were evaluated. The maximum binding increases until a protein concentration of 5.625 µM, and the response drops down for the next two concentrations of 7.5 µM and 9 µM, and again increases for the 11.25 µM and 15 µM protein concentrations (Fig. 4.4, Table 4.2). All responses to study the effect of protein concentrations on the binding of N171 to the terminal 40 nucleotides were carried out using the same flow cell coated with RNA. RNA degrades over time and hence could affect the relative response obtained due to protein binding. Regeneration of the surface to remove bound protein is important as well. If the binding surface does not regenerate completely, a lower response would be obtained on the next cycle. Error in diluting the proteins could also lead to erroneous responses. We did not serially dilute the protein

Table 4.1.

Effect of NaCl concentration on binding of N171 to the terminal 40 nucleotides of the 3'-UTR of IBV

mM NaCl concentration	Relative maximum RU during association
25	3145.2
50	10949.7
100	5961.1
200	6922.0
250	7005.4

Table 4.2.

Effect of protein concentration on binding of N171 to the terminal 40 nucleotides of the 3'-UTR of IBV

µM Protein concentration	Relative maximum RU during association
1.875	567.2
3.75	1148.7
5.625	1469.0
7.5	1048.7
9	951.4
11.25	1792.1
15	1960.0
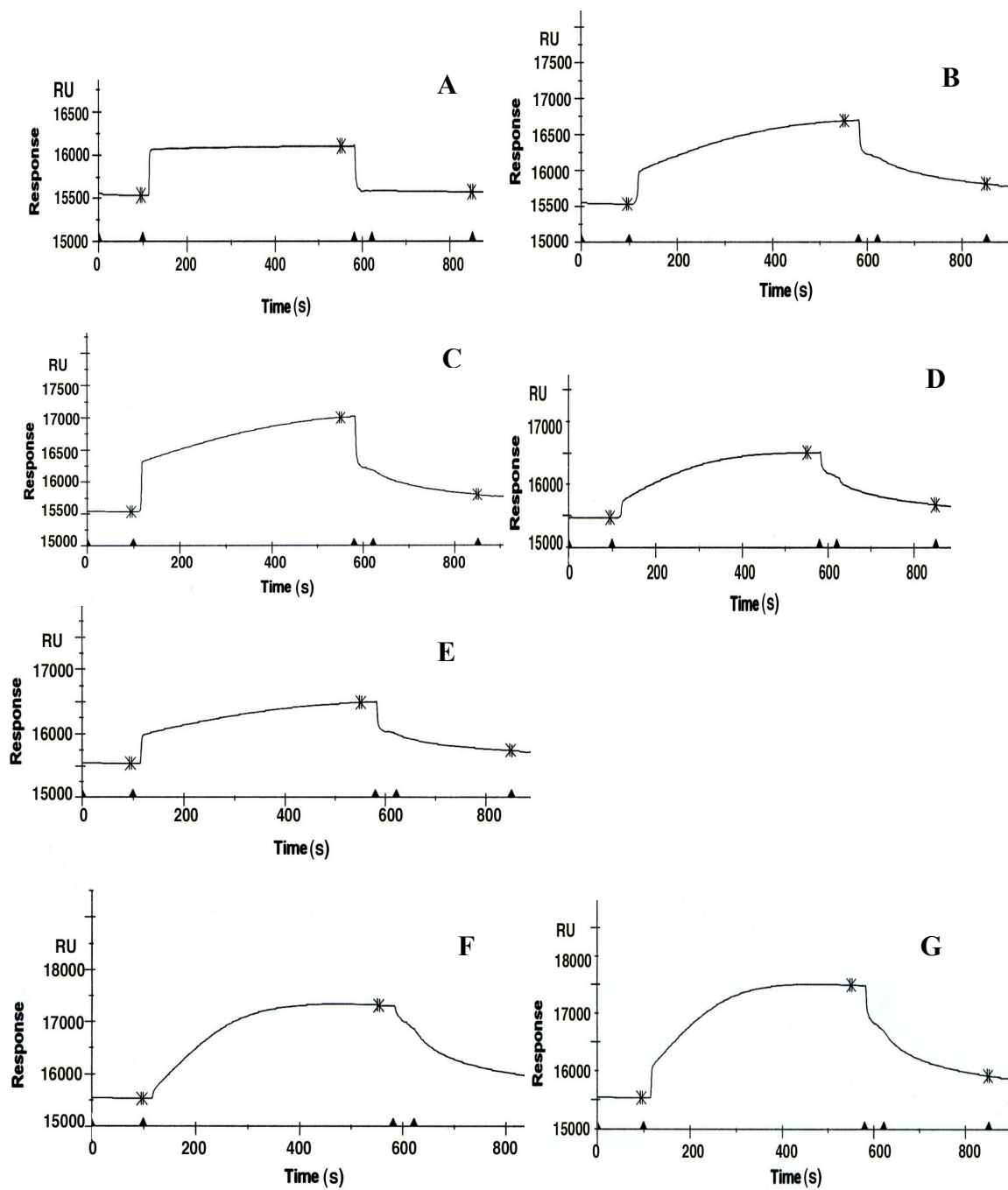
FIG. 4.4. Effect of protein concentration on binding of N171 and 3'-UTR 40 mer RNA of IBV in running buffer using surface plasmon resonance. Binding of (A) 1.875 µM (B) 3.75 µM, (C) 5.625 µM, (D) 7.5 µM, (E) 9 µM, (F) 11.25 µM and (G) 15 µM N171 to 3'-UTR 40 mer RNA.

and hence that could also lead to the observed effect. The experiment was done once and hence we cannot comment on the reproducibility of the relative response obtained.

An attempt was made at determining the rate constants and the equilibrium constant. The data were fit (p values < 0.05) to the simple model A + B ↔ AB, 1:1 stoichiometry. The apparent dissociation rate constant (k_{diss}) was 5.91×10^{-5} s^{-1} and the apparent association rate constant (k_{ass}) was 100 $M^{-1}s^{-1}$. The apparent association equilibrium constant ($kA = k_{ass}/k_{diss}$) was 1.6×10^6 M^{-1}. The analysis should be repeated to confirm the results.

Gel shift assays

IBV N binds sequences containing an elevated U content (Collisson *et al.*, 2001). To determine the ability of IBV N to bind poly U sequences, gel shift assays were carried out with IBV N and a 15- and 40-nucleotide poly U sequence. IBV N protein bound to both a 15-mer and 40-mer poly U RNA as observed by a shift in the RNA band in presence of the N protein. This binding was specific as it occurred in the presence of a large excess of yeast tRNA. To determine the relative ability of IBV N protein to bind U-rich sequences, competitive gel-shift assays were performed with U-rich regions of the IBV genome and the $(U)_{40}$ mer.

IBV N protein binds G2 RNA (N gene + IBV 3'UTR) and CD RNA (terminal 155 nucleotides of the 3'-UTR) (Zhou *et al*, 1996). The 3'-UTR region of the IBV genome is U-rich. Competitive gel shift assays were performed with poly U as competitor and G2 RNA probe and CD RNA probes. All these RNA are predicted to form secondary structures when analyzed by the m-fold program (Zhou, 1999).

Poly U-15 probe
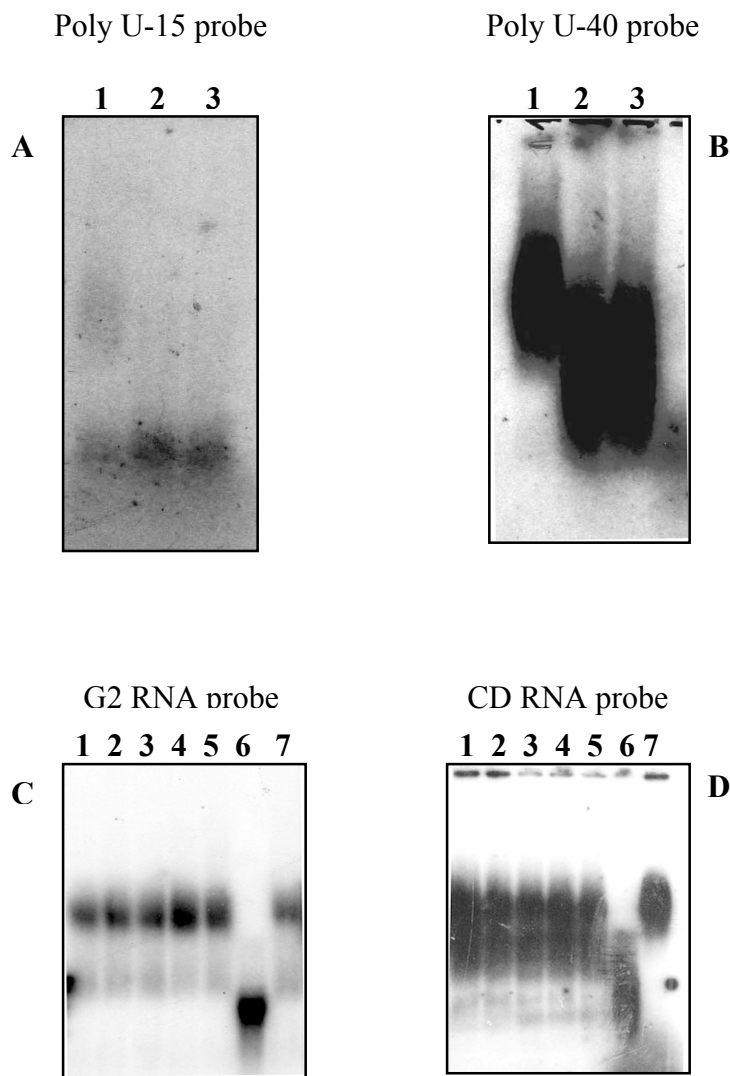
Poly U-40 probe

FIG. 4.5. Gel shift assays using (A) 1 ng poly U_{15} and (B) 1 ng poly U_{40} as probe and 3 μg N protein. Lane 1 represents binding of N protein in presence of yeast-t-RNA; lane 2, free probe and lane 3 shows binding of nonspecific protein BSA to probe. Competitive gel shift assays for cold poly U_{40} as competitor and C) G2 RNA and D) CD RNA probes. Lanes 1 through 5, have labeled probe with 3 μg N protein and two-fold dilutions of competitor starting with 150 ng of poly U_{40} up to 9.375 ng in lane 5; lane 6 is free probe and lane 7 is N protein and probe without the competitor.

Competitive gel shift assays using G2 RNA as probe and $(U)_{40}$ mer as competitor

showed that even a 10^6-fold excess of cold competitor could not compete out the

binding. This is possibly due to the large size of the G2 RNA. Binding of N171 to

0.0189 pmoles of CD RNA was not competed out by approximately 10^6-fold excess of

cold competitor poly U RNA (Fig. 4.5).

DISCUSSION

The genome of IBV is U rich with an average of 32.7% of uridine. The 3'-UTR

and 5'-UTR contain 37% and 29% uridine respectively. The 5' and 3'-UTR's have been

shown to be important in replication of DI's and in subgenomic RNA synthesis. Since

the N protein binds the 3'-UTR and 5'UTR, these effects may be influenced by the

presence of uridine. Sequence specificity and secondary structure are also likely to be

important in binding. Our gel-shift assays are designed to determine the sequence

specificity of binding, and not secondary structure of RNA for protein binding as there

are no ions (such as Mg^{+2} or Zn^{+2}) that help RNA folding. Since the N protein also binds

the $(U)_{15}$ RNA probe, it can be said that such short lengths are not a constraint for

binding of the N protein to form an RNA-protein complex.

The competitive gel shift assay is an effective method to determine the relative

binding affinities of the N protein for the various sequences. The large difference in size

and putative secondary structure of the G2 (1800 nucleotides) and CD (155 nucleotides)

RNA probes may have prevented the competition by cold $(U)_{40}$ RNA. The secondary

structure may facilitate greater binding of the N protein and hence the inability to

compete out binding by $(U)_{40}$. Smaller RNA sequences with varying U percentages would have been very useful to determine the sequence context of uridine for N protein binding.

A preliminary analysis using SPR to study the binding of N171 to the terminal 40 nucleotides of the IBV 3'-UTR was carried out. Since a higher resonance response was obtained in running buffer B (resembled the gel shift assay buffer) than running buffer A, the running buffer B was more appropriate than running buffer A for N binding RNA using the BIAcore. The apparent association and dissociation rate constants were calculated using the BIAcore 2000 BIAevaluation software. Employing gel shift assays, Zhou *et al.* (1996) have characterized the RNA binding domain of the IBV N protein using polypeptide truncations of the IBV N protein and the 3'-UTR RNA. Our results show that SPR can be used in future to further accurately determine the kinetics of binding of the N protein truncations to the 3'-UTR 50 nucleotides. More detailed analysis of the ratio of RNA and protein in the complex was not possible because the original data files were misplaced. Further experiments could not be conducted owing to limited time and financial resources. This technique, however, can be used to model RNA-protein interactions.

CHAPTER V

A RAPID ELISA TECHNIQUE USING THE BIOWAVE MICROWAVE

Reticuloendothelioses virus (REV) and feline immunodeficiency virus (FIV) are retroviruses that infect prairie chickens and cats respectively and infectious bronchitis virus (IBV) is a positive stranded RNA virus that infects chickens. These viruses are pathogens of veterinary interest. Enzyme linked immunosorbent assay (ELISA) is a commonly used technique for detection of virus or viral specific antibodies, however traditional ELISAs can take up to two days for completion versus expensive pre-prepared kits that can yield results within three hours (IDEXX). Traditional ELISAs for the detection of antibody to infectious bronchitis virus (IBV) in chicken serum take at least two days for completion (Ndifuna *et al.*, 1998). ELISAs to detect REV and FIV in cell culture that are routinely performed in our laboratory take 8 hours for completion. We have now developed a rapid ELISA technique using a special type of microwave called the PELCO BIOWAVE (Ted Pella Inc., Redding, CA) that can be completed in less than two hours.

The BIOWAVE microwave (Ted Pella Inc.) has the following unique features. (1) It can maintain a constant, controlled, monitored, temperature from 4°C to 40°C. (2) The wattage in the system can be controlled and it provides continuous microwave energy settings of up to 450 watts. (3) A patented temperature controlled processing surface (PELCO ColdSpot) that eliminates hotspots and ensures uniform heating of the

substance placed within the BIOWAVE. The BIOWAVE has been used for immunochemical techniques such as fluorescent in situ hybridization (FISH) and immunohistochemistry and for tissue embedding for thin section preparation for electron microscopy (Ted Pella Inc., Redding, CA).

We used the PELCO BIOWAVE for the first time to detect REV and FIV in cell culture supernatants and to detect IBV antibody in chicken serum. The BIOWAVE is used to decrease the turn around time for completing an ELISA.

MATERIALS AND METHODS

Preparation of recombinant IBV nucleocapsid protein and REV gag protein

The N gene was cloned into pQE8 expression vector (Qiagen, Chatsworth, CA) and expressed as a histidine-tagged protein in *E. coli* M15 cells (Zhou *et al*., 1996). The fusion protein was purified through a Ni^{+2}-NTA column as described by *Zhou et al*. (1996) and further purified by gel filtration through a Sephadex G200 column. The REV gag protein was cloned in a pet Blue vector (Novagen, San Diego, CA) as a histidine-tagged fusion protein and expressed and purified using the procedure described in the Qiagen manual (Qiagen, Chatsworth, CA).

BIOWAVE

Either completing or breaking the circuit can regulate power output in the BIOWAVE. Completing a circuit allows current to flow through the BIOWAVE thus heating the interior (the on cycle) and breaking the circuit stops current flow (the off cycle) thereby stopping heating within the BIOWAVE. The off cycle essentially allows

the sample being heated to cool down and not be subject to continuous heat energy. The on and off cycles can be programmed for various periods of time. Thus, any heating program can consist of alternate cycles of heating and cooling for up to a total of 6 cycles. The BIOWAVE microwave was set at 250 W and 30°C. Cycle A was programmed for a 2 min on cycle, 2 min off cycle and a 2 min on cycle for a total of 6 minutes. Cycle B was programmed for a 1 min on cycle at 250 W. Cycle A was used for coating antigen (N protein, gag protein or supernatant containing virus), antibody, streptavidin-horse raddish peroxidase conjugate (HRPO) or for the blocking step and cycle B was used for the washing steps. All steps were carried out at 30°C.

IBV ELISA

The traditional ELISA protocol was performed using the method described by Ndifuna *et al.* (1998). 96-well microtiter ELISA plates (Sumitomo Bakelite Co. Ltd.) were coated with 50 µg/100 µl per well IBV recombinant N protein, diluted in bicarbonate/carbonate buffer (Ndifuna *et al.*, 1998). The plates were then blocked with blocking-solution [5% w/v non-fat dry milk, 0.2% Tween 20, 0.02% sodium azide in Tris buffered saline (TBS)]. After one wash with TBS-Tween 20 (0.2%) (TBT-T), 100 µl per well of chicken serum (containing anti-IBV Gray antibody) diluted in blocking solution were added to each well. After washing the plates with TBS-T, 100 µl of a 1:1000 dilution of alkaline phosphatase conjugated goat anti-chicken antibody (KPL, Gaithersburg, Maryland) in blocking buffer were added to the ELISA. After washing with TBS-T, 5-bromo-4-choloro-3-indolyl phosphate (BCIP) and nitroblue tetrazolium (NBT) one component substrate (KPL, Gaithersburg, Maryland) was added to the wells.

The reaction was stopped after 20 minutes with 5% EDTA stop solution (KPL) and the optical density (O.D.) measured at 405 nanometers (nm).

REV and FIV ELISA

Immulon 2HB strips (Thermolab systems, Franklin, MA) were used for the FIV and REV ELISAs. ELISA strips were coated with rabbit anti REV gag polyclonal antibody at a concentration of 20 μg/ml or with 50 μl mouse monoclonal anti FIV gag antibody at a concentration of 20 μg/ml. The plates were then blocked with 300 μl 3% BSA in phosphate buffered saline (PBS) pH 7.4 following which the plates were washed once with PBS containing 0.05% Tween 20 (PBS-T). 20 μl Triton-X 100 per well and 200 μl of various dilutions of REV made in complete Dulbecco's minimal essential medium (DMEM) containing 2% fetal bovine serum (FBS) were then added to the wells. Two fold dilutions of REV gag protein starting with 500 ng up to 1.5 ng were used as standards. For the FIV ELISA, 10 μl Triton-X 100 per well and 100 μl of various dilutions of FIV made in complete DMEM containing 10% FBS were added to the wells. After washing the wells with PBS-T, for the REV ELISA, 100 μl rabbit anti-gag biotinylated IgG (2 μg/ml) diluted in PBS containing 3% FBS were added to the wells and for the FIV ELISA, 100 μl anti-mouse-biotinylated IgG (2 μg/ml) diluted in PBS containing 3% fetal bovine serum (FBS) were added to the plates. The wells were then washed with PBS-T and 100 μl of a 1:1000 dilution of streptavidin-conjugated-HRPO diluted in PBS containing 3% FBS were added to the plates for both ELISAs followed by a wash with PBS-T. Tetramethylbenzidine (KPL, Gaithersburg, Maryland) was used as substrate for HRPO. The reaction was terminated with stop solution (KPL,

Table 5.1.

Comparison of the traditional and the biowave ELISA protocols for REV and FIV detection in cell culture supernatant

	Traditional	Biowave
Antibody	R.T. for two hours	6 min cycle A
Blocking	Overnight at 4°C	6 min cycle A
Wash	Twice at R.T.	1 min cycle B
Antigen	Two hours at R.T.	6 min cycle A
Wash	Four times	1 min cycle B
Biotinylated antibody	30 minutes at R.T.	6 min cycle A
Wash	Thrice	1 min cycle B
Sterptavidin-HRPO conjugate	30 minutes	6 min cycle A
Wash	Five times	1 min cycle B
Substrate	20 min at R.T.	20 min at R.T.

Gaithersburg, Maryland) after 20 minutes. The O.D. was measured at 405 nm. Comparisons of the traditional and BIOWAVE protocols are shown in Table 5.1.

The IBV, FIV and REV ELISAs were also done by using the timings of the Biowave protocol for the various steps, though carried out at room temperature (R.T.) (25 °C) or at 30°C.

RESULTS

IBV ELISA

ELISA was used to determine the presence of anti-IBV antibody in chicken serum by four methods. Method 1 used the protocol of the traditional method (traditional ELISA, slow, R.T.), method 2 (biowave ELISA, fast, 30 ºC) used the BIOWAVE for the biowave protocol outlined in figure 5.1, method 3 (traditional ELISA, fast, 30 ºC) used the biowave protocol timings though the ELISA was carried out at 30°C and method 4 (biowave ELISA, fast, R.T.) used the biowave protocol timings and the ELISA was carried out at R.T. In order to determine the effect of temperature on the ELISAs in the absence of microwave energy, the ELISAs were also carried out with the biowave protocol timings at 25°C and 30°C. The traditional ELISA method is carried out at 25°C and the biowave ELISA was carried out at 30°C. With an increase in antibody dilution, there was a decrease in the O.D. value for both the traditional and biowave ELISA protocols tested. Results for the ELISA for the first three dilutions using method 3 gave lower values as compared to the ELISA results obtained using method 1 and 2,
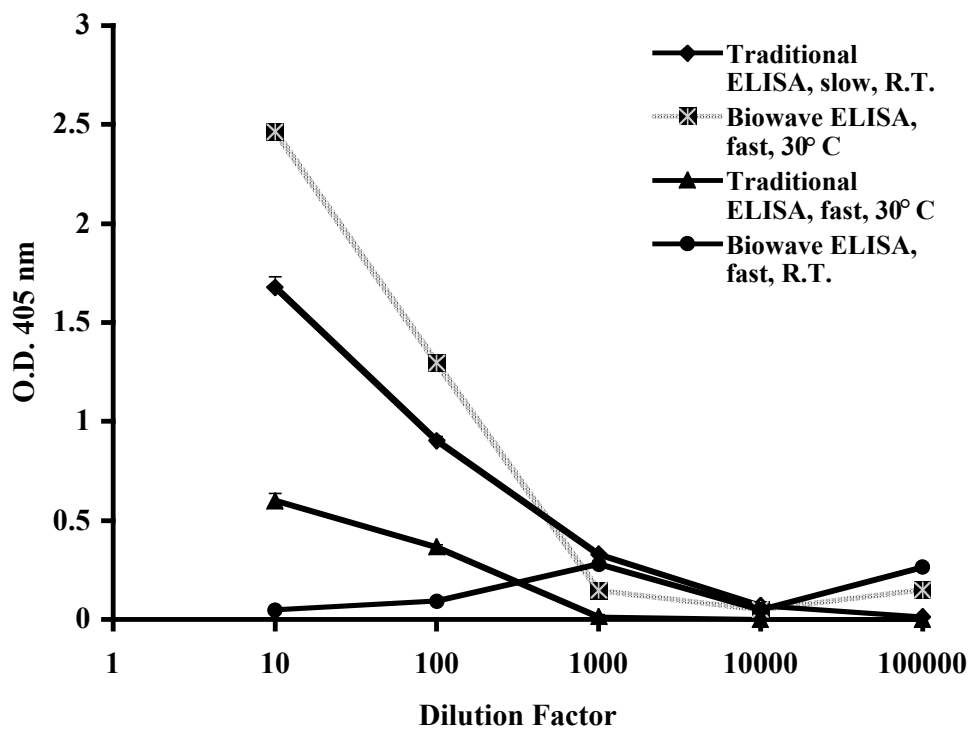
FIG 5.1. Comparison of the traditional and the biowave protocols for IBV ELISA to detect anti-IBV antibody in chicken serum using IBV recombinant nucleocapsid protein as antigen. Values are an average of triplicates. The standard errors are 0.06 or less than 0.06.

following which, the O.D. value dropped to zero. Results for the ELISA using method 4 with anti-IBV Gray antibody and negative serum as a control gave a low background O.D. value. The value was considerably lower than the values obtained by the biowave protocol at lower dilutions of antibody (Fig.5.1).

FIV and REV ELISA

Standardized antigen capture assays were available for detecting FIV and REV. Therefore these assays were modified for detection with the BIOWAVE method. ELISA was used to determine FIV and REV in cell culture supernatants using methods 1 through 4. For the FIV ELISA, with an increase in dilution of the cell culture supernatant, a decrease in O.D. value was obtained for methods 1, 2 and 3. O.D. values with method 3 were lower than those obtained with methods 1 and 2 (Fig. 5.2) and with method 4, the O.D. values were very close to zero or negative (data not shown). The undiluted cell culture supernatant gave a higher O.D. value with method 1 than method 2. Overall, O.D. values using method 1 were lower than those obtained using method 2. O.D. values were obtained with undiluted cell culture supernatants up to a 1:64 dilution of the cell culture supernatant for methods 1 and 2. Hence, both protocols were equally sensitive to the same levels of virus (Fig. 5.2 and Fig. 5.3).

For the REV ELISA, the O.D. values increased with an increasing amount of gag protein for all four methods used. The increase in O.D. values was comparable using methods 1 and 2 up to 300 ng of protein; O.D. values for method 2 were slightly lower than O.D. values for method 1. At 500 ng of protein, the O.D. value obtained with the biowave using method 2 was considerably lower than that using method 1. Method 3

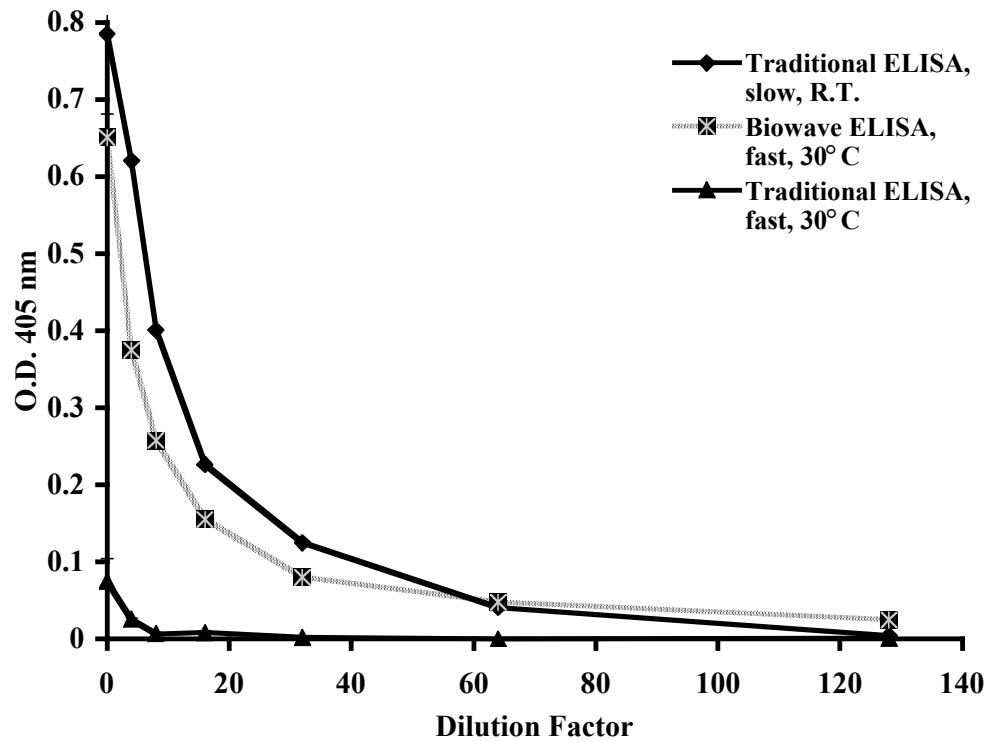**FIG. 5.2.** Comparison of the traditional and the biowave protocols for the detection of FIV in cell culture supernatants using various dilutions of the supernatant. The standard errors are less than 0.05.
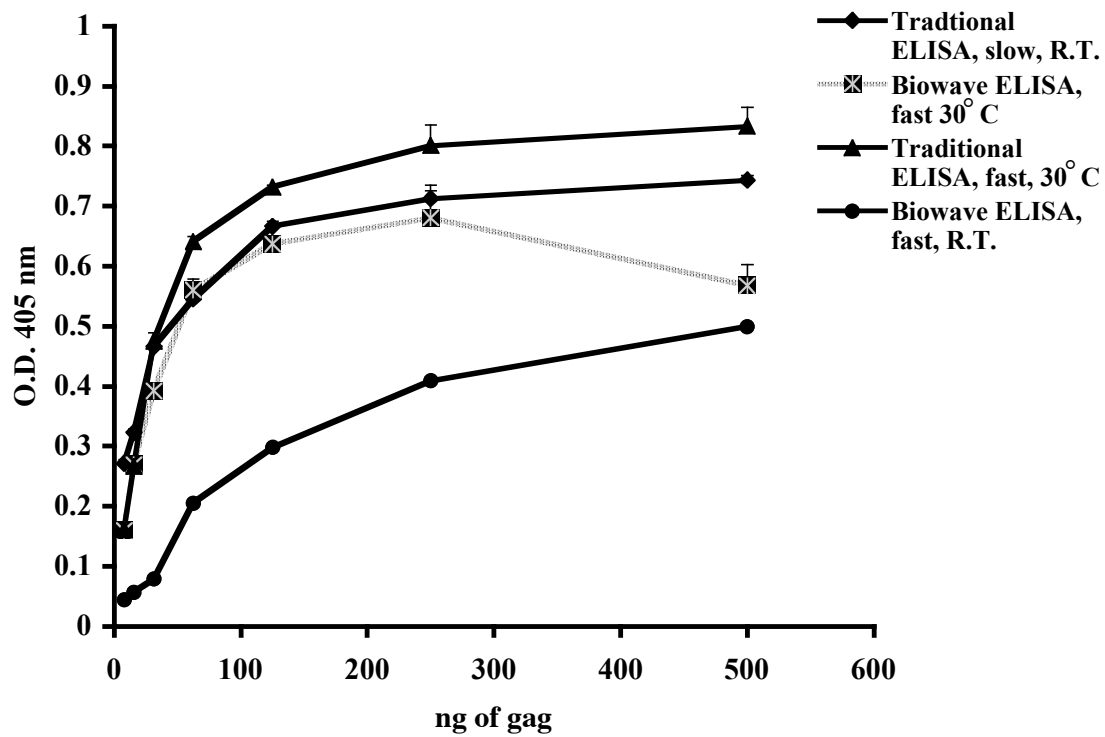
FIG. 5.3. Comparison of the traditional and the biowave protocols for the REV ELISA using REV gag protein standards and antibody to the gag protein raised in rabbits. The standard errors are less than 0.07.

gave higher O.D. values above 50 ng of protein as compared to methods 1 and 2. Method 4 gave an increasing gradation of O.D. values with increasing protein amounts, however the O.D. values were lower than the first three methods. 0.516, 0.377, 0.238 and 0.139 were the O.D. values of virus present in the supernatant obtained using methods 1, 2, 3 and 4. Virus in the supernatant corresponded to approximately 235, 156, 80 and 235 ng of REV gag protein/ml as determined using methods 1, 2, 3 and 4 respectively.

Secondary antibody dilutions

The manufacturer recommended a 1:100 secondary antibody dilution. Very high background O.D. values were obtained with the negative serum when a 1:100 dilution of secondary antibody was used. Hence, a 1:1000 dilution was used. The secondary antibody dilutions for REV and FIV ELISAs were similar to that used for the "traditional" ELISA protocols.

Substrates

For IBV ELISAs, BCIP-NBT was used as alkaline phosphatase substrate and TMB was used as substrate for HRPO for REV and FIV ELISAs. The BIOWAVE works well with both enzyme-substrate systems.

ELISA plates

The IBV ELISA works well only with the simulon flat bottom ELISA plates. Very high backgrounds were obtained when high protein binding plates used for REV and FIV detection was used for the IBV ELISA. On the other hand, the REV ELISA worked well only with the high protein binding ELISA strips.

DISCUSSION

Rapid detection of viruses and antibody to the virus is important in the diagnosis of etiology of disease. ELISAs have been used for the detection of viruses and antibody to the viruses. Traditional ELISAs for antigen or antibody detection take from 8 hours to two days to obtain the results (Ndifuna *et al.*, 1998). We have employed for the first time, a special kind of a microwave called the BIOWAVE to decrease the processing time to obtain the final result for antigen or antibody detection.

Here, we show that chicken serum antibody specific for IBV can be detected by a modified ELISA in about an hour using the BIOWAVE as compared to almost 2 days by the traditional protocol. The process time is considerably reduced greatly accelerating the diagnosis. The biowave method is as sensitive as the traditional ELISA method for detection of IBV antibody in chicken serum. Antibody can be detected up to 1:1000 dilutions by both methods. The O.D. values for the IBV ELISA follow the order, method 2 > method 1 > method 3 > method 4. This suggested that the microwaves in the BIOWAVE positively affect the IBV ELISA and that it is not a temperature-mediated effect alone.

In order to determine the ability to use the BIOWAVE for detection of viral antigens, the standardized ELISAs for the determination of FIV and REV in cell culture supernatants were applied. O.D. values for the FIV ELISA follow the order, method 1 > method 2 > method 3. Furthermore, both methods 1 and 2 for FIV detection were comparable for sensitivity of virus determination. Hence in this case as well the microwaves positively affect the ELISA. In the case of the REV ELISA O.D. values of

protein standards follow the order, method 3 > method 1 > method 2 > method 4. However, when the O.D. values of the virus in the supernatant are compared, they follow the order method 1 > method 2 > method 3 > method 4.

How does microwave energy affect the interaction between proteins to expedite the reaction? The exact mechanism of how microwaves cause heating is not known. Microwaves affect hydrogen bonding of water and increase vibrational energy thereby causing a quick transfer of energy between molecules. In the ELISAs that we have tested, the BIOWAVE gives higher O.D. values as compared to the traditional methods for the IBV and FIV ELISA's. Microwaves probably alter the flexibility of the antibody molecule as well as that of the antigen epitopes thereby enhancing the antigen-antibody interaction. Microwaves also have an effect on the ability to solubilize the viral antigen in presence of the detergent triton-X-100. With the FIV ELISA, the O.D. values for gag detection using the BIOWAVE were closer to the O.D. values obtained using the traditional method. Whereas, for the REV ELISA, the O.D. value for gag detection in the virion using the biowave was lower than the value obtained using the traditional method suggesting that the microwaves are likely to affect solubilization of the viral antigens. In the case of the REV ELISA, the microwave energy did not solubilize the antigen as well as what was obtained with the traditional protocol. Solubilization of viruses to release the antigen is probably dependent on a combination of temperature and time.

The microwaves generated in the PELCO Biowave correspond to a frequency of approximately 2.5 GHz. This frequency corresponds to energy of 0.0002384 kcal/mol. The resonance energy of a peptide bond for most amino acids is 20 kcal/mol, and except

for proline it is 10 kcal/mole. It was proposed that the microwave energy might in some way contribute to the resonance energy of the peptide bond, thereby leading to the diffusion of energy between molecules. However, since the microwave energy is lower than that of the peptide bond, this does not seem to be a possibility. There has to be some other mechanism how microwave enhance the protein-protein interactions.

If the ELISA for virus detection is developed against a virus internal antigen, the virus has to be solubilized using appropriate detergents to expose the internal antigen. Both FIV and REV ELISAs were based on the detection of the gag antigen that is internally present in the virion. Triton-X 100 at a final concentration of 20 % was used to solubilize the virus. Detergent concentration is an important factor for disrupting viruses.

The type of plate used for the ELISA in general is important. For the IBV antibody ELISA, we used the flat bottom simulon ELISA plates. For the REV and FIV antigen ELISA, we used high protein binding strips. A very high background was obtained when we used the high protein binding strips for the IBV-BIOWAVE ELISA.

The BIOWAVE microwave is a practical instrument to improve the processing time of an ELISA. This could be applied to detect viral antigens or antibody to viruses. A laboratory that uses the ELISA technique for the detection of any kind of antigen or antibody to determine etiology of disease can benefit from the use of the BIOWAVE. However, as with the traditional ELISAs, each antigen specific parameter needs to be standardized.

CHAPTER VI

SUMMARY AND CONCLUSION

Coronavirus nucleocapsid (N) protein binds the viral genome forming a helical nucleocapsid (Davies *et al.*, 1981). IBV N protein is phosphorylated and it has been speculated that phosphorylation contributes to the specificity of binding viral RNA. Coronavirus N protein is multi-functional and it has been proposed that phosphorylation might regulate the various roles of the N protein (Masters *et al.*, 1990; Masters and Sturman, 1990; Tahara *et al.*, 1998) . We show here that the N protein is phosphorylated at all times during IBV infection in the cell and from a maximum level of incorporation there is only a 70% drop in the intensity of the labeled protein at the end of one hour. MHV M has been shown to package nonviral RNA with the MHV packaging signal sequence into virus-like particles. The MHV N protein is dispensable for this process (Narayanan *et al.*, 2003a; Narayanan and Makino, 2001). Hence, phosphorylation is unlikely to contribute to specificity of RNA binding. It might however, increase the affinity for viral RNA. Double labeling studies using ^{3}H-leucine and ^{32}P-orthophosphate show that the N protein in the virion is more phosphorylated than the N protein from the virus-infected cell isolated at various times during infection. This result also suggests that enhanced phosphorylation of the N protein is important for some stage in virus assembly. It is not yet known if the N protein is differentially phosphorylated. It is possible that differential phosphorylation of the N protein is important in regulating

transcription, translation, replication and packaging of the viral genome. It is of interest to determine if various phosphorylated forms of the N protein exist in the cell.

Our results indicate that the bacterially expressed IBV N protein is not phosphorylated (data not shown). Zhou *et al.* (1996) have shown that RNA binding by N protein is not dependent on phosphorylation (Zhou *et al.*, 1996). A large complex of the recombinant N protein of molecular mass greater than 450 kilodalton (kDa) is obtained by gel-permeation chromatography. Transmission electron microscopy (TEM) studies of the recombinant N protein show that there are helical structures in the recombinant N protein preparation. These structures resemble nucleocapsid-like structures that are found within the virion. The diameter of the nucleocapsid-like structures ranges from 6 to 10 nm and the lengths vary from 50 to 500 nm. The diameter of the nucleocapsids obtained from the virion range from 10 to 14 nm and the lengths vary from 2 to 6 μm (Davies *et al.*, 1981). The variation in measurements of the virion nucleocapsid usually depends on how compact the nucleocapsid is held. The measurements of the diameter obtained for the IBV recombinant N protein nucleocapsid-like structures compare quite closely to the original measurements. The variation in length may be attributed to N binding to RNA of various lengths and specificity. These nucleocapsid-like structures are not formed by truncations of the N protein that correspond to amino acids 1 to 91, 1 to 171, 203 to 409 and 268 to 407 of the N protein. Amino acids 1 to 171, 203 to 409 and 268 to 407 bind RNA (Zhou *et al.*, 1996). Amino acids 268 to 407 of the carboxyl region of the N protein form large aggregates that elute in the void volume when purified by gel permeation chromatography through a Bio-gel P60 column, indicating that this

region interacts with itself. It is possible that N-N interaction and the RNA binding domain are required for the formation of the nucleocapsid. We show here for the first time that nucleocapsid-like structures are formed in the absence of other viral proteins. Since the bacterially expressed protein is not phosphorylated, phosphorylation is not necessary for the formation of nucleocapsid-like structures although it might be important in specificity of RNA binding.

The significance of formation of nucleocapsid-like structures is relevant in packaging the viral genome into the virion. Since other viral proteins are not required for formation of these structures, it is possible that N protein binds RNA and forms these structures. RNA is associated with the IBV recombinant N protein preparation. However it is not known if RNA is present in these structures. Nucleocapsid proteins have a tendency to oligomerize and self-assemble into such structures with the help of a RNA backbone. Nucleocapsid proteins of negative strand RNA viruses such as vesicular stomatitis virus (VSV), measles virus and rabies virus, form nucleocapsid-like structures in the absence of other viral structural proteins. RNA is associated with these structures. It is highly likely, therefore, that IBV N also forms these structures in the presence of an RNA backbone with which the IBV N protein assembles. It is possible that certain repeating oligomer units associate and form the helical nucleocapsid-like structure as has been observed with the rabies and measles virus nucleocapsid protein (Fooks *et al.*, 1993; Iseni *et al.*, 1998).

Since the coronavirus N protein binds subgenomic RNA and the viral genome (Siddell *et al.*, 1995), it is possible that certain other viral proteins may be required for

specific binding and packaging of the viral genome. MHV M protein, when co-expressed with the E protein, can package non-viral RNA that has the MHV packaging signal sequence and form virus-like particles. The MHV N protein is indispensable for this process (Narayanan *et al.*, 2003a; Vennema *et al.*, 1996). In the work reported by Vennema *et al* (1996), the length of the RNA was only a thousand nucleotides long. Where specificity of packaging likely depends on the interaction of other viral proteins with a packaging signal sequence, packaging of the viral genome (26 to 31 kb) possibly requires the N protein for compacting the genome. In the case of IBV, a putative packaging signal sequence has been identified based on homology with the MHV and BCV packaging signal sequences that are located in the 3' end of ORF 1b (Cologna and Hogue, 2000; Woo *et al.*, 1997). In the case of TGEV, the packaging signal is located in the 5' end of the genome (Escors *et al.*, 2003). However, is not known if the IBV putative packaging signal sequence is functionally relevant.

Double labeling studies using ^{3}H-leucine and ^{32}P-orthophosphate have shown that the ^{32}P:^{3}H cpm ratio is higher in the virion N than the ^{32}P:^{3}H cpm ratio in the N protein from infected cell lysates, suggesting that the virion N protein is more phosphorylated than the N protein from the infected cell lysates. The bacterially expressed IBV recombinant N protein is not phosphorylated and can form nucleocapsid-like structures in the absence of other viral proteins. So why is the N protein more phosphorylated in the virion? It is possible that a) phosphorylation might regulate the interaction of N protein with other viral proteins that are required for virus assembly, b) phosphorylation of N causes better compaction of the viral genome that is packaged as a

nucleocapsid into the virion, or c) phosphorylation increases the affinity of viral RNA binding. Once the sites of phosphorylation on the N protein are identified, mutagenesis of these sites can be performed to give a better idea of the role of phosphorylation of N protein in the virus life cycle. Bordo and Argos (1991) have suggested replacement of serine and threonine with alanine, and tyrosine with phenylalanine. These are considered to be safe replacements because serine, threonine and alanine are closely related to each other in structure and tyrosine and phenylalanine are closely related in structure (Bordo and Argos, 1991). Both alanine and phenylalanine are not putative phosphorylation sites and hence the effect of lack of phosphorylation of the protein can be studied by using these amino acids for replacement.

IBV N protein binds certain viral sequences in the 3'-untranslated region with a higher affinity (Zhou *et al.*, 1996) than other viral sequences. Zhou has shown that RNA binding to the 3'-UTR depends on the presence of U in the sequence. The 3'-UTR is 37% U-rich, which is higher than the rest of the genome. A sequence within the 3'-UTR with a 45% U content was bound better than a sequence with a 6.5% U content (Zhou, 1997). We show here that IBV recombinant N protein binds U_{15}-mer and U_{40}-mer RNA. Although binding to the U oligomer occurred in the presence of a large excess of yeast-t-RNA as non-specific competitor, it is likely that binding of IBV N protein to RNA is sequence and secondary structure dependent. It is possible that, since the 3'-UTR has a higher U content (37%) than the rest of the genome, uridylates may contribute to N binding to the 3'-UTR. The context of the U residues may also affect binding affinity of

binding. It will be interesting to perform competitive gel-shift assays to determine the relative binding of N to RNA U-oligomer and the sequence containing 45% U.

The presence of B cell epitopes on the IBV N protein and the conserved nature of the protein, make it an important serodiagnostic reagent for IBV (Ndifuna *et al*., 1998; Seah *et al*., 2000). IBV recombinant N protein expressed in bacteria has been previously used as a serodiagnostic reagent to detect anti-IBV antibody in the serum of chickens (Ndifuna *et al.*, 1998). We employed the recombinant bacterially expressed histidine-tagged N protein in the development of a rapid ELISA technique using a special microwave called the BIOWAVE to detect anti-IBV antibody in serum of chickens. The technique is superior to the regular ELISA as the time taken for the analysis with the BIOWAVE is around one and a half hours in comparison to the protocol used for the traditional ELISA. The BIOWAVE can be also used for the detection of other viruses as we have shown for the detection of reticuloendotheliosis virus and feline immunodeficiency virus in cell culture supernatants. The BIOWAVE can be used for any ELISA once the process has been standardized.

FUTURE STUDIES

Objective 1. Determine the sites of phosphorylation on the cellular and virion N protein.

Objective 2. Perform alanine/phenylalanine mutagenesis of the phosphorylated sites on the N protein and determine the importance of phosphorylation in the virus life cycle.

Objective 3. Determine if RNA is present in the helical nucleocapsid-like structures that are formed by the bacterially expressed IBV recombinant N protein using RNase-A gold immunolabeling followed by transmission electron microscopy.

Objective 4. Determine using 2D crystallography if repeating oligomers of N-protein are involved in forming the nucleocapsid-like structures.

Objective 5. Crystallize the IBV N protein.

REFERENCES

Adams, M. D., Rudner, D. Z., and Rio, D. C., 1996. Biochemistry and regulation of pre-mRNA splicing. Curr. Opin. Cell Biol. 8, 331-339.

Albassam, M. A., Winterfield, R. W., and Thacker, H. L., 1986. Comparison of the nephropathogenicity of four strains of infectious bronchitis virus. Avian Dis. 30, 468-476.

Alfadhli, A., Love, Z., Arvidson, B., Seeds, J., Willey, J., and Barklis, E., 2001. Hantavirus nucleocapsid protein oligomerization. J. Virol. 75, 2019-2023.

Alterio, J., Mallet, J., and Biguet, N. F., 2001. Multiple complexes involved in tyrosine hydroxylase mRNA stability in rat adrenal medulla, after reserpine stimulation. Mol. Cell Neurosci. 17, 179-189.

Anderson, R., and Wong, F., 1993. Membrane and phospholipid binding by murine coronaviral nucleocapsid N protein. Virology 194, 224-232.

Ausubel, F. M., Brent, R., Kingston, R. E., Moore, D. D., Seidman, J.G., Smith, J. A., and Kevin, S., 1987. Current protocols in molecular biology. John Wiley and Sons, Inc., New York, pp. 10.18.7-10.18.8.

Avellaneda, G. E., Villegas, P., Jackwood, M. W., and King, D. J., 1994. In vivo evaluation of the pathogenicity of field isolates of infectious bronchitis virus. Avian Dis. 38, 589-597.

Baker, S. C., and Lai, M. M., 1990. An in vitro system for the leader-primed transcription of coronavirus mRNAs. EMBO J. 9, 4173-4179.

Balmer, L. A., Beveridge, D. J., Jazayeri, J. A., Thomson, A. M., Walker, C. E., and Leedman, P. J., 2001. Identification of a novel AU-Rich element in the 3' untranslated region of epidermal growth factor receptor mRNA that is the target for regulated RNA-binding proteins. Mol. Cell. Biol. 21, 2070-2084.

Baric, R. S., Nelson, G. W., Fleming, J. O., Deans, R. J., Keck, J. G., Casteel, N., and Stohlman, S. A., 1988. Interactions between coronavirus nucleocapsid protein and viral RNAs: implications for viral transcription. J. Virol. 62, 4280-4287.

Baric, R.S., Stohlman, S.A., and Lai, M.M.., 1983. Characterization of replicative intermediate RNA of mouse hepatitis virus: presence of leader RNA sequences on nascent chains. J. Virol. 48, 633-640.

Baric, R. S., Stohlman, S. A., Razavi, M. K., and Lai, M. M., 1985. Characterization of leader-related small RNAs in coronavirus-infected cells: further evidence for leader-primed mechanism of transcription. Virus Res. 3, 19-33.

Baric, R. S., and Yount, B., 2000. Subgenomic negative-strand RNA function during mouse hepatitis virus infection. J. Virol. 74, 4039-4046.

Baron, M. D., and Forsell, K., 1991. Oligomerization of the structural proteins of rubella virus. Virology 185, 811-819.

Baudoux, P., Carrat, C., Besnardeau, L., Charley, B., and Laude, H., 1998. Coronavirus pseudoparticles formed with recombinant M and E proteins induce alpha interferon synthesis by leukocytes. J. Virol. 72, 8636-8643.

Baumruk, V., Gouyette, C., Huynh-Dinh, T., Sun, J. S., and Ghomi, M., 2001. Comparison between CUUG and UUCG tetraloops: thermodynamic stability and structural features analyzed by UV absorption and vibrational spectroscopy. Nucleic Acids Res. 29, 4089-4096.

Bink, H. H., Hellendoorn, K., van der Meulen, J., and Pleij, C. W., 2002. Protonation of non-Watson-Crick base pairs and encapsidation of turnip yellow mosaic virus RNA. Proc. Natl. Acad. Sci. U.S.A. 99, 13465-13470.

Blattner, F. R., Plunkett, G. 3rd, Bloch, C. A., Perna, N. T., Burland, V., Riley, M., Collado-Vides, J., Glasner, J. D., Rode, C. K., Mayhew, G. F., Gregor, J., Davis, N. W., Kirkpatrick, H. A., Goeden, M. A., Rose, D. J., Mau, B., and Shao, Y., 1997. The complete genome sequence of *Escherichia coli* K-12. Science 277, 1453-1474.

Bontems, S., Di Valentin, E., Baudoux, L., Rentier, B., Sadzot-Delvaux, C., and Piette, J., 2002. Phosphorylation of varicella-zoster virus IE63 protein by casein kinases influences its cellular localization and gene regulation activity. J. Biol. Chem. 277, 21050-21060.

Bordo, D. and Argos, P., 1991. Suggestions for "safe" residue substitutions in site-directed mutagenesis. J. Mol. Biol. 217, 721-729.

Boursnell, M. E., Brown, T. D., Foulds, I. J., Green, P. F., Tomley, F. M., and Binns, M. M., 1987. The complete nucleotide sequence of avian infectious bronchitis virus: analysis of the polymerase-coding region. Adv. Exp. Med. Biol. 218, 15-29.

Brayton, P. R., Lai, M. M., Patton, C. D., and Stohlman, S. A., 1982. Characterization of two RNA polymerase activities induced by mouse hepatitis virus. J. Virol. 42, 847-853.

Brayton, P. R., Stohlman, S. A., and Lai, M. M., 1984. Further characterization of mouse hepatitis virus RNA-dependent RNA polymerases. Virology 133, 197-201.

Brierley, I., Boursnell, M. E., Binns, M. M., Bilimoria, B., Blok, V. C., Brown, T. D., and Inglis, S. C., 1987. An efficient ribosomal frame-shifting signal in the polymerase-encoding region of the coronavirus IBV. EMBO J. 6, 3779-3785.

Brierley, I., Digard, P., and Inglis, S. C., 1989. Characterization of an efficient coronavirus ribosomal frameshifting signal: requirement for an RNA pseudoknot. Cell 57, 537-547.

Bullock, T. L., Sherlin, L. D., and Perona, J. J., 2000. Tertiary core rearrangements in a tight binding transfer RNA aptamer. Nat. Struct. Biol. 7, 497-504.

Burd, C. G., and Dreyfuss, G., 1994. Conserved structures and diversity of functions of RNA-binding proteins. Science 265, 615-621.

Calnan, B. J., Biancalana, S., Hudson, D., and Frankel, A. D., 1991. Analysis of arginine-rich peptides from the HIV Tat protein reveals unusual features of RNA-protein recognition. Genes Dev. 5, 201-210.

Casais, R., Dove, B., Cavanagh, D., and Britton, P., 2003. Recombinant avian infectious bronchitis virus expressing a heterologous spike gene demonstrates that the spike protein is a determinant of cell tropism. J. Virol. 77, 9084-9089.

Cavanagh, D., 1983. Coronavirus IBV glycopolypeptides: size of their polypeptide moieties and nature of their oligosaccharides. J. Gen. Virol. 64, 1187-1191.

Cavanagh, D., 1997. Nidovirales: a new order comprising Coronaviridae and Arteriviridae. Arch. Virol. 142, 629-633.

Chang, R. Y., and Brian, D. A., 1996. *cis* requirement for N-specific protein sequence in bovine coronavirus defective interfering RNA replication. J. Virol. 70, 2201-2207.

Chang, R. Y., Hofmann, M. A., Sethna, P. B., and Brian, D. A., 1994. A cis-acting function for the coronavirus leader in defective interfering RNA replication. J. Virol. 68, 8223-8231.

Chapdelaine, Y., Kirk, D., Karsies, A., Hohn, T., and Leclerc, D., 2002. Mutation of capsid protein phosphorylation sites abolishes cauliflower mosaic virus infectivity. J. Virol. 76, 11748-11752.

Cheley, S., and Anderson, R., 1981. Cellular synthesis and modification of murine hepatitis virus polypeptides. J. Gen. Virol. 54, 301-311.

Chew, P. H., Wakenell, P. S., and Farver, T. B., 1997. Pathogenicity of attenuated infectious bronchitis viruses for oviducts of chickens exposed in ovo. Avian Dis. 41, 598-603.

Chodosh, L. A., 1992. DNA-protein interactions: mobility shift DNA-binding assay using gel electrophoresis, in Ausubel, F. M., Brent, R., Kingston, R. E., Moore,

D. D., Seidman, J.G., Smith, J. A., and Kevin, S. (Eds). Current protocols in molecular biology, supplement 36, John Wiley & Sons, Inc. New York, pp. 12.2.1-12.2.7.

Collisson, E. W., Parr, R. L., Wang, L., and Williams, A. K., 1992. An overview of the molecular characteristics of avian infectious bronchitis virus. Poultry Sci. Rev. 4, 41-55.

Collisson, E. W., Zhou, M., Gershon, P., and Jayaram, J., 2001. Infectious bronchitis virus nucleocapsid protein interactions with the 3' untranslated region of genomic RNA depend on uridylate bases. Adv. Exp. Med. Biol. 494, 669-675.

Cologna, R., and Hogue, B. G., 2000. Identification of a bovine coronavirus packaging signal. J. Virol. 74, 580-583.

Corse, E., and Machamer, C. E., 2000. Infectious bronchitis virus E protein is targeted to the Golgi complex and directs release of virus-like particles. J. Virol. 74, 4319-4326.

Corse, E., and Machamer, C. E., 2002. The cytoplasmic tail of infectious bronchitis virus E protein directs Golgi targeting. J. Virol. 76, 1273-1284.

Corse, E., and Machamer, C. E., 2003. The cytoplasmic tails of infectious bronchitis virus E and M proteins mediate their interaction. Virology 312, 25-34.

Coulis, C. M., Lee, C., Nardone, V., and Prokipcak, R. D., 2000. Inhibition of c-myc expression in cells by targeting an RNA-protein interaction using antisense oligonucleotides. Mol. Pharmacol. 57, 485-94.

Crinion, R. A., and Hofstad, M.S., 1972. Pathogenicity of two embryo-passage levels of avian infectious bronchitis virus for the oviduct of young chicekns of various ages. Avian Dis. 16, 967-973.

Cunnigham, C. H., 1970. Avian infectious bronchitis. Adv. Vet. Sci. Comp. Med. 14, 105-148.

Dalton, K., Casais, R., Shaw, K., Stirrups, K., Evans, S., Britton, P., Brown, T. D., and Cavanagh, D., 2001. cis-acting sequences required for coronavirus infectious bronchitis virus defective-RNA replication and packaging. J. Virol. 75, 125-133.

Davies, H. A., Dourmashkin, R. R., and Macnaughton, M. R., 1981. Ribonucleoprotein of avian infectious bronchitis virus. J. Gen. Virol. 53, 67-74.

Davies, H. A., and Macnaughton, M. R., 1979. Comparison of the morphology of three coronaviruses. Arch. Virol. 59, 25-33.

de Groot, R. J., Maduro, J., Lenstra, J. A., Horzinek, M. C., van der Zeijst, B. A., and Spaan, W. J., 1987. cDNA cloning and sequence analysis of the gene encoding the peplomer protein of feline infectious peritonitis virus. J. Gen. Virol. 68, 2639-2646.

de Haan, C. A., Kuo, L., Masters, P. S., Vennema, H., and Rottier, P. J., 1998. Coronavirus particle assembly: primary structure requirements of the membrane protein. J. Virol. 72, 6838-6850.

de Haan, C. A., Vennema, H., and Rottier, P. J., 2000. Assembly of the coronavirus envelope: homotypic interactions between the M proteins. J. Virol. 74, 4967-4978.

Dea, S., and Tijssen, P., 1988. Viral agents associated with outbreaks of diarrhea in turkey flocks in Quebec. Can. J. Vet. Res. 52, 53-57.

Deng, L., and Gershon, P. D., 1997. Interplay of two uridylate-specific RNA binding sites in the translocation of poly(A) polymerase from vaccinia virus. EMBO J. 16, 1103-1113.

Draper, D. E., 1995. Protein-RNA recognition. Annu. Rev. Biochem. 64, 593-620.

Drosten, C., Gunther, S., Preiser, W., van der Werf, S., Brodt, H. R., Becker, S., Rabenau, H., Panning, M., Kolesnikova, L., Fouchier, R. A., Berger, A., Burguiere, A. M., Cinatl, J., Eickmann, M., Escriou, N., Grywna, K., Kramme,

S., Manuguerra, J. C., Muller, S., Rickerts, V., Sturmer, M., Vieth, S., Klenk, H. D., Osterhaus, A. D., Schmitz, H., and Doerr, H. W., 2003. Identification of a novel coronavirus in patients with severe acute respiratory syndrome. N. Engl. J. Med. 348, 1967-1976.

Du, Z., Yu, J., Andino, R., and James, T. L., 2003. Extending the family of UNCG-like tetraloop motifs: NMR structure of a CACG tetraloop from coxsackievirus B3. Biochemistr*y* 42, 4373-4383.

Dveksler, G. S., Dieffenbach, C. W., Cardellichio, C. B., McCuaig, K., Pensiero, M. N., Jiang, G. S., Beauchemin, N., and Holmes, K. V., 1993. Several members of the mouse carcinoembryonic antigen-related glycoprotein family are functional receptors for the coronavirus mouse hepatitis virus-A59. J. Virol. 67, 1-8.

Dveksler, G. S., Pensiero, M. N., Cardellichio, C. B., Williams, R. K., Jiang, G. S., Holmes, K. V., and Dieffenbach, C. W., 1991. Cloning of the mouse hepatitis virus (MHV) receptor: expression in human and hamster cell lines confers susceptibility to MHV. J. Virol. 65, 6881-6891.

Ellis, E. A., 2002. New embedding formulations using Quetol 651. Microsc. Microanalysis 8 (supp 2): 884 CD.

Errington, W., and Emmerson, P. T., 1997. Assembly of recombinant Newcastle disease virus nucleocapsid protein into nucleocapsid-like structures is inhibited by the phosphoprotein. J. Gen. Virol. 78, 2335-2339.

Escors, D., Camafeita, E., Ortego, J., Laude, H., and Enjuanes, L., 2001. Organization of two transmissible gastroenteritis coronavirus membrane protein topologies within the virion and core. J. Virol. 75, 12228-12240.

Escors, D., Izeta, A., Capiscol, C., and Enjuanes, L., 2003. Transmissible gastroenteritis coronavirus packaging signal is located at the 5' end of the virus genome. J. Virol. 77, 7890-902.

Fernandez-Miragall, O., and Martinez-Salas, E., 2003. Structural organization of a viral IRES depends on the integrity of the GNRA motif. RNA 9, 1333-1344.

Fooks, A. R., Stephenson, J. R., Warnes, A., Dowsett, A. B., Rima, B. K., and Wilkinson, G. W., 1993. Measles virus nucleocapsid protein expressed in insect cells assembles into nucleocapsid-like structures. J. Gen. Virol. 74, 1439-1444.

Fosmire, J. A., Hwang, K., and Makino, S., 1992. Identification and characterization of a coronavirus packaging signal. J. Virol. 66, 3522-3530.

Furuya, T., and Lai, M. M., 1993. Three different cellular proteins bind to complementary sites on the 5'-end-positive and 3'-end-negative strands of mouse hepatitis virus RNA. J. Virol. 67, 7215-7222.

Gallagher, T. M., 1997. A role for naturally occurring variation of the murine coronavirus spike protein in stabilizing association with the cellular receptor. J. Virol. 71, 3129-3137.

Garcia-Gras, E. A., Chi, P., and Thompson, E. A., 2000. Glucocorticoid-mediated destabilization of cyclin D3 mRNA involves RNA-protein interactions in the 3'-untranslated region of the mRNA. J. Biol. Chem. 275, 22001-22008.

Git, A., and Standart, N., 2002. The KH domains of Xenopus Vg1RBP mediate RNA binding and self-association. RNA 8, 1319-1333.

Gombart, A. F., Hirano, A., and Wong, T. C., 1995. Nucleoprotein phosphorylated on both serine and threonine is preferentially assembled into the nucleocapsids of measles virus. Virus Res. 37, 63-73.

Gonzalez, J. M., Gomez-Puertas, P., Cavanagh, D., Gorbalenya, A. E., and Enjuanes, L., 2003. A comparative sequence analysis to revise the current taxonomy of the family Coronaviridae. Arch. Virol. 148, 2207-2235.

Gross, I., Hohenberg, H., and Krausslich, H. G., 1997. In vitro assembly properties of purified bacterially expressed capsid proteins of human immunodeficiency virus. Eur. J. Biochem. 249, 592-600.

Haijema, B. J., Volders, H., and Rottier, P. J., 2003. Switching species tropism: an effective way to manipulate the feline coronavirus genome. J. Virol. 77, 4528-4238.

Hiscox, J. A., Wurm, T., Wilson, L., Britton, P., Cavanagh, D., and Brooks, G., 2001. The coronavirus infectious bronchitis virus nucleoprotein localizes to the nucleolus. J. Virol. 75, 506-512.s

Hogue, B. G., 1995. Bovine coronavirus nucleocapsid protein processing and assembly. Adv. Exp. Med. Biol. 380, 259-63.

Hogue, B. G., and Brian, D. A., 1986. Structural proteins of human respiratory coronavirus OC43. Virus Res. 5, 131-144.

Hoppert, M., and Holzenburg, A., 1998 Electron microscopy in microbiology. RMS Handbook Series, Bios Scientific Publishers Ltd., Oxford, pp. 22-25.

Hou, Y. M., Zhang, X., Holland, J. A., and Davis, D. R., 2001. An important 2'-OH group for an RNA-protein interaction. Nucleic Acids Res. 29, 976-985.

Hou, Y. T., Xin, X. P., Li, L., and Zimmerman, E. M., 2000. Regulation of insulin-like growth factor binding protein-5 mRNA abundance in rat intestinal smooth muscle. Biochem. Biophys. Res. Commun. 275, 422-427.

Hsue, B., Hartshorne, T., and Masters, P. S., 2000. Characterization of an essential RNA secondary structure in the 3' untranslated region of the murine coronavirus genome. J. Virol. 74, 6911-21.

Hsue, B., and Masters, P. S., 1997. A bulged stem-loop structure in the 3' untranslated region of the genome of the coronavirus mouse hepatitis virus is essential for replication. J. Virol. 71, 7567-7578.

Huang, P., and Lai, M. M., 2001. Heterogeneous nuclear ribonucleoprotein A1 binds to the 3'-untranslated region and mediates potential 5'-3'-end cross talks of mouse hepatitis virus RNA. J. Virol. 75, 5009-5017.

Ignjatovic, J., and Sapats, S., 2000. Avian infectious bronchitis virus. Rev. Sci. Tech. 19, 493-508.

Iseni, F., Barge, A., Baudin, F., Blondel, D., and Ruigrok, R. W., 1998. Characterization of rabies virus nucleocapsids and recombinant nucleocapsid-like structures. J. Gen. Virol. 79, 2909-2919.

Jeong, Y. S., and Makino, S., 1992. Mechanism of coronavirus transcription: duration of primary transcription initiation activity and effects of subgenomic RNA transcription on RNA replication. J. Virol. 66, 3339-3346.

Johnson, L., and Gershon, P. D., 1999. RNA binding characteristics and overall topology of the vaccinia poly(A) polymerase-processivity factor-primer complex. Nucleic Acids Res. 27, 2708-2721.

Kalicharran, K., and Dales, S., 1995. Dephosphorylation of the nucleocapsid protein of inoculum JHMV may be essential for initiating replication. Adv. Exp. Med. Biol. 380, 485-489.

Kash, J. C., Cunningham, D. M., Smit, M. W., Park, Y., Fritz, D., Wilusz, J., and Katze, M. G., 2002. Selective translation of eukaryotic mRNAs: functional molecular analysis of GRSF-1, a positive regulator of influenza virus protein synthesis. J. Virol. 76, 10417-10426.

Ke, Y., Sierzputowska-Gracz, H., Gdaniec, Z., and Theil, E. C., 2000. Internal loop/bulge and hairpin loop of the iron-responsive element of ferritin mRNA contribute to maximal iron regulatory protein 2 binding and translational regulation in the iso-iron-responsive element/iso-iron regulatory protein family. Biochemistry 39, 6235-6242.

King, B., and Brian, D. A., 1982. Bovine coronavirus structural proteins. J. Virol. 42, 700-707.

Koloteva-Levine, N., Amichay, M., and Elroy-Stein, O., 2002. Interaction of hnRNP-C1/C2 proteins with RNA: analysis using the yeast three-hybrid system. FEBS Lett. 523, 73-78.

Krijnse-Locker, J., Ericsson, M., Rottier, P. J., and Griffiths, G., 1994. Characterization of the budding compartment of mouse hepatitis virus: evidence that transport from the RER to the Golgi complex requires only one vesicular transport step. J. Cell Biol. 124, 55-70.

Krishnan, R., Chang, R. Y., and Brian, D. A., 1996. Tandem placement of a coronavirus promoter results in enhanced mRNA synthesis from the downstream-most initiation site. Virology 218, 400-405.

Ksiazek, T. G., Erdman, D., Goldsmith, C. S., Zaki, S. R., Peret, T., Emery, S., Tong, S., Urbani, C., Comer, J. A., Lim, W., Rollin, P. E., Dowell, S. F., Ling, A. E., Humphrey, C. D., Shieh, W. J., Guarner, J., Paddock, C. D., Rota, P., Fields, B., DeRisi, J., Yang, J. Y., Cox, N., Hughes, J. M., LeDuc, J. W., Bellini, W. J., and Anderson, L. J., 2003. A novel coronavirus associated with severe acute respiratory syndrome. N. Engl. J. Med. 348, 1953-1966.

Kunkel, M., Lorinczi, M., Rijnbrand, R., Lemon, S. M., and Watowich, S. J., 2001. Self-assembly of nucleocapsid-like particles from recombinant hepatitis C virus core protein. J. Virol. 75, 2119-2129.

Kuo, L., and Masters, P. S., 2002. Genetic evidence for a structural interaction between the carboxy termini of the membrane and nucleocapsid proteins of mouse hepatitis virus. J. Virol. 76, 4987-4999.

Lai, M. M. and Holmes, K. V., 2001. Coronaviridae: the viruses and their replication, in: Knipe, D.M., Howley, P.M., Griffin, D.E., Lamb, R.A., Martin, M.A., Roizman, B., Straus, S.E. (4th Eds.), Fields Virology, Lippincott Raven, Philadelphia, pp 1163-1219.

Lai, M. M., Patton, C. D., Baric, R. S., and Stohlman, S. A., 1983. Presence of leader sequences in the mRNA of mouse hepatitis virus. J. Virol. 46, 1027-1033.

Lai, M. M., Patton, C. D., and Stohlman, S. A., 1982. Replication of mouse hepatitis virus: negative-stranded RNA and replicative form RNA are of genome length. J. Virol. 44, 487-92.

Leibowitz, J. L., and Weiss, S. R., 1981. Murine coronavirus RNA. Adv. Exp. Med. Biol. 142, 227-243.

Li, H. P., Huang, P., Park, S., and Lai, M. M., 1999. Polypyrimidine tract-binding protein binds to the leader RNA of mouse hepatitis virus and serves as a regulator of viral transcription. J. Virol. 73, 772-777.

Li, H. P., Zhang, X., Duncan, R., Comai, L., and Lai, M. M., 1997. Heterogeneous nuclear ribonucleoprotein A1 binds to the transcription-regulatory region of mouse hepatitis virus RNA. Proc. Natl. Acad. Sci. U.S.A. 94, 9544-9549.

Li, W., Moore, M. J., Vasilieva, N., Sui, J., Wong, S. K., Berne, M. A., Somasundaran, M., Sullivan, J. L., Luzuriaga, K., Greenough, T. C., Choe, H., and Farzan, M., 2003. Angiotensin-converting enzyme 2 is a functional receptor for the SARS coronavirus. Nature 426, 450-454.

Lim, K. P., Ng, L. F., and Liu, D. X., 2000. Identification of a novel cleavage activity of the first papain-like proteinase domain encoded by open reading frame 1a of the coronavirus Avian infectious bronchitis virus and characterization of the cleavage products. J. Virol. 74, 1674-1685.

Lim, K. P., Xu, H. Y., and Liu, D. X., 2001. Physical interaction between the membrane (M) and envelope (E) proteins of the coronavirus avian infectious bronchitis virus (IBV). Adv. Exp. Med. Biol. 494, 595-602.

Lin, S. S., Chang, S. C., Wang, Y. H., Sun, C. Y., and Chang, M. F., 2000. Specific interaction between the hepatitis delta virus RNA and glyceraldehyde 3-phosphate dehydrogenase: an enhancement on ribozyme catalysis. Virology 271, 46-57.

Liu, D. X., Brierley, I., Tibbles, K. W., and Brown, T. D., 1994. A 100-kilodalton polypeptide encoded by open reading frame (ORF) 1b of the coronavirus infectious bronchitis virus is processed by ORF 1a products. J. Virol. 68, 5772-5780.

Liu, D. X., and Inglis, S. C., 1991. Association of the infectious bronchitis virus 3c protein with the virion envelope. Virology 185, 911-917.

Liu, D. X., and Inglis, S. C., 1992. Internal entry of ribosomes on a tricistronic mRNA encoded by infectious bronchitis virus. J. Virol. 66, 6143-6154.

Liu, D. X., Shen, S., Xu, H. Y., and Wang, S. F., 1998. Proteolytic mapping of the coronavirus infectious bronchitis virus 1b polyprotein: evidence for the presence of four cleavage sites of the 3C-like proteinase and identification of two novel cleavage products. Virology 246, 288-297.

Liu, D. X., Xu, H. Y., and Brown, T. D., 1997. Proteolytic processing of the coronavirus infectious bronchitis virus 1a polyprotein: identification of a 10-kilodalton polypeptide and determination of its cleavage sites. J. Virol. 71, 1814-1820.

Liu, Q., Johnson, R. F., and Leibowitz, J. L., 2001. Secondary structural elements within the 3' untranslated region of mouse hepatitis virus strain JHM genomic RNA. J. Virol. 75, 12105-12113.

Locker, J. K., Griffiths, G., Horzinek, M. C., and Rottier, P. J., 1992. O-glycosylation of the coronavirus M protein. Differential localization of sialyltransferases in N- and O-linked glycosylation. J. Biol. Chem. 267, 14094-14101.

Locker, J. K., Opstelten, D. J., Ericsson, M., Horzinek, M. C., and Rottier, P. J., 1995. Oligomerization of a trans-Golgi/trans-Golgi network retained protein occurs in the Golgi complex and may be part of its retention. J. Biol. Chem. 270, 8815-8821.

Lomniczi, B., 1977. Biological properties of avian coronavirus RNA. J. Gen. Virol. 36, 531-533.

Lomniczi, B., and Morser, J., 1981. Polypeptides of infectious bronchitis virus. I. Polypeptides of the virion. J. Gen. Virol. 55, 155-164.

Lopez de Quinto, S., Lafuente, E., and Martinez-Salas, E., 2001. IRES interaction with translation initiation factors: functional characterization of novel RNA contacts with eIF3, eIF4B, and eIF4GII. RNA 7, 1213-1226.

Luo, Z., and Weiss, S. R., 1998. Roles in cell-to-cell fusion of two conserved hydrophobic regions in the murine coronavirus spike protein. Virology 244, 483-494.

Machamer, C. E., Mentone, S. A., Rose, J. K., and Farquhar, M. G., 1990. The E1 glycoprotein of an avian coronavirus is targeted to the cis Golgi complex. Proc. Natl. Acad. Sci. U.S.A. 87, 6944-6948.

Macnaughton, M. R., Davies, H. A., and Nermut, M.V., 1978. Ribonucleoprotein-like structures from coronavirus particles. Virology 39, 545-549.

Macnaughton, M. R., and Madge, M. H., 1977. The polypeptide composition of avain infectious bronchitis virus particles. Arch. Virol. 55, 47-54.

Maeda, J., Repass, J. F., Maeda, A., and Makino, S., 2001. Membrane topology of coronavirus E protein. Virology 281, 163-169.

Marra, M. A., Jones, S. J., Astell, C. R., Holt, R. A., Brooks-Wilson, A., Butterfield, Y. S., Khattra, J., Asano, J. K., Barber, S. A., Chan, S. Y., Cloutier, A., Coughlin, S. M., Freeman, D., Girn, N., Griffith, O. L., Leach, S. R., Mayo, M., McDonald, H., Montgomery, S. B., Pandoh, P. K., Petrescu, A. S., Robertson, A. G., Schein, J. E., Siddiqui, A., Smailus, D. E., Stott, J. M., Yang, G. S., Plummer, F., Andonov, A., Artsob, H., Bastien, N., Bernard, K., Booth, T. F., Bowness, D., Czub, M., Drebot, M., Fernando, L., Flick, R., Garbutt, M., Gray, M., Grolla, A., Jones, S., Feldmann, H., Meyers, A., Kabani, A., Li, Y., Normand, S., Stroher, U., Tipples, G. A., Tyler, S., Vogrig, R., Ward, D., Watson, B., Brunham, R. C., Krajden, M., Petric, M., Skowronski, D. M., Upton, C., and Roper, R. L., 2003. The genome sequence of the SARS-associated coronavirus. Science 300, 1399-1404.

Masters, P. S., Parker, M. M., Ricard, C. S., Duchala, C., Frana, M. F., Holmes, K. V., and Sturman, L. S., 1990. Structure and function studies of the nucleocapsid protein of mouse hepatitis virus. Adv. Exp. Med. Biol. 276, 239-246.

Masters, P. S., and Sturman, L. S., 1990. Background paper. Functions of the coronavirus nucleocapsid protein. Adv. Exp. Med. Biol. 276, 235-238.

Matsuyama, S., and Taguchi, F., 2002. Receptor-induced conformational changes of murine coronavirus spike protein. J. Virol. 76, 11819-11826.

McCall, M., Brown, T., Hunter, W. N., and Kennard, O., 1986. The crystal structure of g27d(GGATGGGAG): an essential part of the binding site for transcription factor IIIA. Nature 322, 661-664.

McIntosh, K., Chao, R. K., Krause, H. E., Wasil, R., Mocega, H. E., and Mufson, M. A., 1974. Coronavirus infection in acute lower respiratory tract disease of infants. J. Infect. Dis. 130, 502-507.

Moore, P. B., 1999. Structural motifs in RNA. Annu. Rev. Biochem. 68, 287-300.

Murphy, L. B., Loney, C., Murray, J., Bhella, D., Ashton, P., and Yeo, R. P., 2003. Investigations into the amino-terminal domain of the respiratory syncytial virus nucleocapsid protein reveal elements important for nucleocapsid formation and interaction with the phosphoprotein. Virology 307, 143-153.

Myszka, D. G., 1997. Kinetic analysis of macromolecular interactions using surface plasmon resonance biosensors. Curr. Opin. Biotechnol. 8, 50-57.

Myszka, D. G., 2000. Kinetic, equilibrium, and thermodynamic analysis of macromolecular interactions with BIACORE. Methods Enzymol. 323, 325-340.

Myszka, D. G., and Rich, R. L., 2000. Implementing surface plasmon resonance biosensors in drug discovery. 3, 310-317.

Nanda, S. K., and Leibowitz, J. L., 2001. Mitochondrial aconitase binds to the 3' untranslated region of the mouse hepatitis virus genome. J. Virol. 75, 3352-3362.

Narayanan, K., Chen, C. J., Maeda, J., and Makino, S., 2003a. Nucleocapsid-independent specific viral RNA packaging via viral envelope protein and viral RNA signal. J. Virol. 77, 2922-2927.

Narayanan, K., Kim, K. H., and Makino, S., 2003b. Characterization of N protein self-association in coronavirus ribonucleoprotein complexes. Virus Res. 98, 131-140.

Narayanan, K., Maeda, A., Maeda, J., and Makino, S., 2000. Characterization of the coronavirus M protein and nucleocapsid interaction in infected cells. J. Virol. 74, 8127-8134.

Narayanan, K., and Makino, S., 2001. Cooperation of an RNA packaging signal and a viral envelope protein in coronavirus RNA packaging. J. Virol. 75, 9059-9067.

Ndifuna, A., Waters, A. K., Zhou, M., and Collisson, E. W., 1998. Recombinant nucleocapsid protein is potentially an inexpensive, effective serodiagnostic reagent for infectious bronchitis virus. J. Virol. Methods 70, 37-44.

Nelson, G. W., Stohlman, S. A., and Tahara, S. M., 2000. High affinity interaction between nucleocapsid protein and leader/intergenic sequence of mouse hepatitis virus RNA. J. Gen. Virol. 81, 181-188.

Nguyen, V. P., and Hogue, B. G., 1997. Protein interactions during coronavirus assembly. J. Virol. 71, 9278-9284.

Niemann, H., and Klenk, H. D., 1981. Coronavirus glycoprotein E1, a new type of viral glycoprotein. J. Mol. Biol. 153, 993-1010.

Paoletti, A. C., Shubsda, M. F., Hudson, B. S., and Borer, P. N., 2002. Affinities of the nucleocapsid protein for variants of SL3 RNA in HIV-1. Biochemistry 41, 15423-15428.

Peiris, J. S., Lai, S. T., Poon, L. L., Guan, Y., Yam, L. Y., Lim, W., Nicholls, J., Yee, W. K., Yan, W. W., Cheung, M. T., Cheng, V. C., Chan, K. H., Tsang, D. N., Yung,

R. W., Ng, T. K., and Yuen, K. Y., 2003. Coronavirus as a possible cause of severe acute respiratory syndrome. Lancet 361, 1319-1325.

Perederina, A., Nevskaya, N., Nikonov, O., Nikulin, A., Dumas, P., Yao, M., Tanaka, I., Garber, M., Gongadze, G., and Nikonov, S., 2002. Detailed analysis of RNA-protein interactions within the bacterial ribosomal protein L5/5S rRNA complex. RNA 8, 1548-1557.

Perlman, S., Ries, D., Bogler, E., Chang, L. J., and Stolfus, C. M., 1986. MHv nucleocapsid synthesis in the presence of cycloheximide and the accumulation of negative stranded RNA. Virus Res. 6, 261-272.

Pinto, R. M., Bosch, A., and Bishop, D. H., 1994. Structures associated with the expression of rabies virus structural genes in insect cells. Virus Res. 31, 139-145.

Popova, R., and Zhang, X., 2002. The spike but not the hemagglutinin/esterase protein of bovine coronavirus is necessary and sufficient for viral infection. Virology 294, 222-236.

Raamsman, M. J., Locker, J. K., de Hooge, A., de Vries, A. A., Griffiths, G., Vennema, H., and Rottier, P. J., 2000. Characterization of the coronavirus mouse hepatitis virus strain A59 small membrane protein E. J. Virol. 74, 2333-2342.

Raha, T., Chattopadhyay, D., and Roy, S., 1999. A phosphorylation-induced major structural change in the N-terminal domain of the P protein of Chandipura virus. Biochemistry 38, 2110-2116.

Raha, T., Samal, E., Majumdar, A., Basak, S., Chattopadhyay, D., and Chattopadhyay, D. J., 2000. N-terminal region of P protein of Chandipura virus is responsible for phosphorylation-mediated homodimerization. Protein Eng. 13, 437-444.

Raman, S., Bouma, P., Williams, G. D., and Brian, D. A., 2003. Stem-loop III in the 5' untranslated region is a cis-acting element in bovine coronavirus defective interfering RNA replication. J. Virol. 77, 6720-6730.

Reynolds, E. S., 1963. The use of lead citrate at high pH as an electron dense stain in electron microscopy. J. Cell Biol. 17, 208-212.

Richter, S., Cao, H., and Rana, T. M., 2002. Specific HIV-1 TAR RNA loop sequence and functional groups are required for human cyclin T1-Tat-TAR ternary complex formation. Biochemistry 41, 6391-6397.

Risco, C., Anton, I. M., Enjuanes, L., and Carrascosa, J. L., 1996. The transmissible gastroenteritis coronavirus contains a spherical core shell consisting of M and N proteins. J. Virol. 70, 4773-4777.

Risco, C., Muntion, M., Enjuanes, L., and Carrascosa, J. L., 1998. Two types of virus-related particles are found during transmissible gastroenteritis virus morphogenesis. J. Virol. 72, 4022-4031.

Rota, P. A., Oberste, M. S., Monroe, S. S., Nix, W. A., Campagnoli, R., Icenogle, J. P., Penaranda, S., Bankamp, B., Maher, K., Chen, M. H., Tong, S., Tamin, A., Lowe, L., Frace, M., DeRisi, J. L., Chen, Q., Wang, D., Erdman, D. D., Peret, T. C., Burns, C., Ksiazek, T. G., Rollin, P. E., Sanchez, A., Liffick, S., Holloway, B., Limor, J., McCaustland, K., Olsen-Rasmussen, M., Fouchier, R., Gunther, S., Osterhaus, A. D., Drosten, C., Pallansch, M. A., Anderson, L. J., and Bellini, W. J., 2003. Characterization of a novel coronavirus associated with severe acute respiratory syndrome. Science 300, 1394-1399.

Sachs, A.B., Bond, M.W., and Kornberg, R.D., 1986. A sinlge gene from yeast for both nuclear and cytoplasmic polyadenylate-binding proteins: domain structure and expression. Cell 45, 87-835.

Salanueva, I. J., Carrascosa, J. L., and Risco, C., 1999. Structural maturation of the transmissible gastroenteritis coronavirus. J. Virol. 73, 7952-7964.

Sambrook, S., Fritsch, E. F., and Maniatis, T., 1989. Molecular Cloning- A Laboratory Manual. 2nd edition. Cold Spring Laboratory Press, New York.

Sandalon, Z., and Oppenheim, A., 1997. Self-assembly and protein-protein interactions between the SV40 capsid proteins produced in insect cells. Virology 237, 414-421.

Sawicki, S. G., and Sawicki, D. L., 1990. Coronavirus transcription: subgenomic mouse hepatitis virus replicative intermediates function in RNA synthesis. J. Virol. 64, 1050-1056.

Seah, J. N., Yu, L., and Kwang, J., 2000. Localization of linear B-cell epitopes on infectious bronchitis virus nucleocapsid protein. Vet. Microbiol. 75, 11-16.

Schaad, M. C., and Baric, R. S., 1994. Genetics of mouse hepatitis virus transcription: evidence that subgenomic negative strands are functional templates. J. Virol. 68, 8169-8179.

Schalk, A. F. and Hawn, M.C., 1931. An apparently new respiratory disease of baby chicks. J. Am. Vet. Med. Assoc. 78, 413-422.

Schochetman, G., Stevens, R. H., and Simpson, R. W., 1977. Presence of infectious polyadenylated RNA in coronavirus avian bronchitis virus. Virology 77, 772-782.

Schoehn, G., Iseni, F., Mavrakis, M., Blondel, D., and Ruigrok, R. W., 2001. Structure of recombinant rabies virus nucleoprotein-RNA complex and identification of the phosphoprotein binding site. J. Virol. 75, 490-498.

Sefton, B. M., Beemon, K., and Hunter, T., 1978. Comparison of the expression of the src gene of Rous sarcoma virus in vitro and in vivo. J Virol. 28, 957-971.

Sethna, P. B., Hofmann, M. A., and Brian, D. A., 1991. Minus-strand copies of replicating coronavirus mRNAs contain antileaders. J. Virol. 65, 320-325.

Sethna, P. B., Hung, S. L., and Brian, D. A., 1989. Coronavirus subgenomic minus-strand RNAs and the potential for mRNA replicons. Proc. Natl. Acad. Sci. U.S.A. 86, 5626-5630.

Shen, X., and Masters, P. S., 2001. Evaluation of the role of heterogeneous nuclear ribonucleoprotein A1 as a host factor in murine coronavirus discontinuous transcription and genome replication. Proc. Natl. Acad. Sci. U.S.A. 98, 2717-2722.

Shi, S. T., Huang, P., Li, H. P., and Lai, M. M., 2000. Heterogeneous nuclear ribonucleoprotein A1 regulates RNA synthesis of a cytoplasmic virus. EMBO J. 19, 4701-4711.

Siddell, S. G., 1983. Coronavirus JHM: coding assignments of subgenomic mRNAs. J. Gen. Virol. 64, 113-125.

Siddell, S. G., Barthel, A., and ter Meulen, V., 1981. Coronavirus JHM: a virion-associated protein kinase. J. Gen. Virol. 52, 235-243.

Siddell, S. G., Wege, H., Barthel, A., and ter Meulen, V., 1980. Coronavirus JHM: cell-free synthesis of structural protein p60. J. Virol. 33, 10-17.

Siddell, S. G., 1995. The Coronaviridae. Plenum Press, New York, pp. 14-18, 60-63, 116-122, 141-153.

Sims, A. C., Ostermann, J., and Denison, M. R., 2000. Mouse hepatitis virus replicase proteins associate with two distinct populations of intracellular membranes. J. Virol. 74, 5647-5654.

Singh, R., 2002. RNA-protein interactions that regulate pre-mRNA splicing. Gene Expr. 10, 79-92.

Snijder, E. J., Bredenbeek, P. J., Dobbe, J. C., Thiel, V., Ziebuhr, J., Poon, L. L., Guan, Y., Rozanov, M., Spaan, W. J., and Gorbalenya, A. E., 2003. Unique and conserved features of genome and proteome of SARS-coronavirus, an early split-off from the coronavirus group 2 lineage. J. Mol. Biol. 331, 991-1004.

Song, X., and Singh, S. M., 2001. Distribution and molecular characterization of mRNA-binding proteins specific to the (U)15 region of 3' UTR of the mouse catalase (Cas-1). DNA Cell Biol. 20, 339-348.

Spaan, W. J., Rottier, P. J., Horzinek, M. C., and van der Zeijst, B. A., 1981. Isolation and identification of virus-specific mRNAs in cells infected with mouse hepatitis virus (MHV-A59). Virology 108, 424-434.

Spaan, W. J., Rottier, P. J., Horzinek, M. C., and van der Zeijst, B. A., 1982. Sequence relationships between the genome and the intracellular RNA species 1, 3, 6, and 7 of mouse hepatitis virus strain A59. J. Virol. 42, 432-439.

Spagnolo, J. F., and Hogue, B. G., 2000. Host protein interactions with the 3' end of bovine coronavirus RNA and the requirement of the poly(A) tail for coronavirus defective genome replication. J. Virol. 74, 5053-5065.

Spehner, D., Kirn, A., and Drillien, R., 1991. Assembly of nucleocapsidlike structures in animal cells infected with a vaccinia virus recombinant encoding the measles virus nucleoprotein. J. Virol. 65, 6296-6300.

Steitz, T. A., Rould, M. A., and Perona, J. J., 1990. Structural basis of tRNA discrimination as derived from the high resolution crystal structure of glutaminyl-tRNA synthetase complexed with tRNA(Gln) and ATP. Mol. Biol. Rep. 14, 213-214.

Stern, D. F., and Kennedy, S. I., 1980a. Coronavirus multiplication strategy. I. Identification and characterization of virus-specified RNA. J. Virol. 34, 665-674.

Stern, D. F., and Kennedy, S. I., 1980b. Coronavirus multiplication strategy. II. Mapping the avian infectious bronchitis virus intracellular RNA species to the genome. J. Virol. 36, 440-449.

Stirrups, K., Shaw, K., Evans, S., Dalton, K., Casais, R., Cavanagh, D., and Britton, P., 2000. Expression of reporter genes from the defective RNA CD-61 of the coronavirus infectious bronchitis virus. J. Gen. Virol. 81, 1687-1698.

Stohlman, S. A., Baric, R. S., Nelson, G. N., Soe, L. H., Welter, L. M., and Deans, R. J., 1988. Specific interaction between coronavirus leader RNA and nucleocapsid protein. J. Virol. 62, 4288-4295.

Stohlman, S. A., Fleming, J. O., Patton, C. D., and Lai, M. M., 1983. Synthesis and subcellular localization of the murine coronavirus nucleocapsid protein. Virology 130, 527-532.

Sturman, L. S., and Holmes, K. V., 1977. Characterization of coronavirus II. Glycoproteins of the viral envelope: tryptic peptide analysis. Virology 77, 650-660.

Sturman, L. S., Ricard, C. S., and Holmes, K. V., 1990. Conformational change of the coronavirus peplomer glycoprotein at pH 8.0 and 37 degrees C correlates with virus aggregation and virus-induced cell fusion. J. Virol. 64, 3042-3050.

Tahara, S. M., Dietlin, T. A., Nelson, G. W., Stohlman, S. A., and Manno, D. J., 1998. Mouse hepatitis virus nucleocapsid protein as a translational effector of viral mRNAs. Adv. Exp. Med. Biol. 440, 313-318.

Thiel, V., and Siddell, S. G., 1994. Internal ribosome entry in the coding region of murine hepatitis virus mRNA 5. J. Gen. Virol. 75, 3041-3046.

Thuman-Commike, P. A., 2001. Single particle macromolecular structure determination via electron microscopy. FEBS letter 505, 199-205.

Tsai, M. S., Hsu, Y. H., and Lin, N. S., 1999. Bamboo mosaic potexvirus satellite RNA (satBaMV RNA)-encoded P20 protein preferentially binds to satBaMV RNA. J. Virol. 73, 3032-3039.

Tsu, C. A., Kossen, K., and Uhlenbeck, O. C., 2001. The *Escherichia coli* DEAD protein DbpA recognizes a small RNA hairpin in 23S rRNA. RNA 7, 702-709.

Valentine, R. C., Shapiro, B. M. and Stadtman, E. R., 1968. Regulation of glutamine synthetase. XII. Electron microscopy of the enzyme from *Escherichia coli*. Biochemistry 7, 2143-2152.

Vennema, H., Godeke, G. J., Rossen, J. W., Voorhout, W. F., Horzinek, M. C., Opstelten, D. J., and Rottier, P. J., 1996. Nucleocapsid-independent assembly of coronavirus-like particles by co-expression of viral envelope protein genes. Embo J. 15, 2020-2028.

von Grotthuss, M., Wyrwicz, L. S., and Rychlewski, L., 2003. mRNA cap-1 methyltransferase in the SARS genome. Cell 113, 701-702.

Wang, Y., and Zhang, X., 1999. The nucleocapsid protein of coronavirus mouse hepatitis virus interacts with the cellular heterogeneous nuclear ribonucleoprotein A1 in vitro and in vivo. Virology 265, 96-109.

Warnes, A., Fooks, A. R., Dowsett, A. B., Wilkinson, G. W., and Stephenson, J. R., 1995. Expression of the measles virus nucleoprotein gene in *Escherichia coli* and assembly of nucleocapsid-like structures. Gene 160, 173-178.

Wilbur, S. M., Nelson, G. W., Lai, M. M., McMillan, M., and Stohlman, S. A., 1986. Phosphorylation of the mouse hepatitis virus nucleocapsid protein. Biochem. Biophys. Res. Commun. 141, 7-12.

Williams, A. K., 1993. Analysis of the nucleocapsid protein of IBV and its association with a hypervariable region in te 3' end of the genome. Ph.D. dissertation, Texas A&M University, College Station.

Williams, A. K., Wang, L., Sneed, L. W., and Collisson, E. W., 1992. Comparative analyses of the nucleocapsid genes of several strains of infectious bronchitis virus and other coronaviruses. Virus Res. 25, 213-222.

Williams, G. D., Chang, R. Y., and Brian, D. A., 1999. A phylogenetically conserved hairpin-type 3' untranslated region pseudoknot functions in coronavirus RNA replication. J. Virol. 73, 8349-8355.

Woo, K., Joo, M., Narayanan, K., Kim, K. H., and Makino, S., 1997. Murine coronavirus packaging signal confers packaging to nonviral RNA. J. Virol. 71, 824-827.

Wootton, S. K., and Yoo, D., 2003. Homo-oligomerization of the porcine reproductive and respiratory syndrome virus nucleocapsid protein and the role of disulfide linkages. J. Virol. 77, 4546-4557.

Wurm, T., Chen, H., Hodgson, T., Britton, P., Brooks, G., and Hiscox, J. A., 2001. Localization to the nucleolus is a common feature of coronavirus nucleoproteins, and the protein may disrupt host cell division. J. Virol. 75, 9345-9356.

Xu, H. Y., Lim, K. P., Shen, S., and Liu, D. X., 2001. Further identification and characterization of novel intermediate and mature cleavage products released from the ORF 1b region of the avian coronavirus infectious bronchitis virus 1a/1b polyprotein. Virology 288, 212-222.

Youn, S., 2003. In vitro assembly of an infectious cDNA clone of infectious bronchitis virus and its application as a gene transfer vector. Ph.D. dissertation, Texas A&M University, College Station.

Yount, B., Curtis, K. M., and Baric, R. S., 2000. Strategy for systematic assembly of large RNA and DNA genomes: transmissible gastroenteritis virus model. J. Virol. 74, 10600-10611.

Yount, B., Denison, M. R., Weiss, S. R., and Baric, R. S., 2002. Systematic assembly of a full-length infectious cDNA of mouse hepatitis virus strain A59. J. Virol. 76, 11065-11078.

Zhang, X., and Lai, M. M., 1994. Unusual heterogeneity of leader-mRNA fusion in a murine coronavirus: implications for the mechanism of RNA transcription and recombination. J. Virol. 68, 6626-6633.

Zhang, X., and Lai, M. M., 1995. Interactions between the cytoplasmic proteins and the intergenic (promoter) sequence of mouse hepatitis virus RNA: correlation with the amounts of subgenomic mRNA transcribed. J. Virol. 69, 1637-1644.

Zhou, M., 1997 Interactions of the nucleocapsid protein with the 3' and 5' noncoding regions of genomic RNA of avian infectious bronchitis virus. Ph. D. dissertation, Texas A&M University, College Station.

Zhou, M., and Collisson, E. W., 2000. The amino and carboxyl domains of the infectious bronchitis virus nucleocapsid protein interact with 3' genomic RNA. Virus Res. 67, 31-39.

Zhou, M., Williams, A. K., Chung, S. I., Wang, L., and Collisson, E. W., 1996. The infectious bronchitis virus nucleocapsid protein binds RNA sequences in the 3' terminus of the genome. Virology 217, 191-199.

Ziebuhr, J., Snijder, E. J., and Gorbalenya, A. E., 2000. Virus-encoded proteinases and proteolytic processing in the Nidovirales. J. Gen. Virol. 81, 853-879.

Ziegler, A. F., Ladman, B. S., Dunn, P. A., Schneider, A., Davison, S., Miller, P. G., Lu, H., Weinstock, D., Salem, M., Eckroade, R. J., and Gelb, J., Jr., 2002. Nephropathogenic infectious bronchitis in Pennsylvania chickens 1997-2000. Avian Dis. 46, 847-858.

VITA

Name: Jyothi Jayaram

Permanent Address: 439, Nirmal, 2nd Floor,
Shradhanand Road,
Matunga,
Mumbai 400019,
India.

Education

- **September 1997-May 2004:** Ph.D. Microbiology, Department of Biology, Texas A&M University, College Station, TX, USA

- **July 1994-May 1996:** M.S. Biotechnology, Department of Microbiology and Biotechnology Center, Maharaja Sayajirao University of Baroda, India

- **August 1991-May 1994:** B.S. Microbiology, Ramnarain Ruia College, University of Bombay, Mumbai, India